Effect of Existing Building on Tunneling-induced Ground Movements

By

Rachel Hoi-chee Law

BEng of Civil Engineering
University of Hong Kong
(2001)

Submitted to the Department of Civil and Environmental Engineering in partial fulfillment of the requirements for the degree of
Master of Engineering in Civil and Environmental Engineering

at the

Massachusetts Institute of Technology

June 2012

Signature of Author: _____
Department of Civil and Environmental Engineering
May 11, 2012

Certified by: _____
Andrew J. Whittle
Professor of Civil and Environmental Engineering
Thesis Supervisor

Accepted by: _____
Heidi M. Nepf
Chair, Departmental Committee for Graduate Students

Effect of Existing Building on Tunneling-induced Ground Movements

by
Rachel Hoi-chee Law

Submitted to the Department of Civil and Environmental Engineering
on May 11, 2012 in Partial Fulfillment of the
Requirements for the Degree of Master of Engineering in
Civil and Environmental Engineering

ABSTRACT

The goal of this thesis is to assess the influence of an existing structure on tunneling-induced ground movements. This is accomplished through 2D numerical simulations that are compared with similar prior studies reported by Potts and Addenbrooke (1997). The current study uses the Plaxis finite element code together with the Hardening Soil (HS and HSS) family of constitutive models in order to represent the undrained shear behavior of clay. Input parameters of the HS and HSS models were calibrated for the case of London Clay and compared with results of Potts and Addenbrooke (1997) who used a non-linear elastic model (PJ model). Results have clearly indicated that the choice of soil model has an important influence on the prediction of greenfield ground settlement. The HSS model with the selected set of stiffness parameters provides a reasonable fit with the PJ model and matches closely the greenfield settlement trough expected from empirical models. Numerical analyses are carried out to evaluate the effects of the self-weight, and equivalent elastic bending and axial stiffness of a surface building on tunneling-induced ground movements. For the case of a weightless building, design modification factors for bending and axial stiffness are consistent with results promulgated in Potts and Addenbrooke (1997). For the self-weight scenario, the current analyses indicated that neglecting this factor in the analyses can result in non-conservative estimate of modification factors for deflection ratio and horizontal strain. It is therefore suggested that the effect of building weight cannot be neglected when the boundary effect of building stiffness on the ground is used as a tool to reduce the estimated values of greenfield settlement trough or deflection ratio and horizontal strain of existing buildings in a building damage assessment.

Thesis Supervisor: Andrew J. Whittle
Title: Professor of Civil and Environmental Engineering

Acknowledgements

First and foremost, my biggest thanks go to Prof Andrew Whittle. His in-depth understanding and unparalleled knowledge on geotechnical engineering concepts had guided me through the difficulties encountered in this research. His enlightening opinion on anything related to soil behavior and insightful comments during my study in MIT really benefits me the most.

My sincere thanks also go to Despina, Eva, Gonzalo, Nina, Yixing and everyone in the research team for sharing their valuable experience on geotechnical research and answering my endless questions.

I am grateful to Rob, Shehab, Vasso, Gery and Alessandra for their friendship and all the time we had spent together. They made MIT a lovely place to study and hang out. Without them, my life in MIT would not have been this memorable.

I am indebted to my employer GEO for the comprehensive GEG training that equipped me with the necessary basic geotechnical techniques to enable me to acquire the most deserving knowledge in MIT. Without their support and good blessing, this would not have been possible. My indebtedness also extends to all those colleagues and ex-colleagues in GEO who have heartily helped me through my professional career.

I owe my deepest gratitude to my family (Dad, Mom and sibling Janice) for their patience, support and encouragement. Especially Dad, whose nurture and guidance during my childhood really drove my interest in studying and made me the brightest child. And to my husband (Karl), who always put me on the first priority despite the endless call duty in Brigham. The bits and pieces between two of us during this year's stay in Boston will never be forgotten. Last but not least, to my beloved grandma! Wherever you are, whenever it is, your smile and our sweet memories during my childhood will always be in my heart. Your passion for life really touches me. You all make my life worth living!

Table of Contents

List of Figures

List of Tables

1 Introduction

Tunneling-induced ground movements can cause serious damage to overlying buildings and utilities and have a profound influence on costs associated with tunneling projects. In many cities the urban underground space is very congested with building foundations, transportation and utility tunnels. It is inevitable that the alignment of new tunnels will interact with the existing infrastructures including old, sensitive buildings and tunnels.

The relationship between tunneling-induced ground movements and existing structures is not simple. The problem involves coupled soil-structure interactions, where the tunneling construction affects existing structures, while existing structures also influence the tunneling-induced ground movements. There are three common approaches currently used to estimate tunneling-induced ground movements: 1) empirical, 2) analytical and 3) numerical methods. Among these only numerical analyses are specifically able to model the complexities of soil-structure interactions. Current engineering practice does not take into account the soil-structure interaction in the design of new tunneling projects.

Burland (1995) recommended a three-stage procedure for evaluating the risk of building damage that accounts for beneficial effects of settlement reduction due to stiffness of existing buildings. Potts and Addenbrooke (1997) conducted a parametric study using non-linear finite element methods to assess the influence of an existing structure on ground movements due to tunneling. Their study focused on four key parameters: 1) the width of the structure; 2) its equivalent bending and axial stiffness (based upon elastic

deep beam theory after Burland and Wroth, 1974); 3) building position relative to the tunnel centerline; and 4) the depth of the tunnel. By introducing relative stiffness parameters which combine bending and axial stiffness of the structure with building width and stiffness of the soil, they proposed a unifying framework for estimating building damage parameters (deflection ratio and horizontal strain). This thesis provides a further comparative study of the influence of building properties using numerical analysis. The current study follows the earlier work of Potts and Addenbrooke (1997) and focuses on ground conditions typically found in London (with particular focus on the Crossrail project). However, in contrast to the earlier study[1], this research uses a commercial finite element code *PLAXIS*^{TM} together with the Hardening Soil family of constitutive models (Hardening Soil HS, Schanz, Vermeer and Bonnier 1999 and Hardening Soil Small HSS, Benz 2006).

[1] done with ICFEP and a bespoke soil model proposed by Jardine et.al (1986)

2 Literature Review

2.1 Introduction

This chapter gives an overview of the three common methods for tunneling-induced ground movement predictions (empirical, analytical and numerical) followed by a discussion of the state-of-the-art three-stage approach for the assessment of risk of damage to buildings (Burland, 1995). One of the key steps in this procedure is to compute the relative stiffness of the structure relative to the soil and to account for the relative stiffness in estimating ground response due to tunneling.

2.2 Empirical Method

The empirical method is the most widely-used means to predict magnitude of ground movement. The method uses case history data to predict the magnitude of settlement by assuming a certain geometric shape for the surface settlement distribution. Following Peck (1969) the 2-D transversal settlement trough above a tunnel (under greenfield conditions) is mostly commonly described by a Gaussian distribution function, Figure 2.1:

$$u_y = u_y{}^o \exp\left(\frac{x^2}{2x_i{}^2}\right) \qquad (2.1)$$

where u_y = settlement

$u_y{}^o$ = the maximum settlement at the tunnel centerline

x = the horizontal distance from the tunnel centerline

x_i = the horizontal distance from the tunnel centerline to the point of inflection of the settlement trough

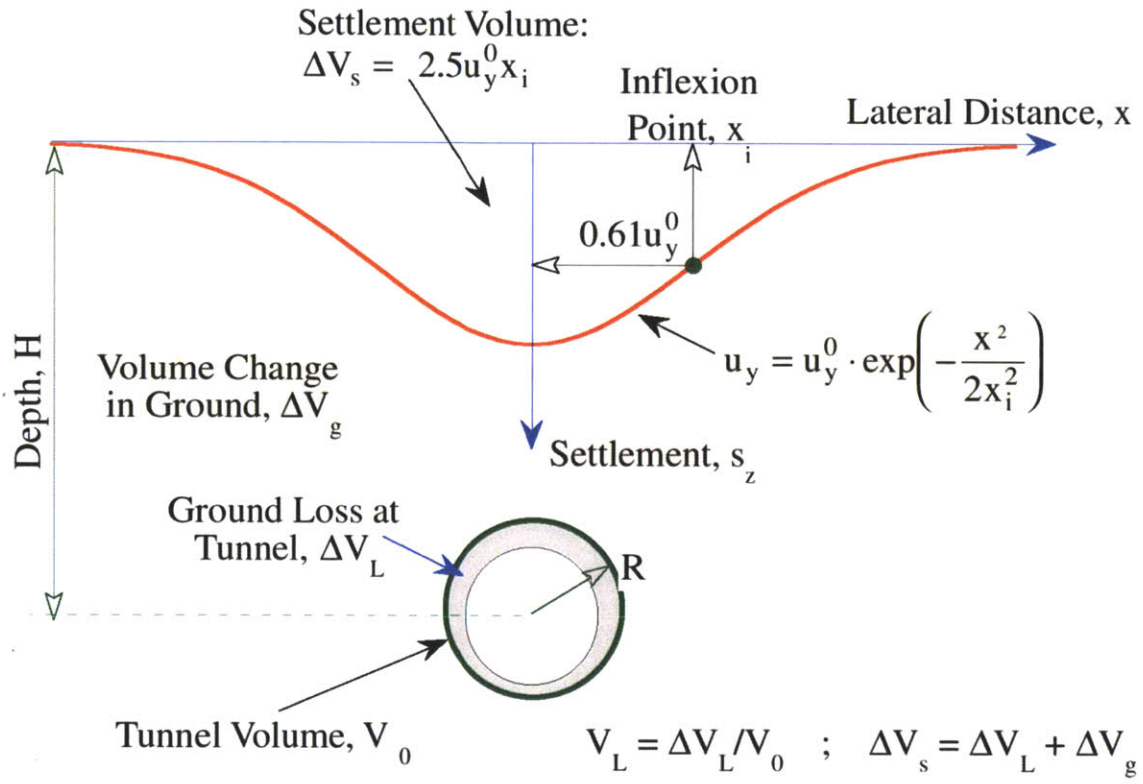

Figure 2.1: Empirical function for transversal, greenfield surface settlement trough (Pinto and Whittle, 2012 after Peck, 1969)

This equation was firstly proposed by Martos (1958) and based on field measurements of settlements above mine openings, and by Schmidt (1969) from tunnel projects for the Chicago subway project.

Mair and Taylor (1997) show that the width of the settlement trough is correlated to the depth of the tunnel, H, and to the characteristics of the overlying soil, see Figure 2.2a.

The same Gaussian function can describe the subsurface vertical ground movements by varying the trough width parameter, such that the point of inflection is defined by:

$$x_i = K\,(H - y) \tag{2.2}$$

where H is the tunnel depth to springline and K is a non-linear function shown in Figure 2.2b.

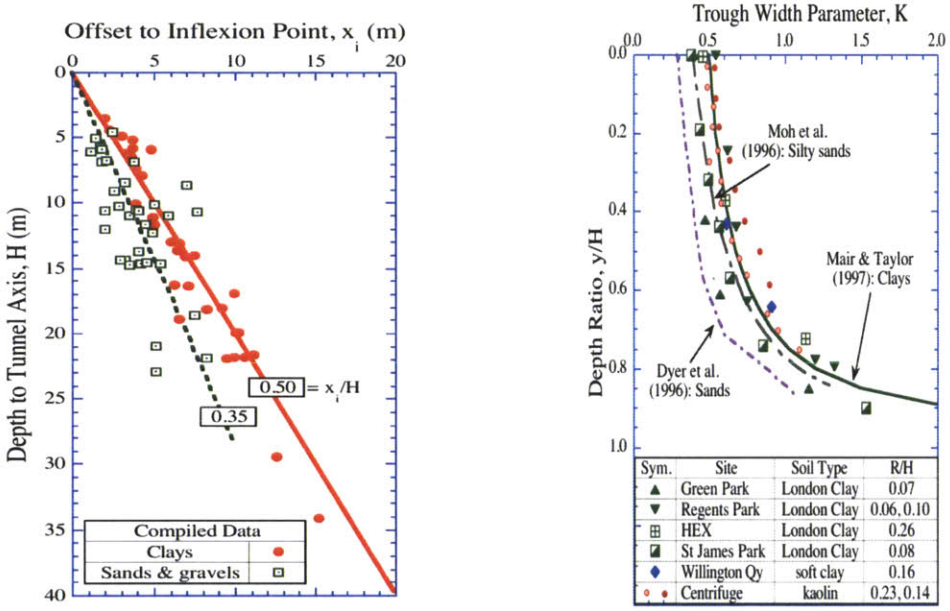

a) Width of surface settlement troughs b) Width of sub-surface settlement troughs

Figure 2.2: Empirical estimation of inflection point (after Mair and Taylor, 1997)

There is not much data for estimating the horizontal components of ground deformations. The common practice is to assume that the displacement vectors are directed to a point on or close to the center of the tunnel as proposed by Attewell (1978) and O'Reilly and New (1982):

$$u_x \approx \frac{x}{H} u_y \tag{2.3}$$

By integrating equation (2.1), the volume of surface settlement trough, ΔV_s, per unit advancement of the tunnel can be obtained:

$$\Delta V_s = \sqrt{2\pi} x_i S_{max} \tag{2.4}$$

The volume loss ΔV_L, which represents the ground loss around the tunnel, is obtained by:

$$\Delta V_L = \Delta V_s + \Delta V_g \tag{2.5}$$

where ΔV_g represents the volume change of the ground.

It is worth noting that the volume loss at the tunnel cavity ΔV_L is not necessarily equal to the surface volume ΔV_s. For example, when tunneling in dense sand under drained conditions, Cording and Hansmire (1975) report that $\Delta V_s < \Delta V_L$ due to soil dilation. On the other hand, when tunneling in clay where short-term (i.e., end of construction) ground movements usually occur under undrained (constant volume) conditions, it is generally expected that $\Delta V_s = \Delta V_L$ (Mair and Taylor, 1997). Macklin (1999) has assumed that measurements of surface settlements are associated with ground loss at the tunnel heading and hence, can be correlated to the stability conditions at the tunnel face.

Figure 2.3 shows Macklin (1999)'s correlations between the volume loss ΔV_L (= ΔV_s) for shallow tunnels in clay and the load factor, LF = N/N_c, where N_c is the critical stability number derived by Kitamura and Mair (1981) and N is:

$$N = (\sigma_v - \sigma_T)/S_u \tag{2.6}$$

where σ_v is the overburden stress at the springline elevation, σ_T the face pressure at the loading and S_u, the undrained shear strength of the clay.

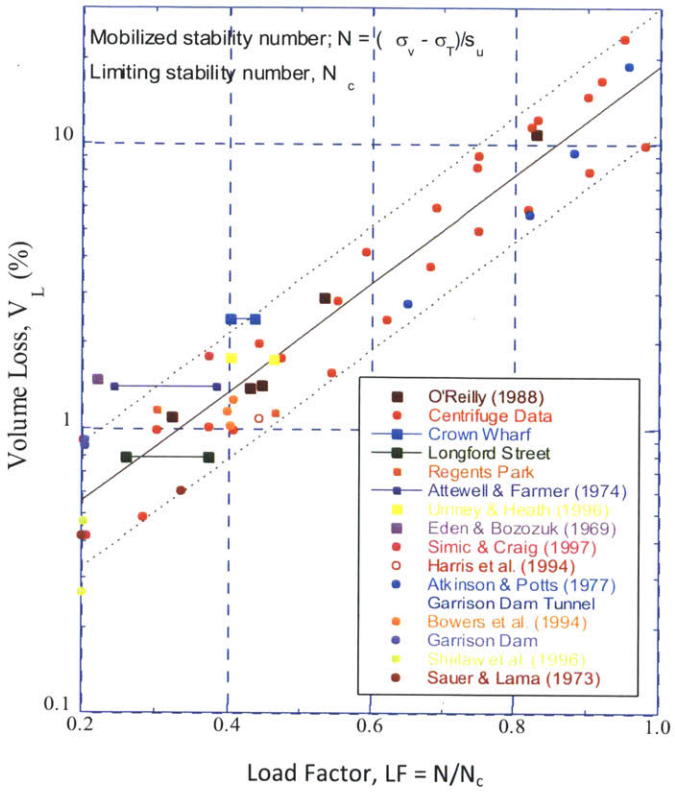

(a) Empirical estimate of ground loss for shallow tunnel in Clays (Macklin, 1999)

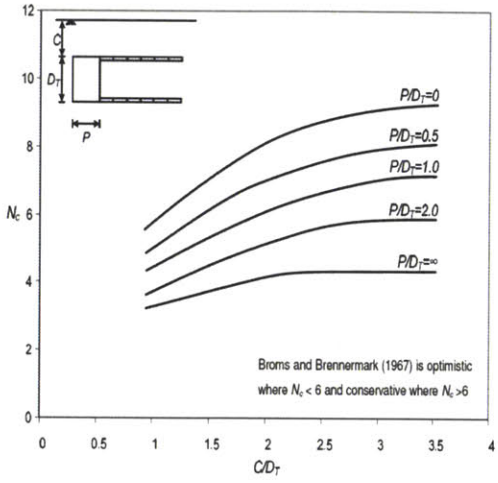

(b) Critical advanced stability of unsupported headings of tunnels in clay (Kitamura & Mair, 1981)

Figure 2.3: Empirical estimate of ground loss at the tunnel heading and correlation with stability number

Empirical method mainly depends on past field observations. However in reality, ground movement depends on various factors such as tunnel geometry and depth, tunnel construction method, workmanship and behavior of soil around the tunnel. Therefore, failing to consider these site-specific factors could be an important limitation of the empirical method.

2.3 Analytical method

Analytical solutions provide a complete framework to describe the distribution of far-field ground deformations based on a prescribed set of displacements around the tunnel cavity. Figure 2.4 shows that the ground deformations can be expressed as the summation of three modes of tunnel cavity deformation, namely 1) uniform convergence, u_ε; 2) ovalization, u_δ; and 3) vertical translation, Δu_y. The analytical solutions make gross approximations of the constitutive behavior of the soil (e.g., assuming linear, elastic soil properties), yet fulfill all of the principles of continuum mechanics.

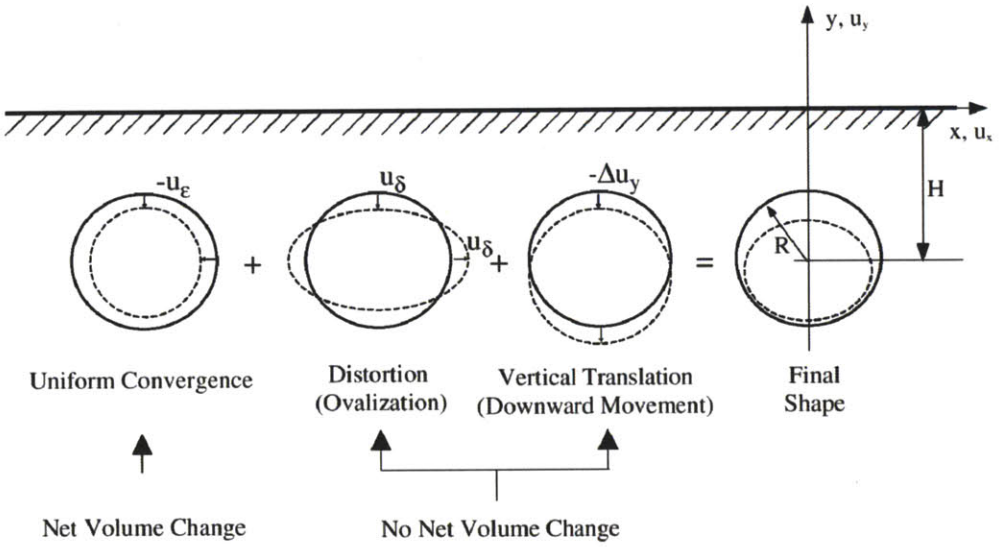

a) Notation and sign convention

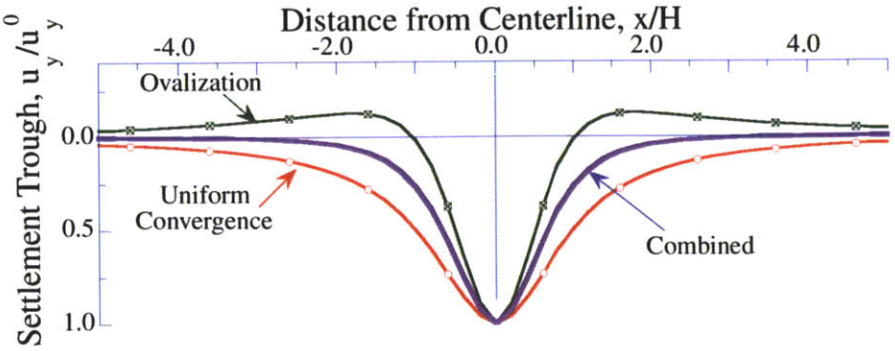

b) Component contributions to surface settlement trough

Figure 2.4: Modes of deformation around tunnel cavity (Sagaseta and Whittle, 2003)

In fact, there are a variety of analytical solutions for estimating settlement distribution for shallow tunnels in soft ground, using either exact (complex variable, Verruijt, 1997) or approximate (superposition of line sources) methods (Sagaseta, 1987; Verruijt and Booker, 1996; Gozalez and Sagaseta, 2001). For the approximate methods, the 'far-field' ground movements caused by shallow tunneling processes (excavation and support) are solved as a linear superposition of the above three deformation modes occurring at the tunnel cavity. Pinto and Whittle (2011) have shown that closed-form solutions obtained by the approximate methods by superposition of singularity solutions (after Sagaseta, 1987) provide a good approximation of the more complete ('Exact') solutions obtained by representing the finite dimensions of a shallow tunnel in an elastic soil (after Verruijt, 1996). Pinto and Whittle (2011) have also shown how the results are influenced by soil plasticity (close to the tunnel) and have developed closed-form solutions for uniform convergence of a 3-D tunnel heading.

The analytical method requires a small number of physically meaningful input parameters, which can be obtained in principle from a small number of independent field measurements of ground displacements. Pinto et al. (2011) have shown how these can be estimated from a series of case studies. The analytical solutions offer a more complete framework for estimating the distribution of ground movements around a tunnel in greenfield conditions. However, they rely on the calibration of tunnel cavity parameters (u_ε and u_δ) to processes of tunnel construction. They also do not address directly the role of soil-structure interaction.

2.4 Numerical method

Empirical and analytical methods have been well-developed to provide a reasonable estimate of greenfield tunneling-induced ground movements. However, these methods can become deficient in the absence of adequate case history data. More importantly, some factors affecting ground movement, notably pressures at the excavated face, long term settlement and effects of the construction sequencing are not fully taken into account in these methods. These limitations have encouraged widespread adoption of numerical methods for analyzing ground deformations caused by tunneling.

Non-linear finite element methods are the most commonly used numerical analysis for tunnels. Finite element models can be used to simulate deformation coupled deformation and flow[1], as well as stability analyses[2]. Finite element analyses can 1) incorporate constitutive soil models of varying complexity; 2) represent structural support conditions for the tunnel analyses; and 3) consider interactions with pre-existing structures.

Finite element analyses are capable of simulating the construction of a tunnel in stages. The tunnel linings are typically modeled by plates or shell elements, while tunnel excavation and grouting processes are simulated by deactivating and activating soil clusters. Two dimensional models of tunneling are routinely used to represent the construction process. In these situations, the volume losses are simulated mainly by two methods, either by 1) directly applying a contraction at the tunneling cavity; or 2)

[1] Both drained and undrained situations can be modeled and the effect of time can be taken into account for time-dependent geotechnical process, such as consolidation.

[2] Done by c-phi reduction methods

assuming that the in-situ stresses are partitioned between a fraction (1 - β) that is internally redistributed within the soil mass and a fraction (β) that is applied to the tunnel lining.

2.5 Assessment of risk to buildings

Given a set of predictions of tunneling-induced ground movements for greenfield conditions, it is necessary to quantify their potential effects on existing buildings. Burland (1995) considered this problem and suggested a three-stage approach for assessment of risk of damage to buildings by tunneling works:

1) Preliminary assessment

In the preliminary assessment stage, ground settlement contours are drawn using empirical predictions of greenfield conditions. If the maximum predicted settlement of a building $\rho \leq 10$mm or the greenfield trough imposes a rotation, $\theta < 0.002$ (Figure 2.5), no further assessment is necessary. Burland (1995) noted that the slope, θ is not a satisfactory building performance parameter as it gives no indication of the possible distortion of the building. The preliminary assessment based on the slope and settlement of the ground surface only provides a conservative initial basis for identifying those buildings along the tunnel alignment requiring further study.

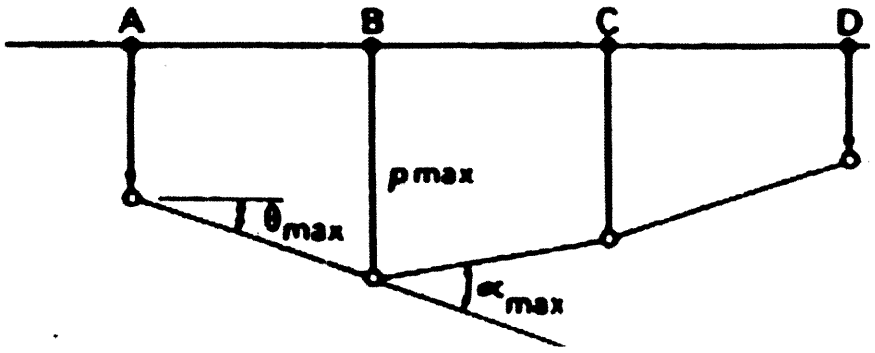

Figure 2.5: Definition of rotation (slope), θ

2) Second stage assessment

The second stage assessment introduces the concept of a limiting tensile strain. Following Polshin and Tokar (1957), Burland and Wroth (1974) conducted numerous large scale tests on masonry panels and walls at the UK Building Research Establishment and showed that the onset of visible cracking is associated with a critical tensile strain, ε_{crit} which is not sensitive to the mode of deformation. Burland et al. (1977) noted that the critical tensile strain (ε_{crit}) causing the onset of visible cracking is not a fundamental material property because it does not necessarily represent a limit of serviceability (as it may be acceptable to allow deformation well beyond the initiation of visible cracking). Therefore, they introduced the concept of limiting tensile strain (ε_{lim}), which takes into account the effects of differing materials and serviceability limit states.

Boscardin and Cording (1989) analyzed seventeen case records of damage (covering a variety of building types) due to ground movement induced by open cutting and tunneling, and proposed that the limiting tensile strain (ε_{lim}) can be related to the five categories of building damage (Table 2.1) originally proposed by Burland et al. (1977)

(Table 2.2), by reference to visible damage to walls (with particular reference to ease of repair of plaster and brickwork or masonry).

Category of damage	Normal degree of severity	Limiting tensile strain (ε_{lim}) (%)
0	Negligible	0 - 0.05
1	Very slight	0.05 - 0.075
2	Slight	0.075 - 0.15
3	Moderate*	0.15 - 0.3
4 to 5	Severe to very severe	> 0.3

Table 2.1: Relationship between category of damage and limiting tensile strain (Boscardin and Cording, 1989)

Category of damage	Normal degree of severity	Description of typical damage* (ease of repair is in italic)
0	Negligible	Hairline cracks less than about 0·1 mm
1	Very slight	*Fine cracks which are easily treated during normal decoration.* Damage generally restricted to internal wall finishes. Close inspection may reveal some cracks in external brickwork or masonry. Typical crack widths up to 1 mm
2	Slight	*Cracks easily filled. Redecoration probably required. Recurrent cracks can be masked by suitable linings.* Cracks may be visible externally and *some repointing may be required to ensure weathertightness.* Doors and windows may stick slightly. Typical crack widths up to 5 mm
3	Moderate	*The cracks require some opening up and can be patched by a mason. Repointing of external brickwork and possibly a small amount of brickwork to be replaced.* Doors and windows sticking. Service pipes may fracture. Weathertightness often impaired. Typical crack widths are 5 to 15 mm or several up to 3 mm
4	Severe	*Extensive repair work involving breaking-out and replacing sections of walls, especially over doors and windows.* Windows and door frames distorted, floor sloping noticeably.† Walls leaning† or bulging noticeably, some loss of bearing in beams. Service pipes disrupted. Typical crack widths are 15 to 25 mm but also depends on the number of cracks
5	Very severe	*This requires a major repair job involving partial or complete rebuilding.* Beams lose bearing, walls lean badly and require shoring. Windows broken with distortion. Danger of instability. Typical crack widths are greater than 25 mm but depend on the number of cracks

*Crack width is only one factor in assessing category of damage and should not be used on its own as a direct measure of it.
†Local deviation of slope, from the horizontal or vertical, of more than 1.100 will normally be clearly visible. Overall deviations in excess of 1.150 are undesirable.

Table 2.2: Classification of visible damage to walls with particular reference to ease of repair of plaster and brickwork or masonry (Burland et al., 1977)

The limiting tensile strain provides a convenient measure of the damage that can be related to deformations for different types of structure. Burland and Wroth (1974) proposed the deep beam approach (Figure 2.6) in which the structure is represented as a deep beam with equivalent elastic axial and bending stiffness. The analysis considered the sagging ratio Δ/L (see Figure 2.6(a)) for two extreme modes of beam behavior in bending about a neutral axis at the centre (Figure 2.6(b)) and in shearing only (Figure 2.6(c)).

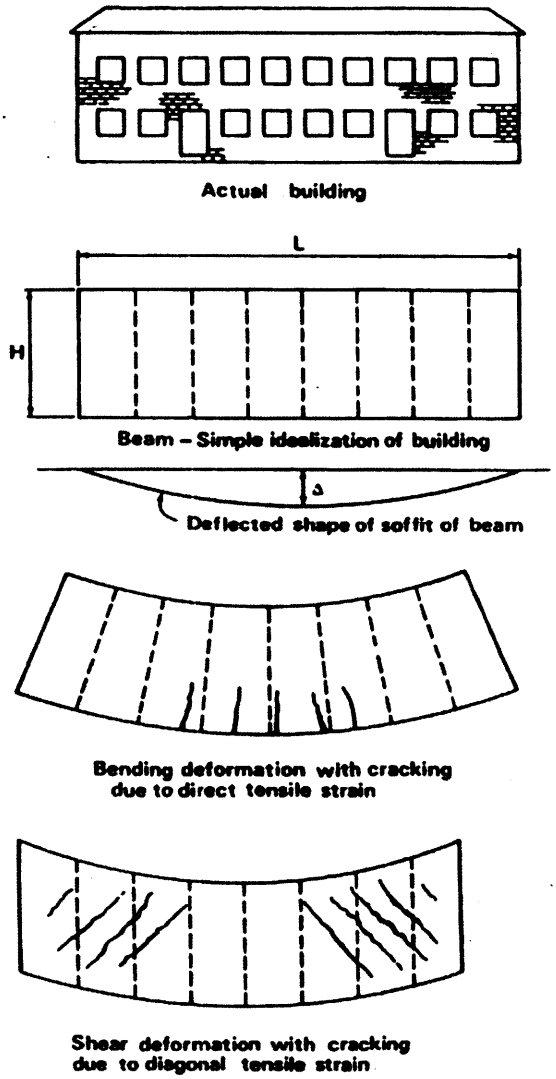

(a) Actual building and equivalent deep beam as well as definition of deflection ratio

(b) Cracking in bending

(c) Cracking in shear

Figure 2.6: Cracking of a simple beam (After Burland and Wroth, 1974)

The deflection of a deep beam in bending and shear (after Timoshenko, 1955, see Figure 2.7) is:

$$\Delta = \frac{PL^3}{48EI}\left(1 + \frac{18EI}{L^2HG}\right) \tag{2.7}$$

where E is Young's modulus, G is shear modulus, I is the second moment of area (about a defined neutral axis and P is the vertical load of the building represented as a point load)[1].

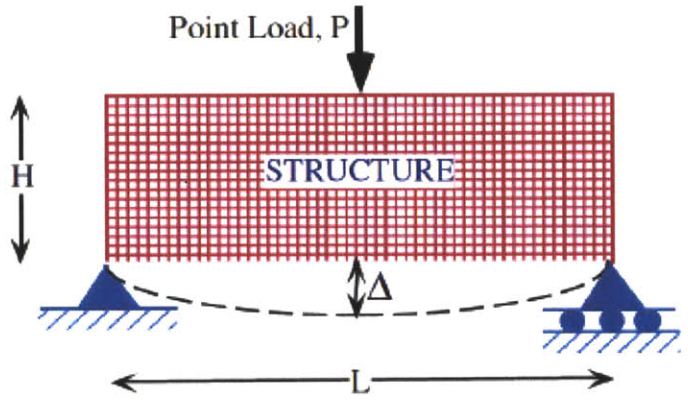

Figure 2.7: Deflection of deep beam with bending and shear (Timoshenko, 1955)

Equation (2.7) can be written in terms of deflection ratio and maximum fibre strain, ε_{bmax}:

Bending:
$$\frac{\Delta}{L} = \left(\frac{L}{12} + \frac{3I}{2tL^2H}\frac{E}{G}\right)\varepsilon_{bmax} \tag{2.8}$$

Diagonal shear:
$$\frac{\Delta}{L} = \left(1 + \frac{1L^2}{4H^2}\right)\varepsilon_{bmax} \tag{2.9}$$

where t is the distance of the neutral axis from the edge of the beam in tension.

[1] Burland and Wroth (1974) show that the dead-weight load distribution has little impact on the subsequent results.

As building damage can also result from horizontal strains, Boscardin and Cording superimposed horizontal tensile strain, ε_h to the above analysis (i.e., assuming that the deflected beam is subjected to uniform extension over its full depth). For bending, equation (2.7) can be rewritten to represent the resultant extreme fibre strain ε_{br} in terms of ε_{bmax} and ε_h:

$$\varepsilon_{br} = \varepsilon_{bmax} + \varepsilon_h \tag{2.10}$$

From the Mohr's circle of strain, the resultant diagonal tensile strain in the shearing region can also be given in terms of ε_{dmax} and ε_h:

$$\varepsilon_{dr} = \varepsilon_h \left(\frac{1-\mu}{2}\right) + \sqrt{\varepsilon_h^2 \left(\frac{1+\mu}{2}\right)^2 + \varepsilon_{dmax}^2} \tag{2.11}$$

where μ is the Poisson's ratio.

The larger of ε_{br} and ε_{dr} defines the maximum strain, ε_{max} in the beam. Based on equations (2.8), (2.9), (2.10) and (2.11), the maximum strain can be computed for a given value of Δ/L and ε_h, in terms of t, E/G and μ. The value of ε_{max} can then be used to assess the category of building damage by Tables 2.1 and 2.2, associated with the given values of building damage parameters: Δ/L (deflection ratio) and ε_h (horizontal strain).

Burland (1997) admitted that the second stage assessment, although more detailed, is still very conservative and is likely to overestimate damage to buildings. He attributed this to the fact that the building conforms to the 'greenfield site' settlement trough. This is in

contrast to practice, where the inherent stiffness of the building will interact with the supporting ground and tend to reduce both deflection ratio and horizontal strains.

3) Detailed evaluations

This stage is undertaken for buildings where a "moderate" level of damage has been predicted in stage two. The approach is to carry out a refined version of stage two taking into account the particular features of the building and the tunneling scheme (i.e., soil-structure interaction). The key factors suggested to be considered include:

- The sequence and method of tunneling (factors such as face pressure and wait time for support affect the volume loss and hence, can reduce potential ground movements);
- Building details, such as the beneficial effects of structural continuity including those of framed structures, strip footings and rafts;
- Adverse effects of having buildings oriented at a significant skew to the tunnel axis;
- Beneficial effects of predicted greenfield settlement reduced by the stiffness of existing buildings.

Protective measures will then be considered for buildings remaining in the "moderate" or higher damage categories, following the completion of the three-stage assessment.

2.6 Modeling Soil Structure Interaction by the Relative Stiffness Approach

There is a coupled relationship between tunneling and performance of existing buildings. Tunneling-induced settlements affect existing structures, while the stiffness and weight of existing structures also influence the distribution and magnitude of tunneling-induced soil movements. Burland (1997) highlighted this issue by asserting the fact that failing to consider the effect of soil-structure interaction will usually over-estimate the degree of building damage.

To address this issue quantitatively, Potts and Addenbrooke (1997) proposed a relative stiffness method, based on a parametric study using non-linear finite element methods. The four key parameters in their study included: 1) the width of the structure, B; 2) the equivalent bending, EI and axial stiffness, EA (represented as an equivalent elastic deep beam after Burland and Wroth, 1974); 3) building position relative to the tunnel centerline, e; and 4) the depth to tunnel springline, H. It is noted that in all cases the dead and live loads of the structure are not modeled (i.e., no vertical load).

Potts and Addenbrooke (1997) focused on a specific circular tunnel with diameter, d = 4.146 m, and depth from the soil surface to the tunnel axis, H = 20m or 34m (typical for proposed tunnel construction in London). An equivalent elastic beam of width B resting on the soil surface was used to model the effect of existing structures. The contact surface is assumed to be rough (i.e., no slip between beam and soil). The numerical

analysis in their study was done using the ICFEP program and a bespoke soil model proposed by Jardine et al. (1986), referred to subsequently as the PJ model.

The soil model described by Jardine et al. (1986) is capable of representing the non-linear elastic pre-yield behavior as well as plastic behavior (by a Mohr-Coulomb yield surface and plastic potential). In their analyses, Potts and Addenbrooke (1997) modeled strength parameters c' = 10kPa; ϕ' = 25°, with an angle of dilation ψ = 12.5°, a saturated bulk unit weight γ_s = 20kN/m^3 and a coefficient of earth pressures at rest K_0 = 1.5. Subsequent publications (e.g., Franzius, 2003) clarify that Potts and Addenbrooke (1997) adopted a zone of reduced K_o around the tunnel (see Figure 2.8) as an artifact to obtain better predictions of the greenfield surface settlement trough. Potts and Zdravkovic (2001) assert that this modeling assumption represents some of the 3D effects of tunneling and appears to represent measured performance for a series of cases studies for the JLE project[1]. The results in Figure 2.9 show modest levels of improvement that are achieved through the reduced K_o zone. It is, however, abundantly clear that numerical simulations for K_o = 1.5 underestimate surface settlements above the tunnel and predict wider settlement troughs than the measured data. Potts and Zdravkovic (2001) also carried out three dimensional analyses and found that tunneling construction causes a reduction in the effective stress ratio at the springline. They therefore envisage that the reduced K_o-approach may be a logical assumption to represent the stress change ahead of tunnel face.

[1] JLE project at Regant's Park (34m depth), Green Park (29m depth) and St. James's Park (30m depth)

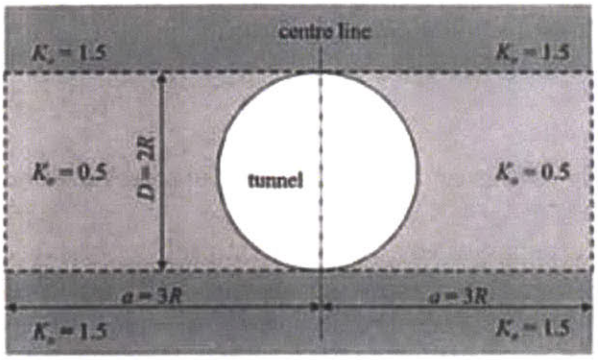

Figure 2.8: Layout of zone of reduced Ko (after Potts and Zdrakovic, 2001)

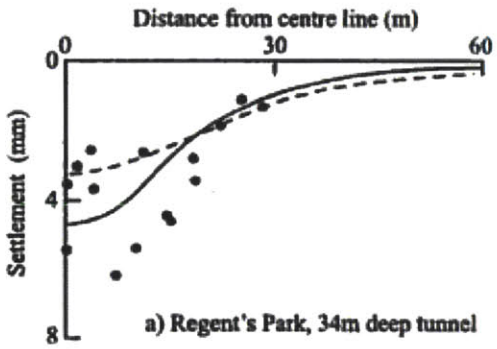

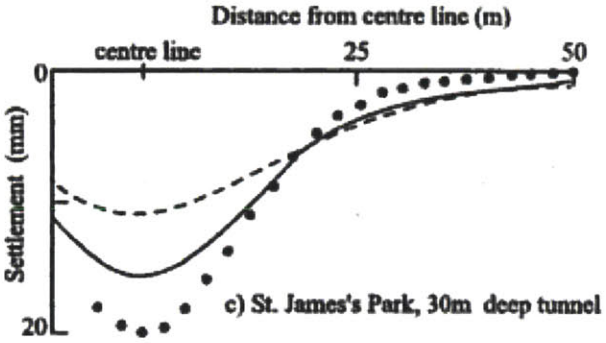

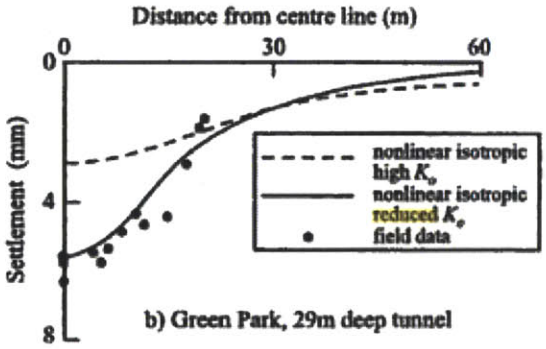

Figure 2.9: Effects of initial stress conditions on settlement prediction

As for the stiffness properties, the PJ model represents isotropic secant shear and bulk moduli parameters as functions of the shear and volumetric strains. Secant stiffness that describe the variation of shear and bulk moduli are given by:

$$\frac{3G}{p'} = A + B\cos\left[\alpha\left(Log_{10}\left(\frac{E}{\sqrt{3}C}\right)\right)^{\gamma}\right] \tag{2.12}$$

$$\frac{K}{p'} = R + S\cos\left[\delta\left(Log_{10}\left(\frac{\epsilon_v}{T}\right)\right)^{\lambda}\right] \tag{2.13}$$

where G = secant modulus, K = secant bulk modulus, p' = mean effective stress, E = deviatoric strain invariant= $\left(\frac{2}{3}\right)^{\frac{1}{2}}[(\varepsilon_1-\varepsilon_2)^2+(\varepsilon_1-\varepsilon_3)^2+(\varepsilon_2-\varepsilon_3)^2]^{\frac{1}{2}}$ = volumetric strain and A, B, C, R, S, T, α, δ, γ and λ are constants with values used by Potts and Addenbrooke (1997) listed in Table 2.3 below:

Strata	A	B	C (%)	α	γ
London Clay	1120	1016	1 x 10^{-4}	1.335	0.617
	R	S	T (%)	δ	λ
	549	506	1 x 10^{-3}	2.069	0.420

Table 2.3: Input parameters for the PJ model (after Jardine et al., 1986)

Potts and Addenbrooke (1997) used the following relative bending and axial stiffness to account for the stiffness of both the beam (structure) and the soil in presenting the results of their analyses:

Relative bending stiffness: $$\boldsymbol{\rho^* = \frac{EI}{E_s(\frac{B}{2})^4}} \tag{2.14}$$

Relative axial stiffness: $$\boldsymbol{\alpha^* = \frac{EA}{E_s(\frac{B}{2})}} \tag{2.15}$$

where E, I and A are equivalent Young's modulus, second moment of area and equivalent cross sectional area of the existing structure; B is the width of the existing structure; and E_s is the secant Young's modulus that would be obtained at an axial strain, $\varepsilon_a = 0.01\%$ in a triaxial compression test performed on a sample retrieved at a depth, $z = H/2$.

The expression ρ^* is similar to that used by Fraser and Wardle (1976) and Potts and Bond (1994). Fraser and Wardle (1976) carried out a series of numerical analysis of rectangular rafts on layered soil foundations and concluded that the dimensionless stiffness factor (embracing influence of raft rigidity I and its length to breath ratio, soil depth and Poisson's ratio, in an expression resembling ρ^*) can markedly affect both vertical movement and bending moments in raft foundations. Similar factors were also adopted for retaining wall analyses by Potts and Bond (1994). On the other hand, the expression for α^* is similar to the normalized dimensionless grade beam stiffness (embracing influence of soil stiffness, depth of soil cut as well as Young's modulus and area of grade beam) used by Boscardin and Cording (1989). Boscardin and Cording (1989) studied the effect of the normalized dimensionless grade beam stiffness on the angular distortion, diagonal strain and lateral strain on the grade beams. It should be noted that as Potts and Addenbrooke (1997) concern plane strain conditions, α^* is dimensionless while ρ^* has dimensions of m^{-1}. The value of E_s adopted in the Potts and Addenbrooke (1997) study is the secant stiffness at 0.01% axial strain in a drained triaxial compression test performed on a sample retrieved from a depth of half the tunnel depth (i.e., E_s = 103MPa and 163MPa for tunnel depths of 20m and 40m respectively), assuming E_s increases linearly with depth.

Tunnel excavation was modeled by incremental support removal of the solid elements within the tunnel boundary, which is represented by incremental reduction of the stresses that the soil within the tunnel applied to the tunnel boundary. For each increment, the movements of tunnel boundary were monitored and used to calculate the volume loss of soil moving into the tunnel. The percentage volume loss ΔV_L can then be obtained by dividing the calculated volume loss by the original tunnel cross-section ($\pi D^2/4$ per unit length of the tunnel). For the greenfield case, the stress reduction at which the accumulated volume loss $\Delta V_L = 1.5\%$ was chosen to represent the field conditions. All the analyses with surface structures in this study were terminated at the same stress reduction and the volume loss is recorded. As the volume loss varies slightly between analyses (1.41% to 1.51%), the results are all corrected by linear interpolation that correspond to the same $\Delta V_L = 1.5\%$ on the basis that the relationship between the volume loss and the maximum surface settlement can be assumed linear over the range (see Figure 2.10).

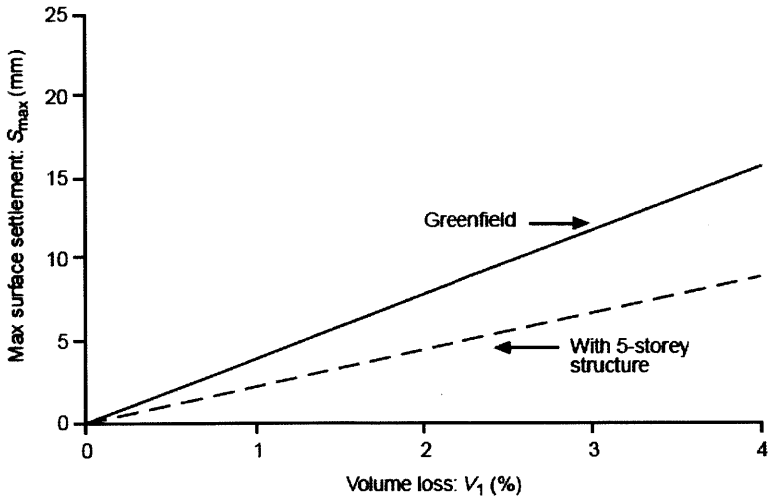

Figure 2.10: Variation of Maximum surface settlement with volume loss in Potts and Addenbrooke (1997)

Potts and Addenbrooke (1997) used two building damage parameters, namely deflection ratio and horizontal strain (Boscardin and Cording, 1989; Burland, 1995) to assess the effects of tunneling on existing buildings.

While the horizontal strain can be directly obtained from the computer output, the other building damage parameters, deformation ratios DR_{sag} and DR_{hog} for sagging and hogging respectively are defined in Figure 2.11. The deflection ratio was then calculated for both sagging and hogging by dividing the maximum deflection Δ by the length L connecting the points of inflection with the end of the structure or with each other. In Franzius (2003), it was clarified that the points of inflection were determined graphically in Potts and Addebrooke (1997).

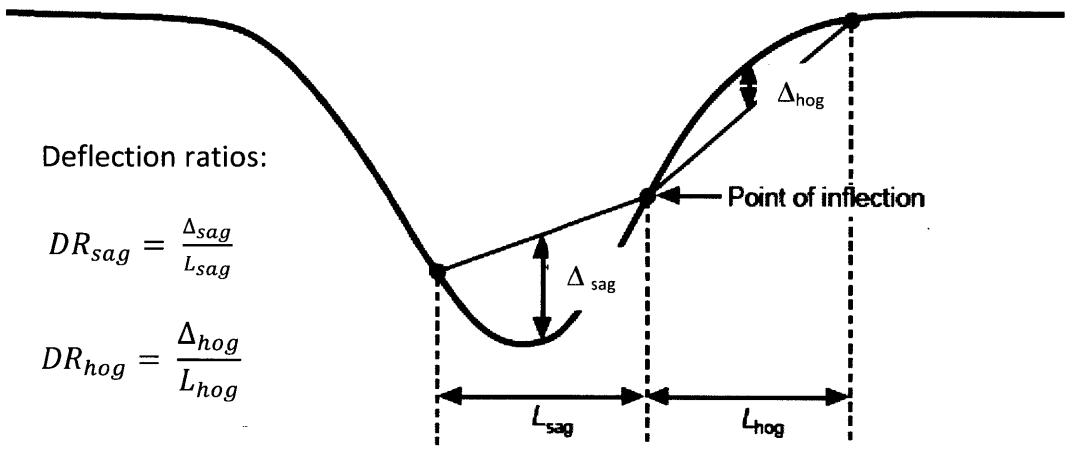

Figure 2.11: Definition of deflection ratios strain (Potts and Addenbrooke, 1996)

Potts and Addebrooke (1996) compared the results from the analyses with a beam (a structure) with those from the greenfield conditions, and define the following modification factors for deflection ratio:

$$M^{DR_{sag}} = \frac{DR_{sag}}{DR^{g}_{sag}} \tag{2.16}$$

$$M^{DR_{hog}} = \frac{DR_{hog}}{DR^{g}_{hog}} \tag{2.17}$$

where DR^{g}_{sag} and DR^{g}_{hog} are deflection ratios for that portion of the greenfield settlement trough which lies directly beneath the structure. Similarly, the modification factors for the maximum compressive and tensile horizontal strains are defined as:

$$M^{\varepsilon_{hc}} = \frac{\varepsilon_{hc}}{\varepsilon^{g}_{hc}} \tag{2.18}$$

$$M^{\varepsilon_{ht}} = \frac{\varepsilon_{ht}}{\varepsilon^{g}_{ht}} \tag{2.19}$$

where ε^{g}_{hc} and ε^{g}_{ht} are the greenfield values of horizontal compressive and tensile strains for that portion of settlement trough which lies directly beneath the structure.

Based on the results of their finite element analyses, design curves specifying the modification, by stiffness of structures, to greenfield settlement trough were established for the building damage parameters (Figure 2.12 and Figure 2.13).

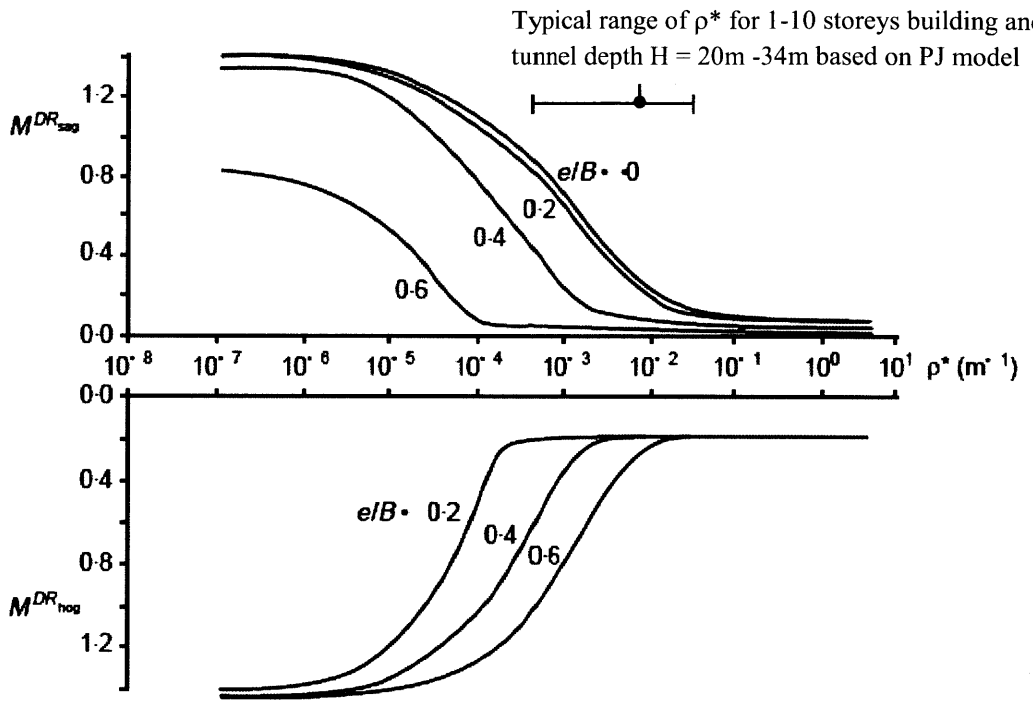

Figure 2.12: Design curves for modification factors to deflection ratio (Potts and Addenbrooke, 1997)

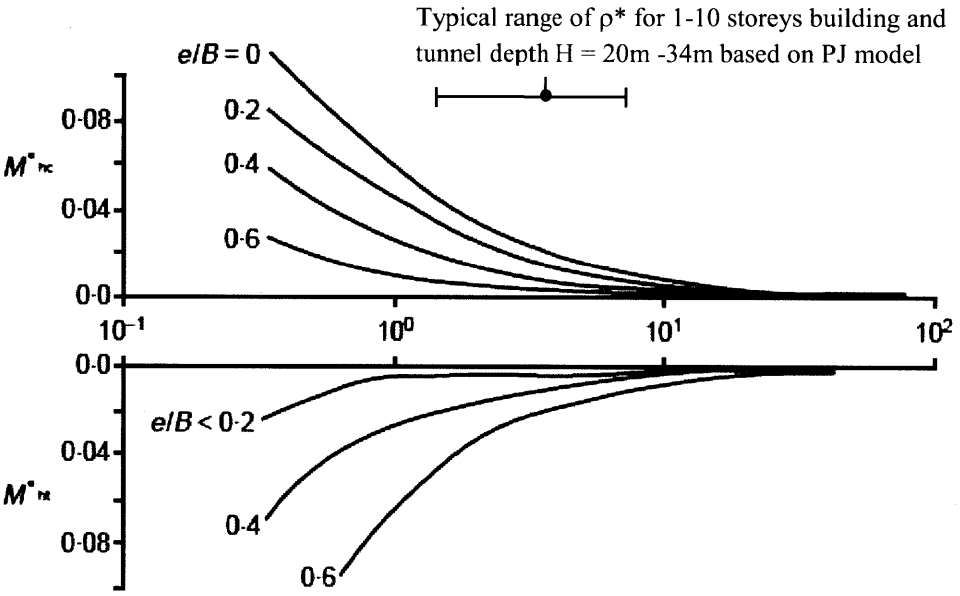

Figure 2.13 : Design curves for modification factors to horizontal strain (Potts and Addenbrooke, 1997)

When the greenfield values of deflection ratio and horizontal strain are known for a particular project, the greenfield values are multiplied by the respective modification factors to obtain those likely to be imposed on the structure (taking into account the effect of building stiffness on ground movement), by equations 2.17, 2.18, 2.19 and 2.20.

In addition, the combination of modified deflection ratio and horizontal strain can be used to determine the building damage category (Table 2.2 by Burland, 1995), see Figure 2.14.

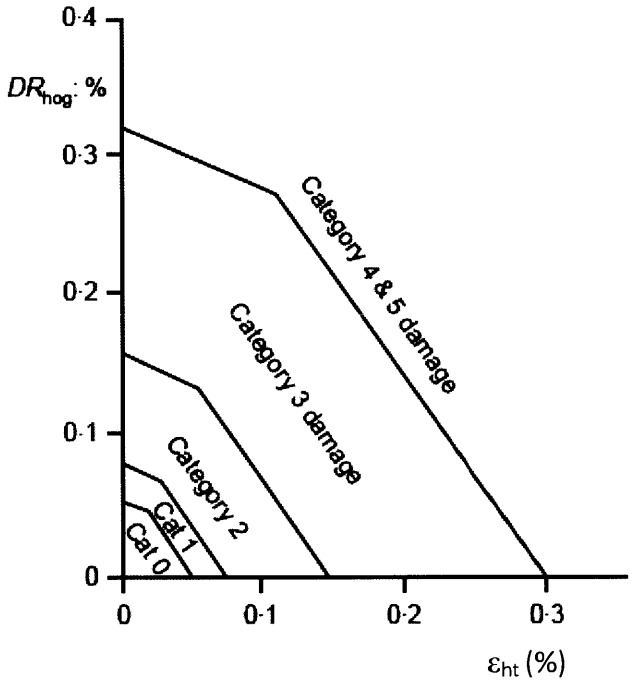

Figure 2.14: Relationship of damage category to deflection ratio and horizontal tensile strain for hogging (Burland 1995)

In practice, it is very uncommon to conduct numerical modeling directly taking into account the influence of buildings. Instead, deformations of buildings are assessed mostly by subjecting their foundations to the excavation-induced greenfield ground movements with no account of any influence of the existing structures' stiffness or the

buildings' weight. Therefore, the design curves introduced in Potts and Addenbrooke (1997) are very useful in giving initial estimates of the likely building damage, although it should be noted that the curves were developed based on specific ground conditions and structure characteristics.

2.7 Evaluation of the Relative Stiffness Approach

2.7.1. Building load

As stated above, the effects of building loads are not considered in Potts and Addenbrooke (1997). Franzius et al. (2004) carried out a series of numerical analyses to assess the effect of building weight on tunneling-induced ground and building movements. In addition to the two key steps of: 1) constructing a weightless beam with a stiffness to represent a certain number of building storeys and 2) applying incremental stress reduction to simulate tunnel excavation, they added an intermediate step, which is to apply a uniform stress above the weightless beam to simulate the effect of building weight. They modeled this stage as being fully drained (assuming consolidation would have largely completed before tunnel excavation). As they considered that in reality ageing of the soil may affect the soil stiffness properties during the consolidation time, the high initial soil stiffness to p' ratio was reset prior to tunnel excavation (achieved by resetting the strain before applying incremental stress reduction for tunnel excavation). By doing so, the initial soil stiffness before tunnel excavation depends only on the stress level p' (governed by insitu stress state and building loads). Franzius et al. (2004)

concluded that the addition of weight in the numerical analyses performed originally by Potts and Addenbrooke (1997) has only a small influence on the calculated deflection ratios for both hogging and sagging modes and horizontal strain. In order words, they considered that building stiffness (instead of building load) dominates the settlement reduction in the relevant greenfield case.

2.7.2. Relative stiffness expression

Franzius (2003) carried out a systematic investigation of the various parameters used in the original relative stiffness approach proposed by Potts and Addenbrooke (1997). Among the various parameters investigated, their findings related to the relative stiffness expression have a material influence on the application of the approach. Based on his analyses which cover a wider range of building features than the earlier study, Franzius (2003) showed that the original definition of relative bending stiffness ($\rho^* = EI/E_s(B/2)^4$ - equation 2.14) over-estimates the influence of B by incorporating it raised to a power of 4 in the denominator of ρ^*. His analyses also indicated that, in contrast, the tunnel depth is not sufficiently represented in the relative stiffness expression, as the tunnel depth is included in ρ^* only via the soil stiffness E_s which is taken from half tunnel depth. Franzius (2003) proposes refining ρ^* to:

$$\rho^*_{mod} = \frac{EI}{E_s H B^2 L} \qquad (2.20)$$

The above expression modified the original one by incorporating H (tunnel depth to springline) and reducing the influence of B. The length of building in the longitudinal direction (L) is introduced so that the expression is dimensionless whether it is used in 2D or 3D analysis[1]. Franzius (2003) justifies the modified expression based on the results of their numerical analysis which show that the modified expression produced less scatter for $M^{DR_{sag}}$ though the scatter increases slightly for $M^{DR_{hog}}$ which is still within the upper bound of the design curves proposed in Potts and Addenbrooke (1997). For axial strain it was found that the original definition of relative axial stiffness ($\alpha^* = EA/E_sH$ – equation 2.15) gives a good correlation with $M^{\varepsilon ht}$ for all cases analyzed. Nevertheless, similar to ρ^*_{mod}, the expression is modified to include L to make it dimensionless whether it is used in 2D or 3D analysis:

$$\alpha^*_{mod} = \frac{EA}{E_s BL} \tag{2.21}$$

Franzius (2003) justified the use of the building width B rather than the half width of building B/2 (as adopted by Potts and Addenbrooke (1997)) to be consistent with the expression of degree of eccentricity as e/B. It was shown that the use of the building width B rather than the half width of building B/2 has no implication on the relative position of the results to each other when plotted against a log-scale of relative stiffness. Franzius (2003) proposes a new set of design curves for modification factors adopting the modified relative bending and axial stiffness (Figure 2.15 and Figure 2.16).

[1] In 2D the effect of L cancels out from the numerator (I) and denominator

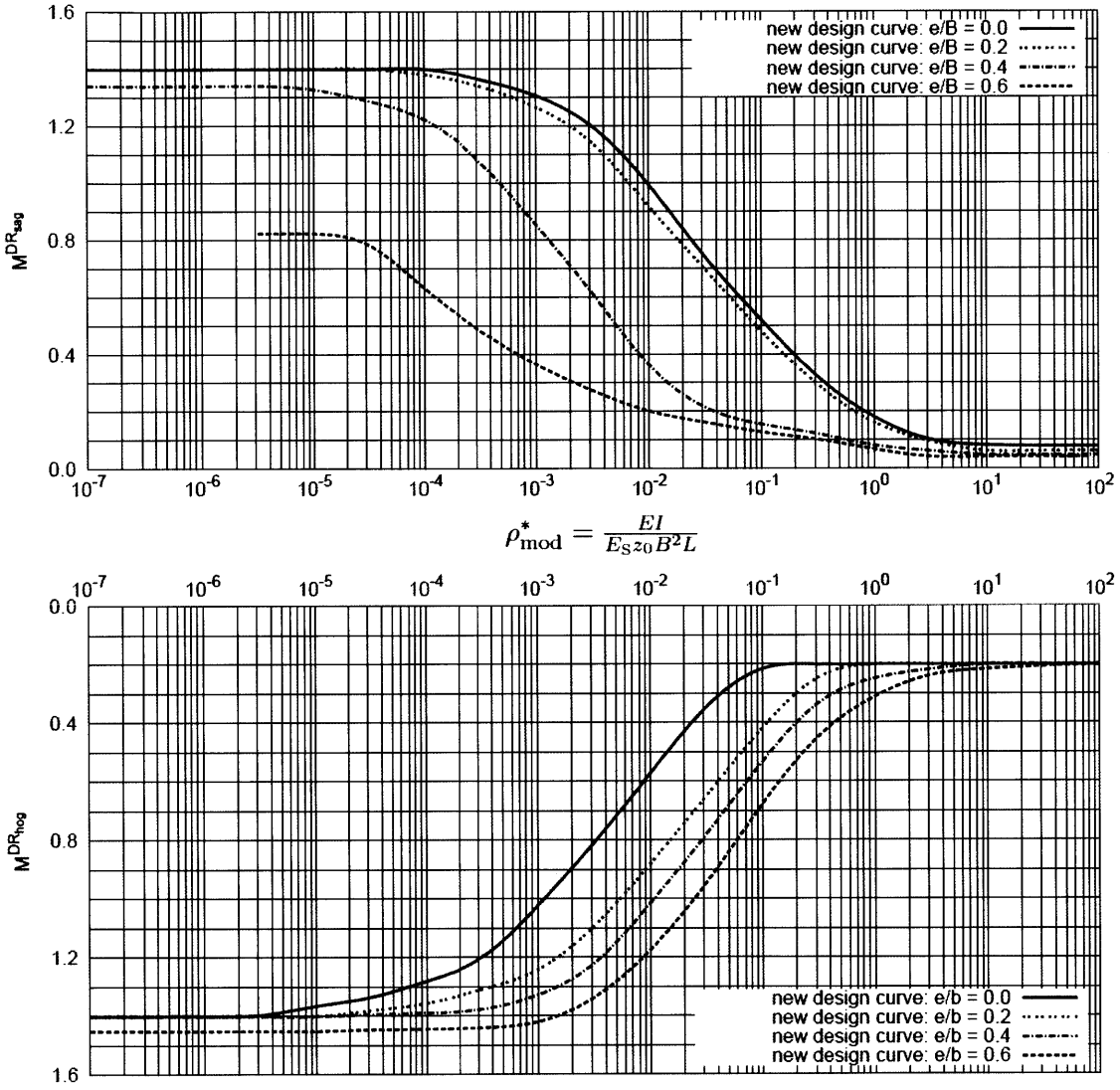

Figure 2.15: Proposed design curves for M^{DR} adopting the modified relative bending stiffness ρ^*_{mod}.

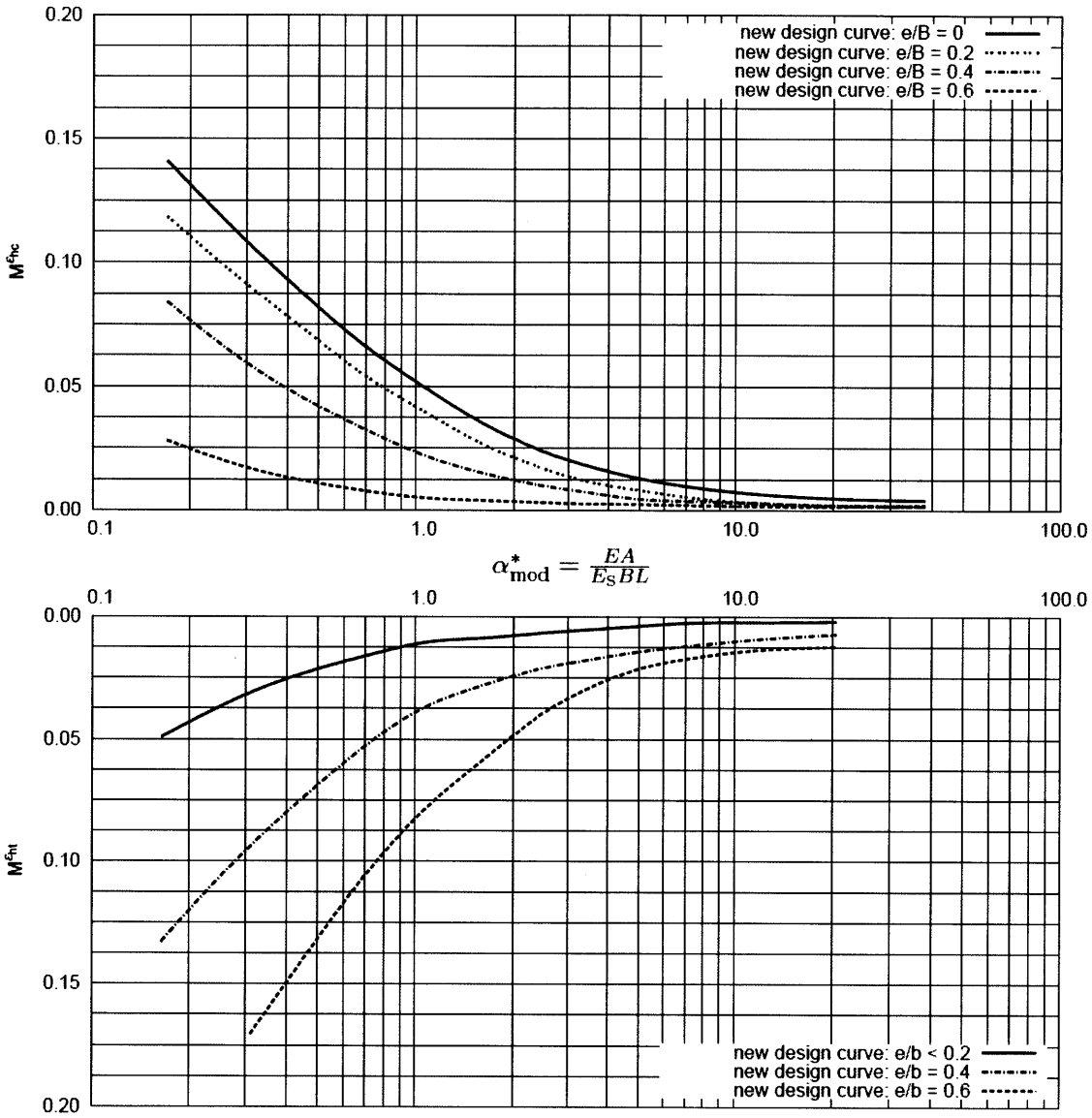

Figure 2.16: Proposed design curves for M^{DR} adopting the modified relative axial stiffness α^*_{mod}.

2.7.3. Building stiffness

Dimmock and Mair (2008) review the method of deriving building stiffness (numerator of the relative stiffness) and hence the relative stiffness. In their study, the progressive response of two- to three-storey masonry buildings (at Moodkee Street and Keetons Estate) to bored tunneling for the Jubilee Line Extension project in London was investigated. Based on the modification factors back-analyzed from the observed ground movement, they inferred the back-analyzed relative bending stiffness in sagging and hogging using the design charts in Potts and Addenbrooke, 1997 (Figure 2.17).

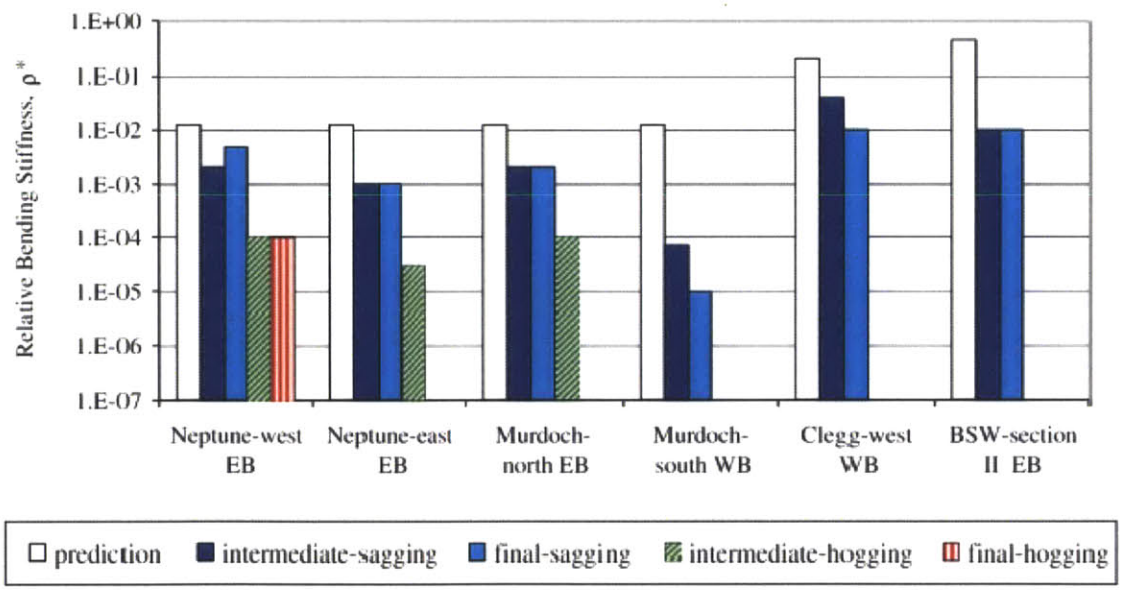

Figure 2.17: Approximate relative bending stiffness estimated from modification factor for the masonry facades at Moodkee Street and Keetons Estate (Dimmock and Mair, 2008)

By comparing the back-analyzed relative bending stiffness with that suggested in Potts and Addenbrooke (1997), they suggested the following modifications for estimating

relative bending stiffness of low-rise masonry structures for future use with design charts in Potts and Addenbrooke (1997):

- Only the foundation, instead of the entire building, can be considered in the estimation of relative bending stiffness for hogging. They explained that the observed behavior was probably due to inability of the masonry in the upper part of the wall to withstand significant tensile stresses.

- The second recommendation is to reduce the estimated relative bending stiffness in sagging by one order of magnitude to account for the presence of door and window openings.

3 Method of Analysis

3.1. Finite element analysis

This thesis provides a comparative study to the earlier work of Potts and Addenbrooke (1997) on the influence of building properties on tunneling-induced ground movements by numerical analysis. As such, the current numerical analyses largely follow the prior work in terms of problem geometry, soil profile (London clay) and method of simulating tunnel excavation. In contrast to the earlier study, this research uses a commercial finite element code *PLAXIS*^{TM} together with hardening soil family of constitutive models (Hardening Soil HS, Schanz, Vermeer and Bonnier 1999 and Hardening Soil Small HSS, Benz 2006). As such, some features of the numerical analyses have to be modified to suit this study. A dedicated calibration process is required to identify hardening soil model (HS and HSS) parameters that represent London clay and approximate the stiffness behavior simulated by Potts and Addenbrooke (1997) (using an earlier non-linear elastic model presented by Jardine et al., 1986). This chapter describes the finite element analyses and gives a full account of the soil model calibration process.

Geometry

The reference geometry comprises a circular diameter, d = 4.146m and fixed depth from the soil surface to the tunnel springline, H = 20m. Figure 3.1 shows a typical half-model mesh used in the 2D, plain strain analysis, comprising 15-node triangular elements with

fourth order interpolation for displacement. The mesh has been refined to ensure the model gives numerical results with adequate degree of accuracy for the problem. The structure is represented by a surface elastic beam centered above the crown of the tunnel (i.e., zero eccentricity). The soil-beam (structure) interface is assumed to be perfectly rough (i.e., no slip).

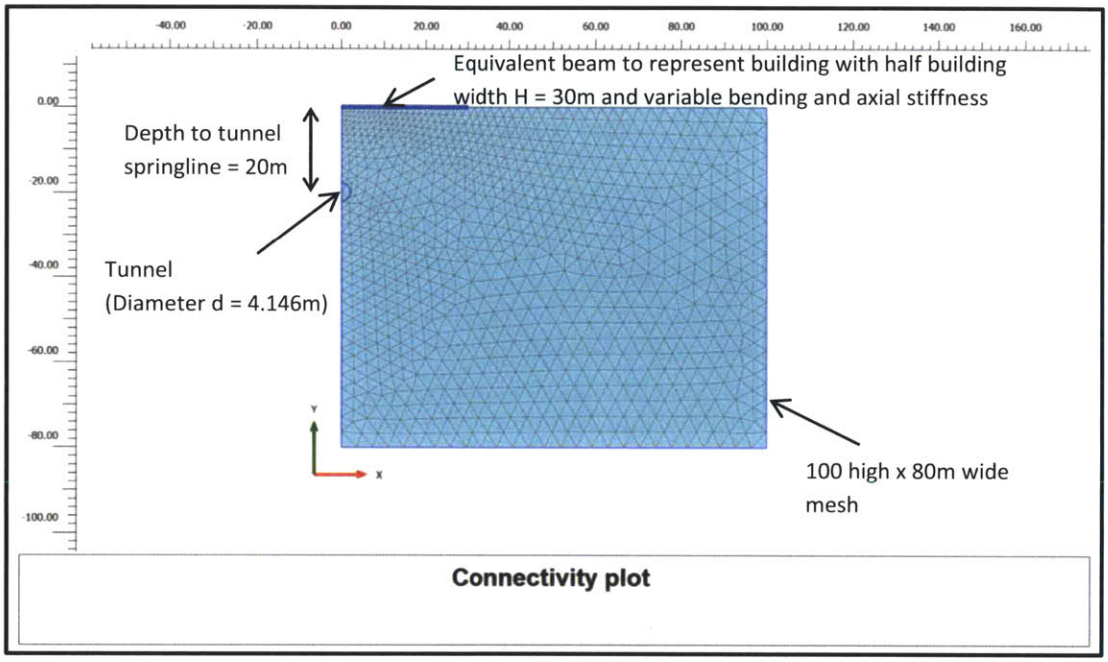

Figure 3.1: Typical half model for analyses

This study considered buildings to be a concrete frame structure consisting of 1 to 10 storeys. For a building with m storeys, the equivalent properties of the elastic beam were calculated assuming that the building consists of m+1 slabs at a vertical spacing of 3.4m. The thickness of each slab is assumed to $t_{stab} = 0.15$m. An individual slab with thickness $t_{stab} = 0.15$m is assumed to have the following properties:

Elastic modulus $E_c = 23 \times 10^6$ kN/m^2 (3.1)

Area $A_{slab} = 0.15$ m^2/m (3.2)

Second moment of area $I_{slab} = 2.8125 \times 10^{-4}\ m^4/m$ (3.3)

Axial stiffness $(E_cA)_{slab} = 3{,}450{,}000\ kN/m$ (3.4)

Bending stiffness $(E_cI)_{slab} = 6468.75\ kNm^2/m$ (3.5)

(bending about mid-plane)

The axial and bending stiffness for an equivalent beam, comprising m storeys (m+1 slabs) are then calculated using the parallel axis theorem (Timoshenko, 1995), assuming the neutral axis to be at the mid-height of the building:

$$(E_cA)_{structure} = (m+1)\ (E_cA)_{slab} \tag{3.6}$$

$$(E_cI)_{structure} = E_c \sum_1^{(n+1)} (I_{slab} + A_{slab}H^2) \tag{3.7}$$

All properties in equations 3.6 and 3.7 assume plane strain conditions with unit width. In order to get a consistent set of parameters (based on equivalent thickness and young's modulus of beam, t_{fe} and E_{fe}), the above stiffness expressions can be converted to:

$$(E_cA)_{structure} = \frac{E_{fe}t_{fe}}{12} \tag{3.8}$$

$$(E_cI)_{structure} = \frac{E_{fe}t_{fe}^3}{12} \tag{3.9}$$

By rearranging equations 3.8 and 3.9 the expression of equivalent thickness t_{fe} can be obtained by:

$$t_{fe} = \sqrt{\frac{12(E_c I)_{structure}}{(E_c A)_{structure}}} \tag{3.10}$$

The input parameters for beam in finite element code *PLAXIS*™ are $(E_c A)_{structure}$ and $(E_c I)_{structure}$. In addition, *PLAXIS*™ computes the equivalent thickness t_{fe} which is shown in the input window for checking.

In this study, 1-, 3-, 5-, 8- and 10-storey buildings are considered in evaluating the effect of building stiffness and building load on tunneling-induced ground settlement. The corresponding stiffness parameters are given in Table 3.1:

Building	Bending stiffness $(EI)_{structure}$ [kNm^2/m]	Axial stiffness $(EA)_{structure}$ [kN/m]	T_{fe} [m]	Building weight [kPa]
Slab	6.47 x 10^3	3.45 x 10^6	0.15	N/A
1	2.00 x 10^7	6.90 x 10^6	5.89	50
3	1.99 x 10^8	1.38 x 10^7	13.17	50
5	6.98 x 10^8	2.07 x 10^7	20.12	50
8	2.39 x 10^9	3.11 x 10^7	30.41	50
10	4.39 x 10^9	3.80 x 10^7	37.25	50

Table 3.1: Stiffness of building

Soil properties

This study focuses on the ground conditions typically found in London. The hardening soil family of constitutive models (HS, Schanz, Vermeer and Bonnier 1999 and HSS, Benz 2006) are chosen among various constitutive models available in *PLAXIS*™. These

models are advanced elastic-plastic models for simulating the behavior of soil. In contrast to the elastic-perfectly plastic soil model (Mohr Coulomb model), the yield surfaces of the HS model are not fixed in principal stress space, but harden due to plastic straining. In addition, the HSS model uses additional parameters to describe small-strain non-linear stiffness properties as functions of stress and strain. This is a key model feature that is particularly relevant to this study as the average shear strain of the analyses is typically in the range of 0.1% to 0.01%.

The analyses focus on the short-term response of the ground and hence, the clay is assumed to be undrained. The shear strength is described by conventional effective stress strength parameters, apparent cohesion (c') = 10kPa, internal friction (ϕ') = 25° with dilatancy angle (ψ) = 12.5°. The HS family of constitutive models use separate input parameters to simulate the soil stiffness associated with plastic strain due to primary deviatoric loading and primary compression, as well as elastic unloading and re-loading. The HS family of constitutive models are calibrated against the PJ model of Jardine et al. (1986) that was used in Potts and Addenbrooke (1997) in order to identify input stiffness parameters that represent a similar stress-strain characteristics to the previous study. This calibration process aims to enable a direct comparison on results obtained by numerical analyses using these two different soil models (PJ model vs hardening soil family of constitutive models). Further details of the calibration process are provided in sub-paragraph 3.2 below.

Initial Stress

The analyses assume that the coefficient of at-rest earth pressure K_o = 0.577 (i.e., K_o = 1-sinϕ), which is similar to the reduced K_o = 0.5 used by Potts and Addenbrooke (1997). Despite the use of reduced K_o in the numerical simulation in this study, it should be noted that the actual K_o value of over-consolidated London clay is expected in the range K_o = 1 to 1.5. The reasoning to use lower values of K_o is mentioned in Potts and Zdravkovic (2001) as a method to simulate the influence of the 3D stress field caused by tunneling. Nevertheless, Franzius (2003) carried out a series of numerical analysis and concluded that the calculating modification factors of deflection ratio and horizontal strain (obtained by normalizing with the greenfield trough), only differ slightly for these different initial conditions (zone of reduced K_o = 0.5 vs global K_o = 1.5). This may be explained by the fact that the reported modification factors are normalized by the greenfield predictions and therefore the influence of initial stress conditions is cancelled out. As such, the assumption of reduced K_o is further justified for the purpose of this study, in which building deformations are mainly quantified by building damage parameters (deflection ratio and horizontal strain), and the respective modification factors for deflection ratio and horizontal strain were proved by Franzius (2003) to be relatively insensitive to the change of initial stress conditions.

Modeling of tunnel excavation

The tunnel excavation was modeled by the β method (details given in Chapter 2). To apply this in *PLAXIS*^{TM}, the staged construction option is used to emulate a reduced ultimate level of ΣM-stage. For example, for a value of 0.6 ΣM-stage, β is equal to 1 -

ΣM-stage (i.e 0.4), and the physical meaning is that only 40% of the initial stress is applied to the tunnel lining. In the tunnel excavation simulation, β is decreased from 1 in incremental reduction towards 0. For each incremental reduction of β value, the movements were monitored and used to calculate the volume loss by integrating the surface settlement trough with respect to the original ground level (due to undrained conditions, the surface volume loss corresponds to the volume loss at the tunnel cavity). It is assumed to be the same as the ground movements into the tunnel as the soil is assumed to be undrained. The volume is then divided by the original cross-sectional area of the tunnel in order to obtain the percentage volume loss (ΔV_L). The termination criterion of all the analyses in this study is set at a fixed β value based on the analyses of the greenfield conditions with a cumulative volume loss, ΔV_L = 1.5%, to represent the field conditions after tunneling. In contrast to Potts and Addenbrooke (1997) where the results were adjusted by linear interpolation to the specific volume loss (1.5%), no correction is needed in the current analysis. This issue is significant as subsequent results show that the modification factors (for both deflection ratio and horizontal strain) are not linearly correlated to the volume loss. Nevertheless, the approximation has negligible effect in terms of making comparison with the results in Potts and Addenbrooke (1997), where there are small variations in volume loss (1.41% to 1.51%) and adjustments are small.

Building stiffness parameters

Potts and Addenbrooke (1997) proposed definitions for relative bending and axial stiffness parameters, $\rho^* = EI/E_s(B/2)^4$ and $\alpha^*=EA/E_s(B/2)$, to describe their results. This

approach introduces a reference value of soil stiffness E_s (defined as the secant stiffness for an average point in the overlying soil at depth = H/2 and at a shear strain $\gamma = 0.01\%$). The purpose of this parameter is to normalize the results of the numerical analysis. Subsequent studies by Franzius (2003) have shown some limitations associated with the definition of E_s. Given that the current study focuses on a unique settlement profile and tunnel, we present the results in terms of the properties of the structure. Further numerical simulations with different tunnel geometry and stiffness properties are needed in order to evaluate the best choice of normalizing parameters.

Building deformation criteria

The building damage parameters (a quantitative measure of the effect of tunneling on building) used in this study are the deflection ratio DR (refer to Figure 2.10) and horizontal strain ε_h. To calculate DR, it is necessary to determine the point of inflection which separates the zones of the sagging and hogging moments. The point of inflection is found by calculating the rate of change of the slope of surface settlement trough ($du_y^2/dx^2 = 0$) numerically in a spreadsheet and locating the change of sign. The deflection ratio is calculated for sagging and hogging by dividing the maximum defection by the length L connecting the points of inflection or connecting one of the points of inflection with the end of structure. The horizontal strain ε_h is given as the maximum compressive or tensile horizontal strain at the neutral axis (by referring the strain to the neutral axis, any effects of bending are eliminated). This is obtained by dividing the axial force by the beam sectional area, where axial force is directly obtained from the computer output.

3.2 Calibration of soil model

The HS family of constitutive models and the PJ model (PJ, Jardine et al. 1986) used by Potts & Addenbrooke (1997) are based on different sets of soil parameters. In order to calibrate a HS to be consistent with the PJ model, the stress-strain behaviors of the two models are compared in three different aspects, which are: 1) the deviatoric stress-strain behavior in drained triaxial shearing ($q = (\sigma_1 - \sigma_3)$ vs ε_a); 2) the secant modulus profile at selected shear strain levels (E_{sec} vs z); and 3) the surface settlement trough profile resulting from tunnel excavation. The stress-strain behavior of the PJ model is predicted from its original trigonometric expressions (equations 2.12 & 2.13) by spreadsheet calculations, where the stress-strain behavior of the hardening soil model in *PLAXIS*^{TM} is obtained by numerical integration of the incremental stress-strain relations.

Triaxial compression using PJ model

The non-linear elastic PJ model describes the secant soil moduli as non-linear functions of the strain level using trigonometric expressions (equations 2.12 & 2.13). In order to predict the deviatoric stress-vertical strain ($(\sigma_1 - \sigma_3)$ vs ε_a) relationship, the tangent elastic shear and bulk modulus are obtained by differentiation as follows:

$$\frac{G}{p'} = A + B\cos(\beta X^{\gamma}) - \frac{B\beta\gamma X^{\gamma-1}}{2.303}\sin(\beta X^{\gamma}) \quad \text{with } X = \log_{10}\left(\frac{E_d}{\sqrt{3}C}\right) \tag{3.11}$$

$$\frac{K}{p'} = R + S\cos(\beta Y^{\mu}) - \frac{S\delta\mu Y^{\mu-1}}{2.303}\sin(\delta Y^{\mu}) \quad \text{with } Y = \log_{10}\left(\frac{|\varepsilon_{vol}|}{T}\right) \tag{3.12}$$

where p' is the mean effective stress, E_d is the deviatoric strain invariant, ε_{vol} is the volumetric strain, and A, B, C, R, S, T, δ, β, γ and μ are constants. Values of these constants for London clay are retrieved from Franzius et al. (2005) and tabulated in Table 3.2 below:

Strata	A	B	C (%)	β	γ
London	373.3	338.7	1×10^{-4}	1.335	0.617
Clay	R	S	T (%)	δ	λ
	549	506	1×10^{-3}	2.069	0.420

Table 3.2: Input parameters for the Potts soil model (tangent stiffness) for London Clay

For elastic stress-strain relations in the triaxial space, the following equation holds:

$$\begin{Bmatrix} \Delta p' \\ \Delta q' \end{Bmatrix} = \begin{bmatrix} K' & 0 \\ 0 & 3G' \end{bmatrix} \begin{Bmatrix} \Delta \varepsilon_{vol} \\ \Delta \varepsilon_s \end{Bmatrix} \tag{3.13}$$

where p' is the mean effective stress, q' is the deviatoric stress, K' and G' are respectively the tangent bulk and shear moduli and ε_{vol} and ε_s are respectively the volumetric and shear strains.

From equation 3.13, $$\Delta q' = 3G\Delta\varepsilon_s \tag{3.14}$$

Since $\Delta\varepsilon_s = \frac{2}{3}(\Delta\varepsilon_v - \Delta\varepsilon_h)$, where $\Delta\varepsilon_v$ and $\Delta\varepsilon_h$ are respectively the vertical and horizontal strain components. Equation 3.14 can be written as:

$$\Delta q' = 2G\,(\Delta\varepsilon_v - \Delta\varepsilon_h) \tag{3.15}$$

On the other hand, by definition volumetric strain $\Delta\varepsilon_{vol}$ can be defined in terms of ε_v and ε_h as:

$$\Delta\varepsilon_{vol} = (\Delta\varepsilon_v + 2\Delta\varepsilon_h)/3 \tag{3.16}$$

Assuming undrained conditions in triaxial shear test (i.e., $\Delta\varepsilon_{vol} = 0$), equation 3.16 can be written as:

$$\Delta\varepsilon_h = -0.5\Delta\varepsilon_v \tag{3.17}$$

Using the correlation in equation 3.17, equation 3.15 can be rewritten to describe the change in deviatoric stress $\Delta q'$ in relation to the change in vertical strain $\Delta\varepsilon_v$:

$$\Delta q' = 3G\Delta\varepsilon_v \tag{3.18}$$

Hence the undrained shear stress-axial strain behavior is controlled by 3G, which can be obtained from equation 3.11 above. As the value of G in the PJ model is dependent on the current state of mean effective stress (p') and the deviatoric strain (E_d) (see equation 3.11), the current state of p' and E_d have to be obtained before the current state of G can be known. While the deviatoric strain E_d can be simply obtained from the vertical strain (which is an input in the spreadsheet calculations), $\Delta p'$ has to be computed by rewriting equation 3.13 as:

$$\Delta p' = K\Delta\varepsilon_{vol} \tag{3.19}$$

As the soil is assumed to be undrained in this computation, $\Delta\varepsilon_{vol} = 0$. As such, $\Delta p'$ can also be taken as zero and the value of mean effective stress p' can be treated as a constant (i.e., applied confining stress). Deviatoric stress q can also be computed accordingly using equation 3.18 for incremental step increase of vertical strain ε_v. Based on the above procedures, the stress-strain behavior for the PJ model for London clay under confining stresses of 400kPa and 680kPa (relevant stress levels for 20m and 34m deep

tunnel respectively, which are typical depths for the London underground tunnel) are computed and plotted in Figure 3.2.

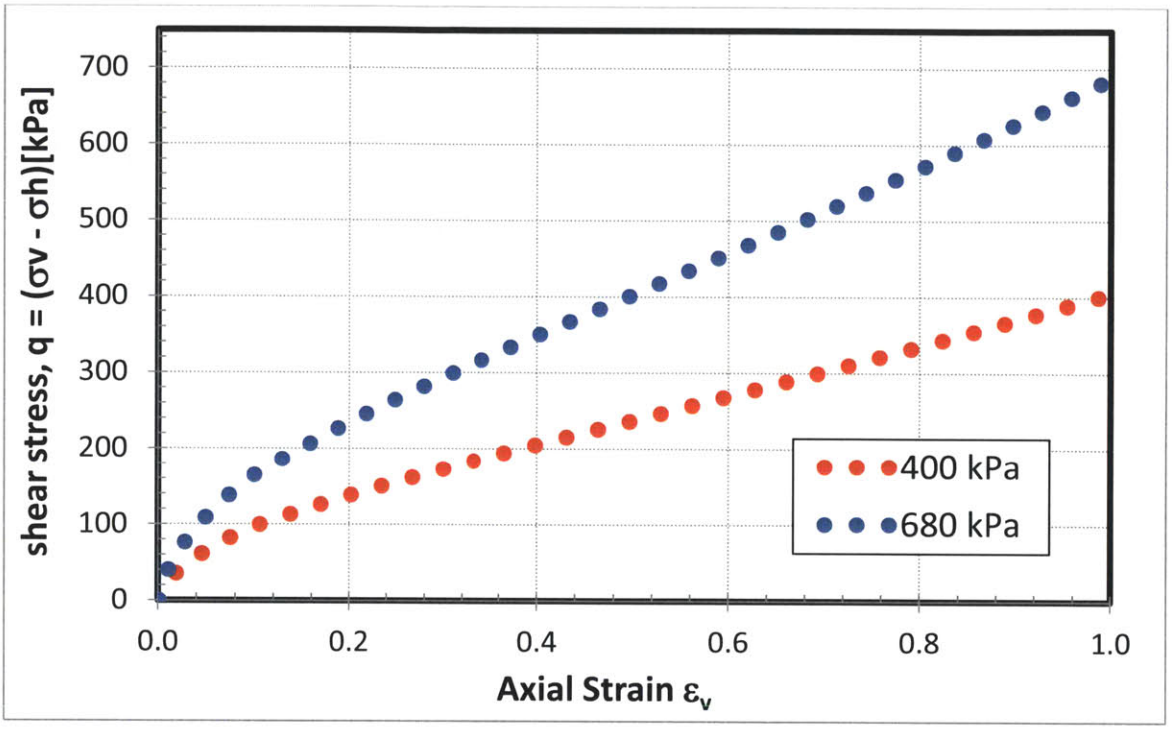

Figure 3.2: Plot of deviatoric stress q vs vertical strain εv for confining stresses of 400kPa and 680kPa

Triaxial compression by HS and HSS models

The stress-strain behavior of the HS and HSS models are obtained by numerical simulations in *PLAXIS*™. The basic stiffness characteristics of the HS model are controlled by the following parameters:

Controlling behaviour	Input Parameters	Note
Plastic straining due to primary deviatoric loading	E_{50}^{ref}	Secant stiffness in standard drained triaxial test
Plastic straining due to primary compression	E_{oed}^{ref}	Tangent stiffness for primary oedometer loading
Elastic unloading / loading	E_{ur}^{ref}	Unloading / reloading stiffness

Table 3.3: Key input stiffness parameters for HS model

The current analyses follow default assumptions in PLAXIS™ in that $E_{ur}^{ref} = E_{50}^{ref}$ and $E_{oed}^{ref} = E_{50}^{ref}$. The HSS model adds two additional parameters to describe non-linear stiffness at small-strain levels:

- The initial or small-strain shear modulus G_0;
- The shear strain level, $\gamma_{0.7}$, at which the secant shear modulus $G_s = 0.7\ G_o$.

These parameters are selected as G_o = 324MPa and $\gamma_{0.7}$ = 0.009% based on site investigation results from the Crossrail project geotechnical sectional interpretative report for Royal Oak to Liverpool Street done by the Geotechnical Consulting Group. As the values of E_{oed}^{ref} and E_{ur}^{ref} are dependent on E_{50}^{ref}, and the values of G_0 and $\gamma_{0.7}$ are fixed, the only parameter varied in this calibration exercise (for HS and HSS) is E_{50}^{ref}. Figure 3.3 and Figure 3.4 show simulations for a set of drained triaxial tests for selected values of E_{50}^{ref} at p_o' = 400kPa and K_o = 1. Similar results are shown in Figure 3.5 and Figure 3.6 at p_o' = 680kPa.

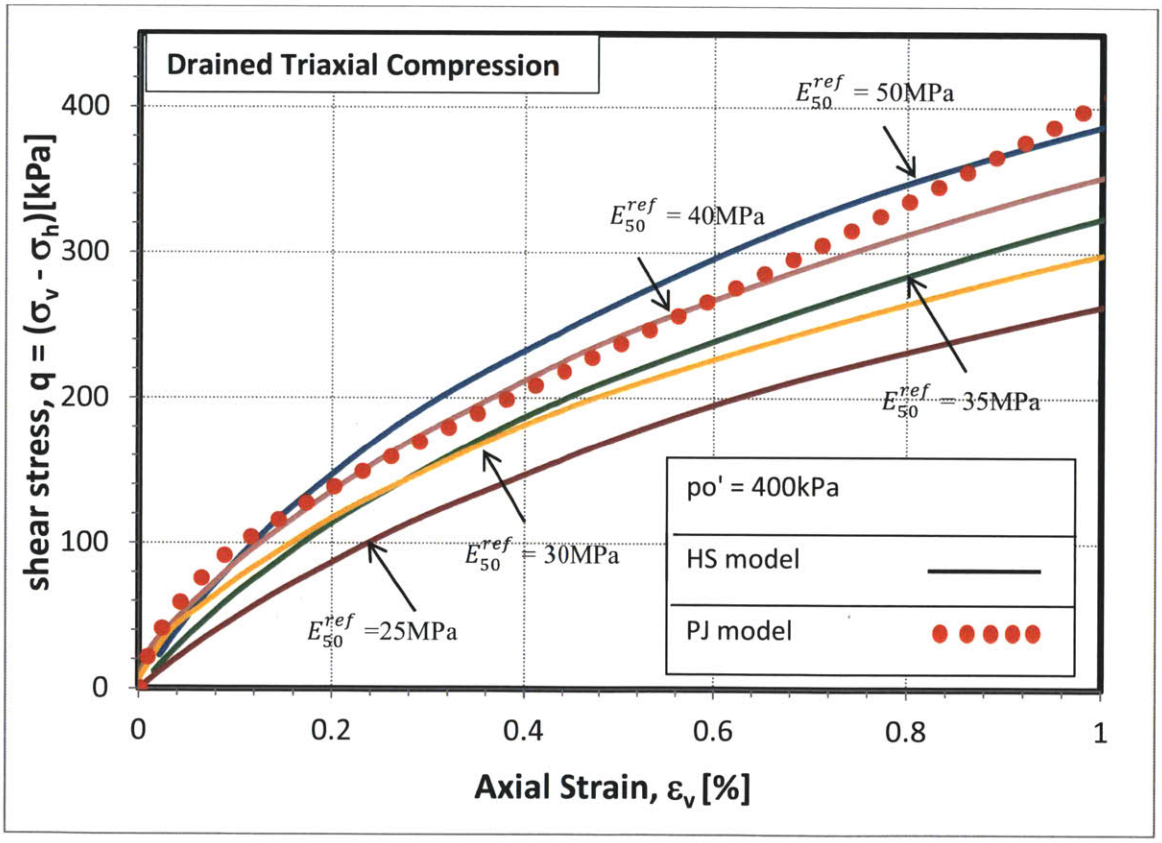

Figure 3.3: Shear stress-vertical strain ε_v for HS model (p_o' = 400kPa)

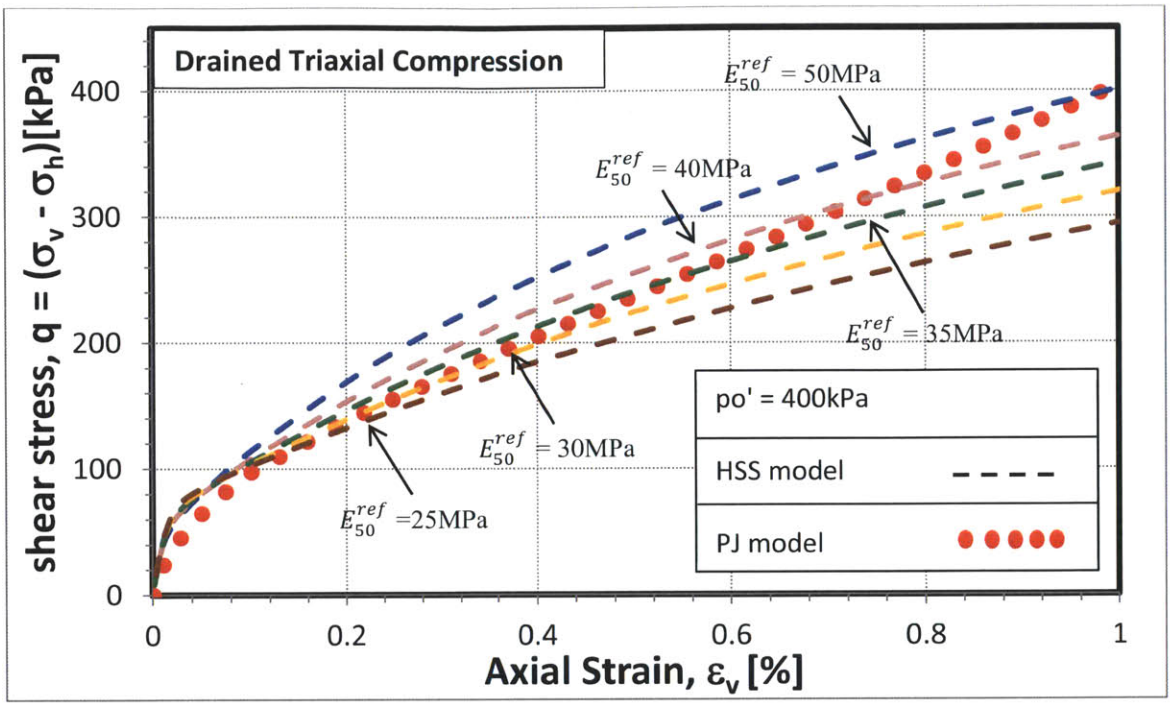

Figure 3.4: Shear stress - vertical strain ε_v for HSS model (p_o' = 400kPa)

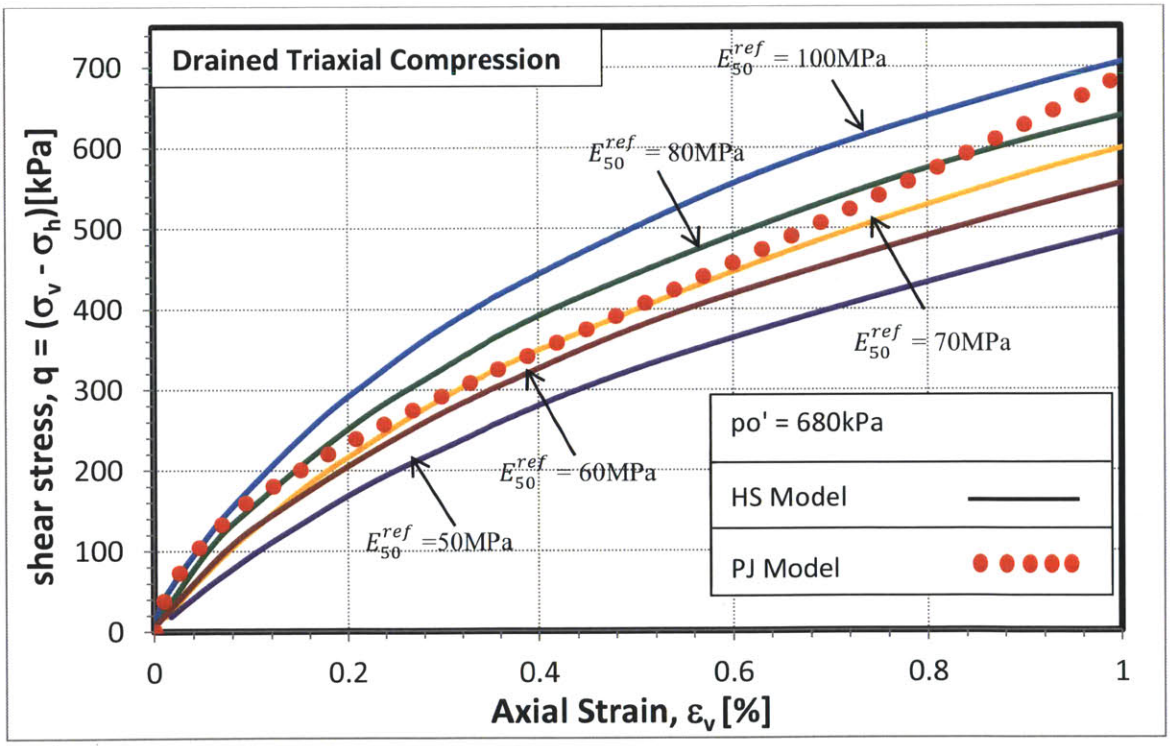

Figure 3.5: Shear stress - vertical strain ε_v for HS model (p_o' = 680kPa)

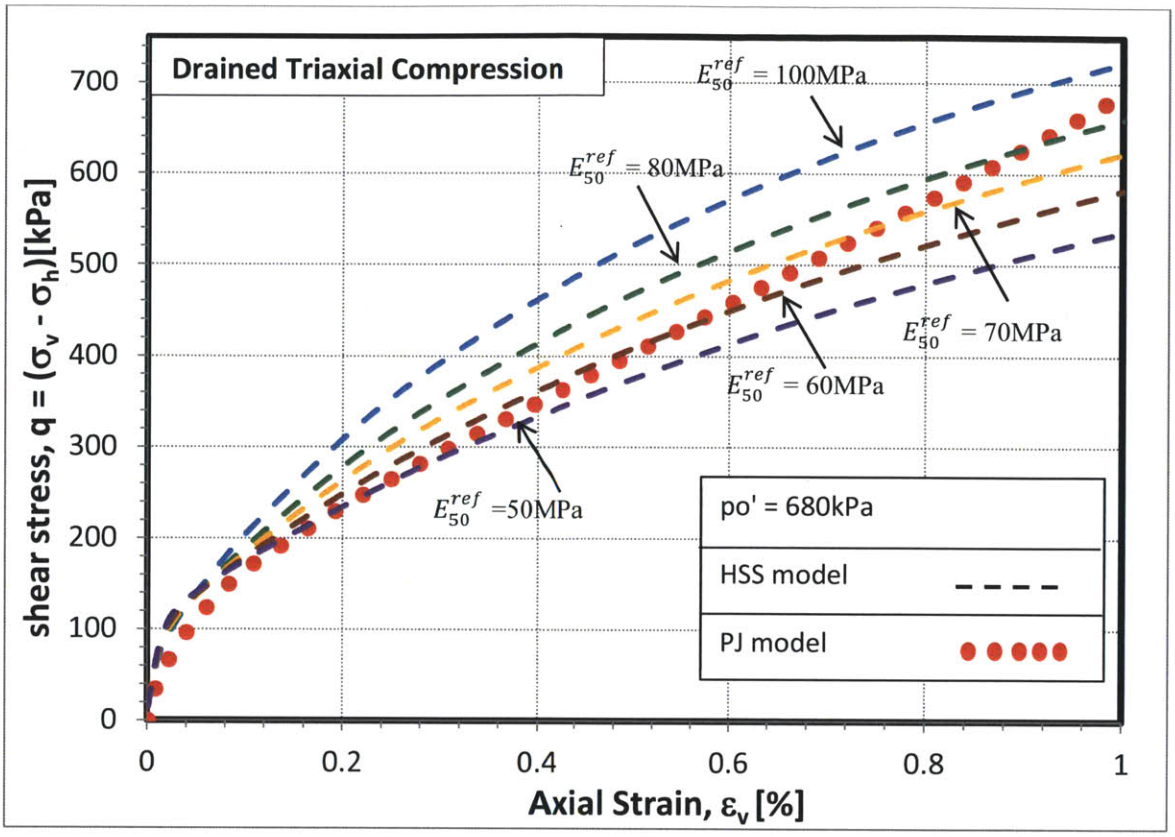

Figure 3.6: Shear stress - vertical strain ε_v for HSS model (p_o' = 680kPa)

By comparing the results in Figure 3.3 and Figure 3.4 (p_o' = 400kPa), the best fits for the HS and HSS models fit with the PJ model results corresponding to 40MPa and 30MPa respectively. To enable a comparison of the best-fit stiffness of the two soil models (HS and HSS with PJ model), the chosen stiffness is re-plotted in Figure 3.7:

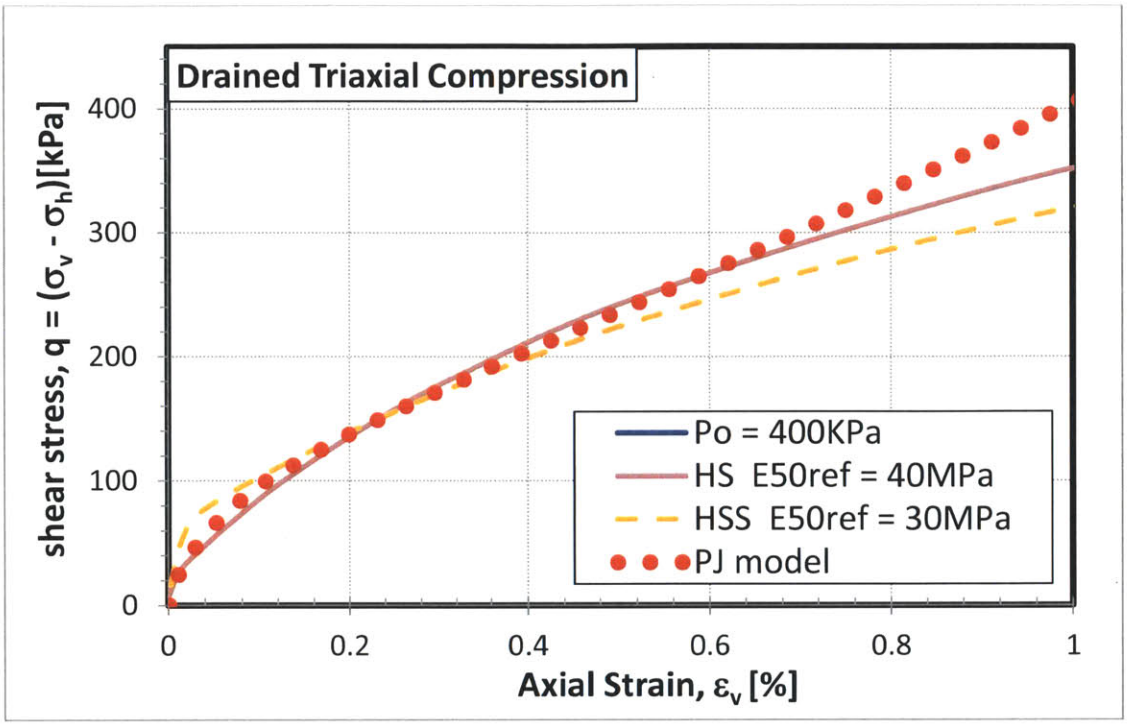

Figure 3.7: Comparison of best-fit input stiffness for HS and HSS models (p_o' = 400kPa)

It is evident that the HS model provides the better fit to the PJ model. In particular at small strain the stiffness estimated by the HSS model is much higher than that predicted from the PJ model. The HS and PJ models diverge for $\varepsilon_v > 0.6\%$.

On the other hand, the comparing of results for p_o' = 680kPa (Figure 3.5 and Figure 3.6) gives the best fits for HS and HSS models with E_{ref}^{50} = 80MPa and 50MPa respectively, as shown in Figure 3.8:

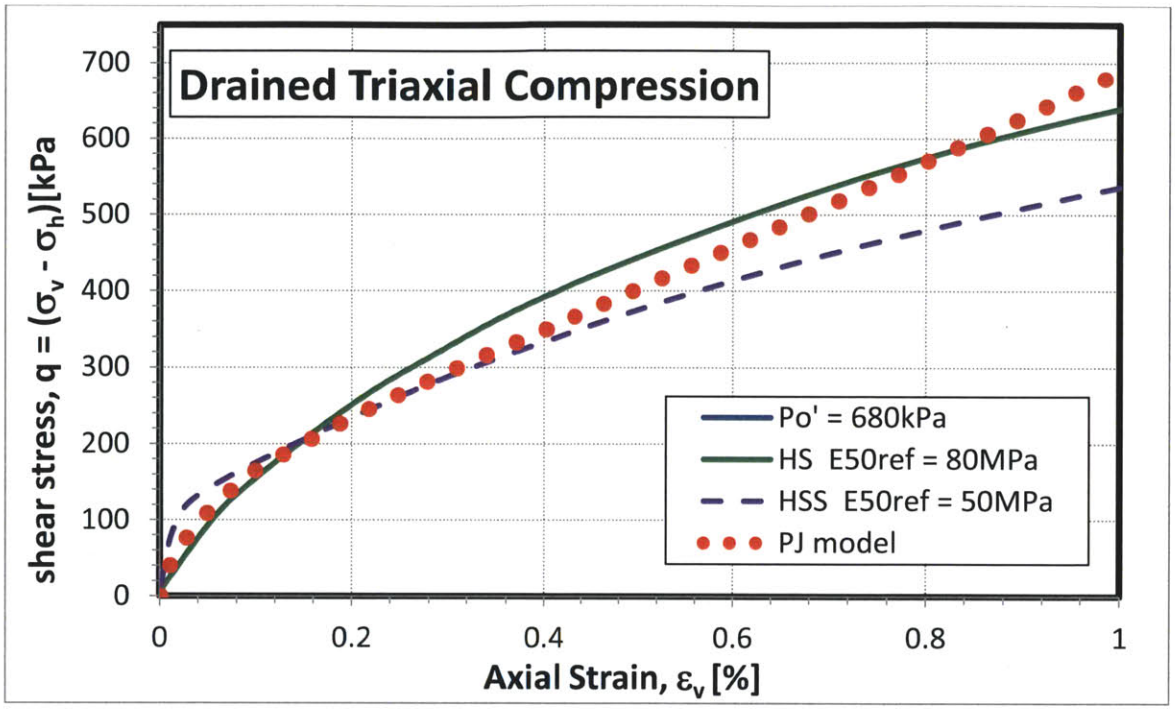

Figure 3.8: Comparison of best-fit input stiffness for HS and HSS models (p_o' = 680kPa)

The HS model again appears to fit better with the PJ model and in particular at small strain. The HS and PJ models diverge for $\varepsilon_v > 0.4\%$.

The preceding results show the range of stiffness parameters for relevant depths of tunnels in London, which range from E_{ref}^{50} = 40 – 80 MPa (for the HS model) and E_{ref}^{50} = 30 – 50 MPa (for the HSS model). Subsequent calculations assume 60MPa for HS model and 40MPa for HSS model.

Secant modulus profile at selected shear strain levels (E_{sec} vs z)

Further drained triaxial simulations have been conducted using the average E_{ref}^{50} at p_o' values corresponding to depths, z = 5m, 20m and 34m below ground surface (i.e., p_o' = 100kPa, 400kPa and 680kPa). The resulting secant stiffness-depth relations at axial strain levels of ε_v = 0.01%, 0.1% and 1% are plotted in Figure 3.9 and Figure 3.10.

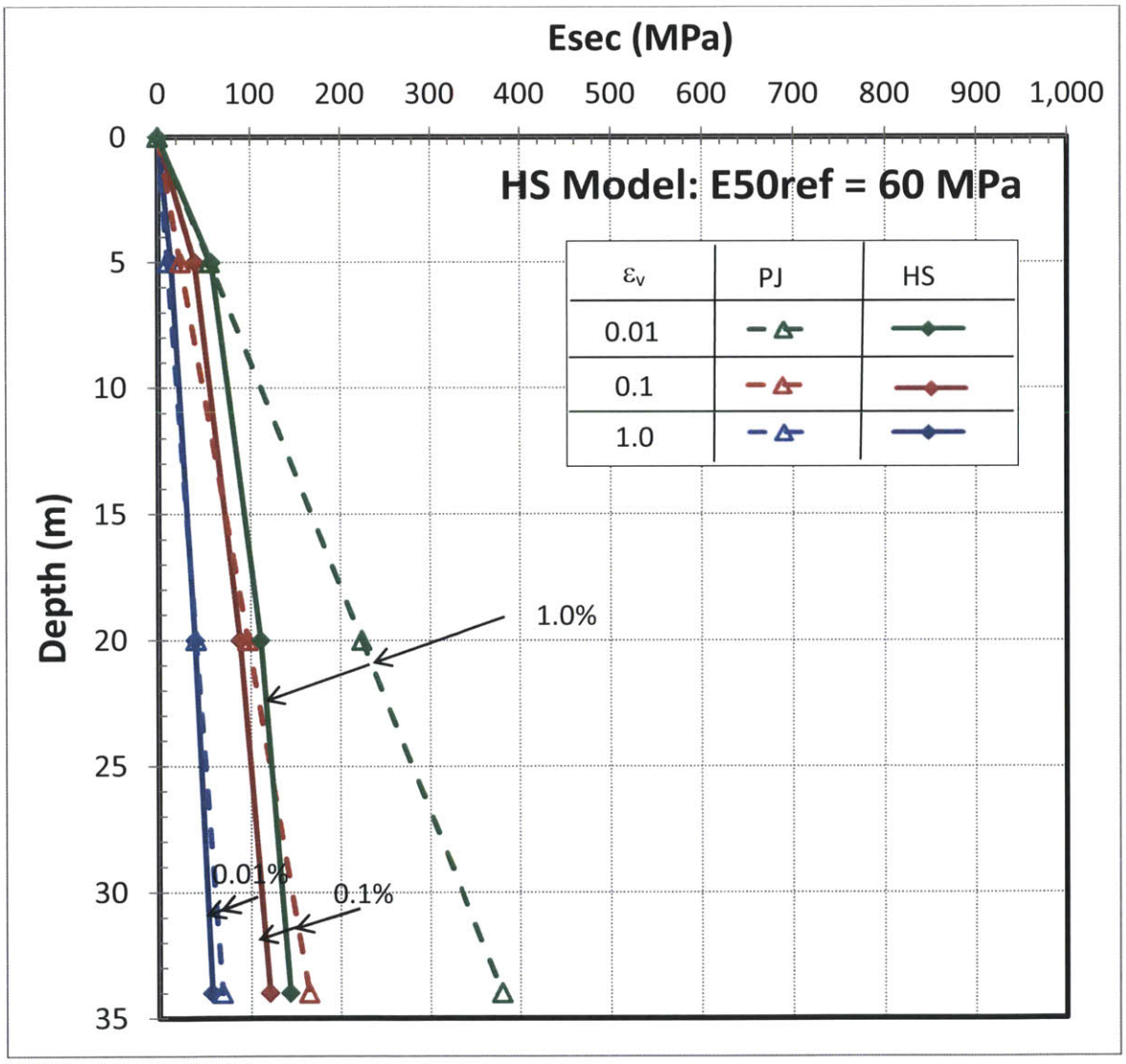

Figure 3.9: E_{sec} vs depth at various strain levels for HS model ($\boldsymbol{E_{ref}^{50}}$=60MPa)

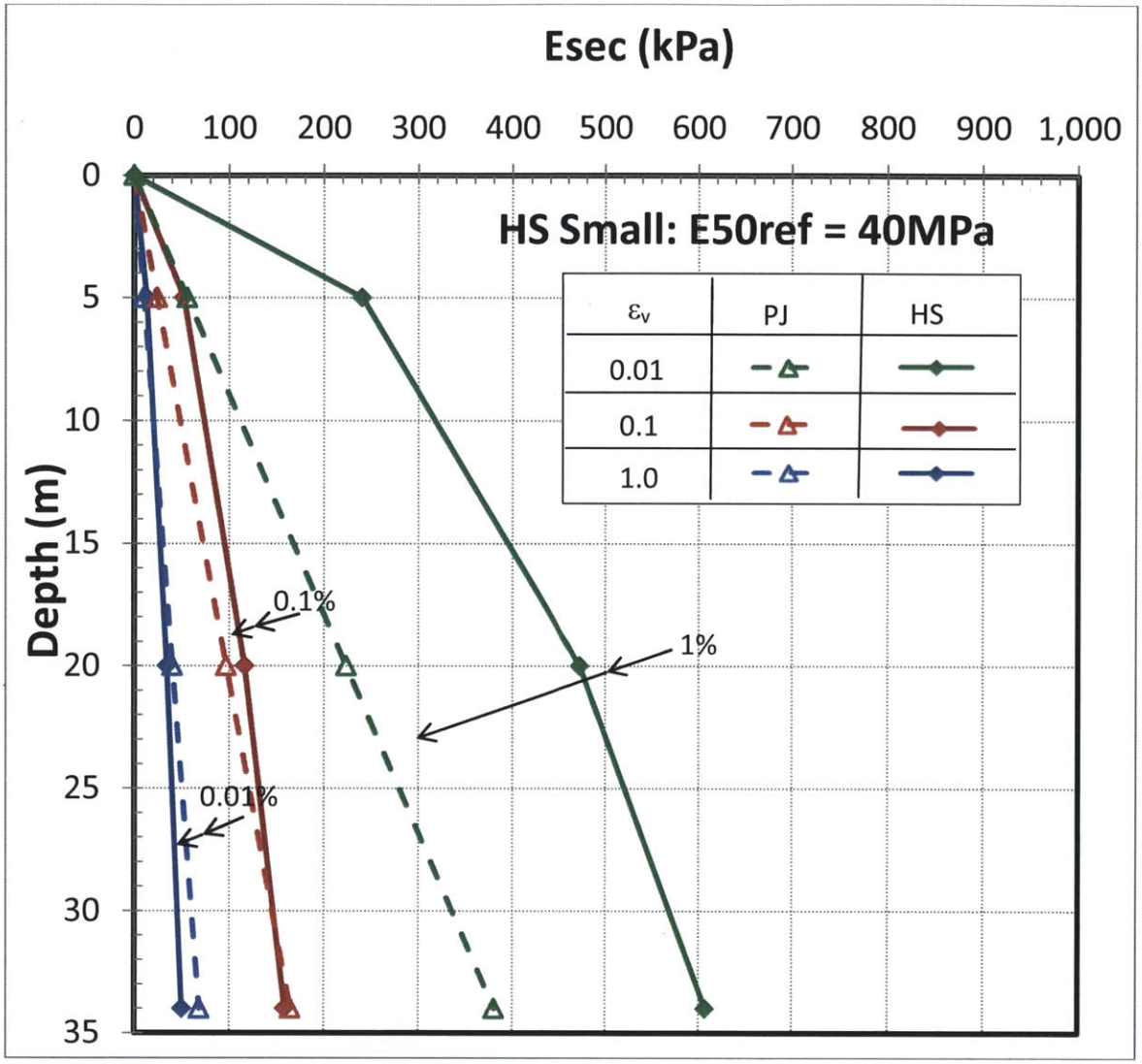

Figure 3.10: E_{sec} vs depth at various strain levels for HSS model ($\boldsymbol{E_{ref}^{50}}$=40MPa)

Figure 3.9 and Figure 3.10 show that the value of E_s in the PJ model increases approximately linearly with depth, such that the reference parameters E_s for the tunnels[1] at depths are 111MPa and 189MPa for the PJ model, as compared to E_s = 103MPa and 163MPa reported in Potts and Addenbrooke (1997). The minor difference is probably attributed to the fact that E_s values adopted in Potts and Addenbrooke (1997) were

[1] Es is taken at ε_a = 0.01%, at z = H/2 (Potts and Addenbrooke, 1997)

obtained by drained triaxial compression tests while this study assumes undrained shear conditions.

Both HS and HSS models agree reasonably well with the PJ model in terms of stiffness at axial strain ε_v = 0.1% and 1% strains, although HSS model fits slightly better over the depth. It should however be noted that at ε_v = 0.01% strain, the stiffness obtained by both models does not agree perfectly with the PJ model (with difference between 37% to 211% across the depth).

Based on the above calibration, the following are the best-fit input stiffness parameters for the hardening soil family of constitutive models (Table 3.4):

	E_{50}^{ref} [MPa]	E_{oed}^{ref} [MPa]	E_{ur}^{ref} [MPa]	G_0 [MPa]	$\gamma_{0.7}$ [%]
HS model	60	60	180	--	--
HSS model	40	40	120	324	0.009

Table 3.4: Best-fit input stiffness parameters for HS and HSS models

This section compares the tunneling-induced greenfield settlement troughs for the HS and HSS models with prior published results using the PJ model. The results focus on a 4.146m diameter tunnel located at 20m below the ground surface. The tunnel cavity support ratio, β, at the tunnel cavity is adjusted to produce a volume loss at the ground surface, ΔV_s = 1.5% (evaluated by numerical integration of the settlement trough).

Figure 3.11 and Figure 3.12 show volume loss ΔV_s (= ΔV_L) as a function of the tunnel release ratio (1-β) for the HS and HSS models respectively.

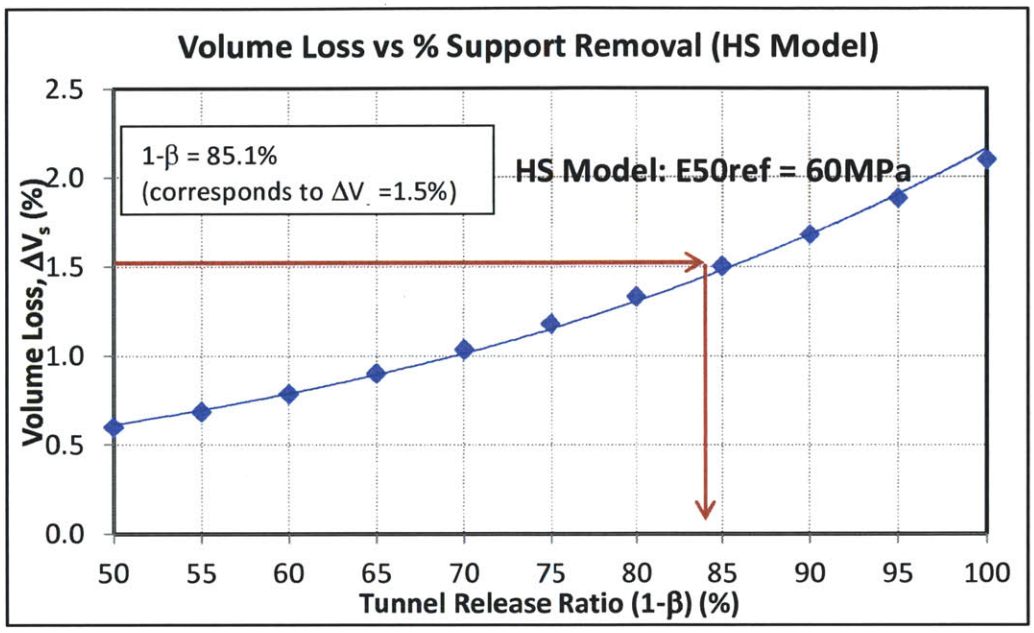

Figure 3.11: Variation of volume loss with percentage support removed for HS model

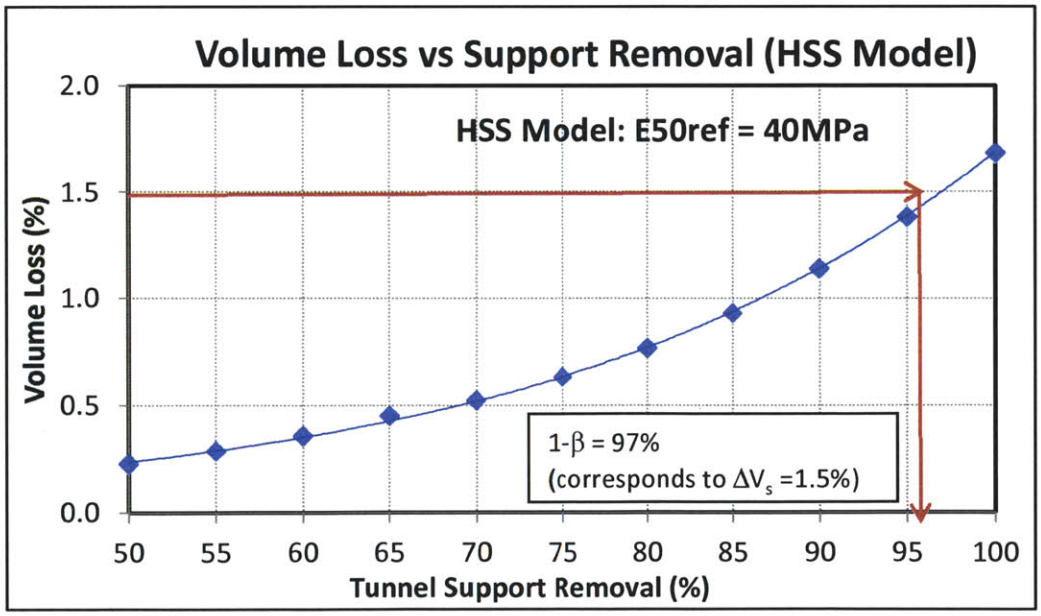

Figure 3.12: Variation of volume loss with percentage support removed for HSS model

Figure 3.13 compares the normalized settlement troughs (for $\Delta V_L = 1.5\%$) for the PJ, HS and HSS models (with inflection points, x_i = 12.7m, 17.7m and 11.2m from tunnel centerline respectively). The results show that the HSS model predicts a narrower settlement trough than the HS model confirming the importance of small strain non-linearity. There is a good match between results of the PJ and HSS models above the tunnel ($x < 5$m). The PJ model generally predicts larger far-field settlements ($x > 20$m) than either the HS or HSS models.

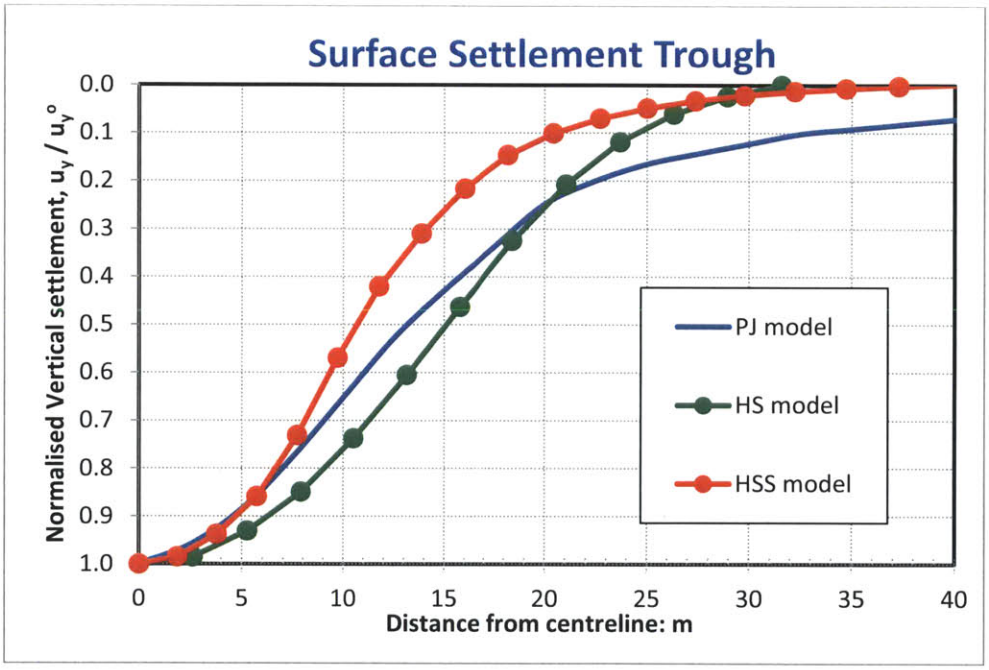

Figure 3.13: Comparison of greenfield settlement trough shape for Potts soil model, HS model and HSS model under common volume loss of 1.5%

Figure 3.14 includes a further comparison of the HSS and PJ settlement with the expected empirical behavior, described by the Gaussian function (equation 2.1) with $x_i/H = 0.5$ (Mair and Taylor, 1997), where x_i is the offset of point of inflection from tunnel

centerline and H is the depth to tunnel springline (see Figure 3.14). The HSS model clearly shows a much better match with the empirical data, than the PJ model.

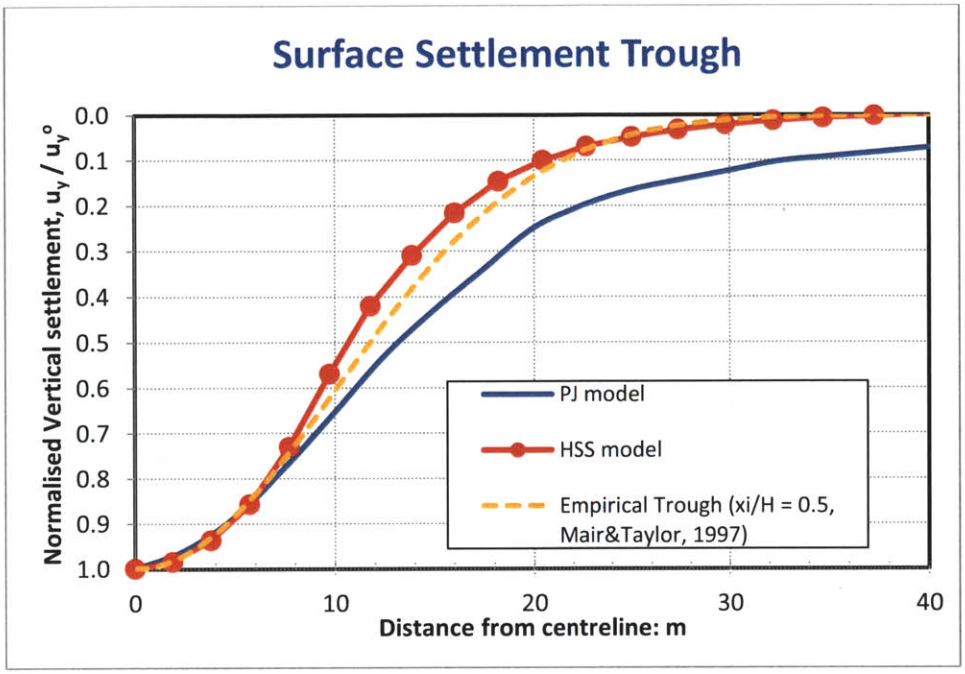

Figure 3.14: Empirical Trough predicted by Gaussian equation with $x_i/H = 0.5$

In this sub-section, it has clearly indicated that the choice of soil model has an important influence on the prediction of greenfield ground settlement. The preceding calibration exercise has shown that the HSS model with the selected set of stiffness parameters provides a reasonable fit with the PJ model and matches closely the greenfield settlement trough expected from empirical models. It can therefore be concluded that given two soil models with similar stiffness characteristics, the calculating greenfield settlement trough can vary depending on the soil model used. This result is reasonable because the two soil models are fundamentally different in that the stress-strain relationship in the PJ model is

represented by a periodic logarithmic function while that of the hardening soil family of constitutive models are represented by a hyperbolic function.

3.3 Conclusions

This chapter explains the method of analysis in this study, including the modeling of geometry, building, soil properties, initial stresses, soil-structure interface, and tunnel excavation in the finite element analysis as well as the chosen building stiffness for presenting the results of analyses and the building deformation criteria adopted to quantify the effect of ground movement on structures.

To enable a comparison to be made between the result of this study (analyzed using the hardening soil family of constitutive models) and that of the earlier study in Potts and Addenbrooke (1997) (done with ICFEP and the bespoke PJ model proposed by Jardine et.al (1986)), the stiffness parameters used in the hardening soil model in this study are calibrated with the PJ model by matching the stress-strain behavior and the greenfield settlement trough shape resulting from tunnel excavation.

4 Effects of Building Stiffness

4.1 Introduction

It was concluded in Chapter 3 that the best-fit HSS model and the corresponding PJ model produce different settlement troughs due to tunnel excavation. As the effects of building properties are to be assessed through modification factors relative to the greenfield conditions, the results are inevitably influenced by the choice of soil model. The HSS model appears to fit closely the empirical data, and a series of finite element analyses have been carried out to assess effects of building properties using the best-fit HSS model. The elastic building properties are varied in the same range proposed by Potts and Addenbrooke (1997).

4.2 Results and Interpretation

A total of 48 finite element analyses have been performed in which the depth of tunnel, the width and eccentricity of the surface beam are unchanged, while the axial and bending stiffness of the structure is varied. These analyses are summarized in Table 4.1:

B (m)	e (m)	Z (m)	EA kN/m	EI kNm	$M^{DR\ sag}$	$M^{DR\ hog}$	$M^{\varepsilon ht}$	$M^{\varepsilon hc}$
60	0	20	1.50×10^{8}	4.32×10^{3}	1.01	1.20	0.0002	0.0001
60	0	20	1.50×10^{8}	4.32×10^{5}	0.96	1.16	0.0002	0.0001
60	0	20	1.50×10^{8}	4.32×10^{6}	0.70	0.80	0.0001	0.0001
60	0	20	1.50×10^{8}	4.32×10^{7}	0.38	0.10	0.0000	0.0000
60	0	20	1.50×10^{8}	4.32×10^{8}	0.19	0.00	0.0000	0.0000
60	0	20	1.50×10^{8}	4.32×10^{10}	0.01	0.01	0.0000	0.0000
60	0	20	1.50×10^{7}	4.32×10^{3}	1.01	1.21	0.0022	0.0014
60	0	20	1.50×10^{7}	4.32×10^{5}	0.96	1.15	0.0021	0.0014
60	0	20	1.50×10^{7}	4.32×10^{6}	0.70	0.81	0.0018	0.0012
60	0	20	1.50×10^{7}	4.32×10^{7}	0.38	0.13	0.0011	0.0007
60	0	20	1.50×10^{7}	4.32×10^{8}	0.19	0.05	0.0003	0.0002
60	0	20	1.50×10^{7}	4.32×10^{10}	0.06	0.06	0.0004	0.0003
60	0	20	1.50×10^{6}	4.32×10^{3}	1.01	1.18	0.0402	0.0263
60	0	20	1.50×10^{6}	4.32×10^{5}	0.95	1.14	0.0402	0.0264
60	0	20	1.50×10^{6}	4.32×10^{6}	0.72	0.83	0.0416	0.0273
60	0	20	1.50×10^{6}	4.32×10^{7}	0.47	0.37	0.0397	0.0260
60	0	20	1.50×10^{6}	4.32×10^{8}	0.35	0.32	0.0333	0.0219
60	0	20	1.50×10^{6}	4.32×10^{10}	0.32	0.35	0.0287	0.0188
60	0	20	1.50×10^{5}	4.32×10^{3}	0.98	1.10	0.3269	0.2145
60	0	20	1.50×10^{5}	4.32×10^{5}	0.94	1.07	0.3420	0.2244
60	0	20	1.50×10^{5}	4.32×10^{6}	0.82	0.93	0.3576	0.2346
60	0	20	1.50×10^{5}	4.32×10^{7}	0.76	0.86	0.3570	0.2342
60	0	20	1.50×10^{5}	4.32×10^{8}	0.75	0.86	0.3536	0.2320
60	0	20	1.50×10^{5}	4.32×10^{10}	0.74	0.86	0.3530	0.2316
60	0	20	1.50×10^{4}	4.32×10^{3}	0.96	1.08	0.8126	0.5332
60	0	20	1.50×10^{4}	4.32×10^{5}	0.94	1.06	0.8162	0.5355
60	0	20	1.50×10^{4}	4.32×10^{6}	0.93	1.05	0.8130	0.5334
60	0	20	1.50×10^{4}	4.32×10^{7}	0.92	1.05	0.8114	0.5324
60	0	20	1.50×10^{4}	4.32×10^{8}	0.92	1.05	0.8112	0.5322
60	0	20	1.50×10^{4}	4.32×10^{10}	0.92	1.05	0.8112	0.5322
60	0	20	1.50×10^{3}	4.32×10^{3}	0.96	1.10	0.9886	0.6487
60	0	20	1.50×10^{3}	4.32×10^{5}	0.95	1.09	0.9868	0.6475
60	0	20	1.50×10^{3}	4.32×10^{6}	0.95	1.09	0.9868	0.6475
60	0	20	1.50×10^{3}	4.32×10^{7}	0.95	1.09	0.9864	0.6473
60	0	20	1.50×10^{3}	4.32×10^{8}	0.95	1.09	0.9864	0.6473
60	0	20	1.50×10^{3}	4.32×10^{10}	0.95	1.09	0.9864	0.6473
60	0	20	1.50×10^{2}	4.32×10^{3}	0.96	1.10	1.0533	0.6911
60	0	20	1.50×10^{2}	4.32×10^{5}	0.96	1.10	1.0533	0.6911
60	0	20	1.50×10^{2}	4.32×10^{6}	0.96	1.10	1.0533	0.6911
60	0	20	1.50×10^{2}	4.32×10^{7}	0.96	1.10	1.0533	0.6911
60	0	20	1.50×10^{2}	4.32×10^{8}	0.96	1.10	1.0533	0.6911
60	0	20	1.50×10^{2}	4.32×10^{10}	0.96	1.10	1.0533	0.6911

Table 4.1: Analyses with 60m beam with zero eccentricity

Figure 4.1 illustrates typical predictions of surface settlement troughs for cases a) where the axial stiffness varies (at constant bending stiffness) and b) where the bending stiffness varies (at constant axial stiffness). Figure 4.1(a) shows that despite the high bending stiffness (EI = 4 x 10^{10} kNm), the settlement troughs follow very closely the greenfield case for axial stiffness EA $\leq$ 1.5 x 10^{4} kN/m. However, as the axial stiffness is increased, the structure modifies the settlement to give a shallower trough towards the limiting case (EA = 1.5 x 10^{8} – 1.5 x 10^{9} kN/m), where the settlement trough is uniform beneath the beam. However, the influence of the structure decreases rapidly beyond the edge of the beam and the greenfield settlement curve is fully recovered within a horizontal distance 3m of the edge. Figure 4.1(b) shows that for beams with constant axial stiffness but varying bending stiffness, the trough follows very closely the greenfield profile for EI $\leq$ 4 x 10^{5} kNm. It is then shown that the greater the bending stiffness, the more the beam modifies the greenfield settlement trough. At the highest bending stiffness (EI = 4.322 x 10^{10} kNm), the settlement trough is uniform across the beam width and again the greenfield curve is fully recovered within a horizontal distance 3m of the edge. These results give a very clear message that both the axial stiffness and bending stiffness affect the settlement trough within the range of EA and EI being varied.

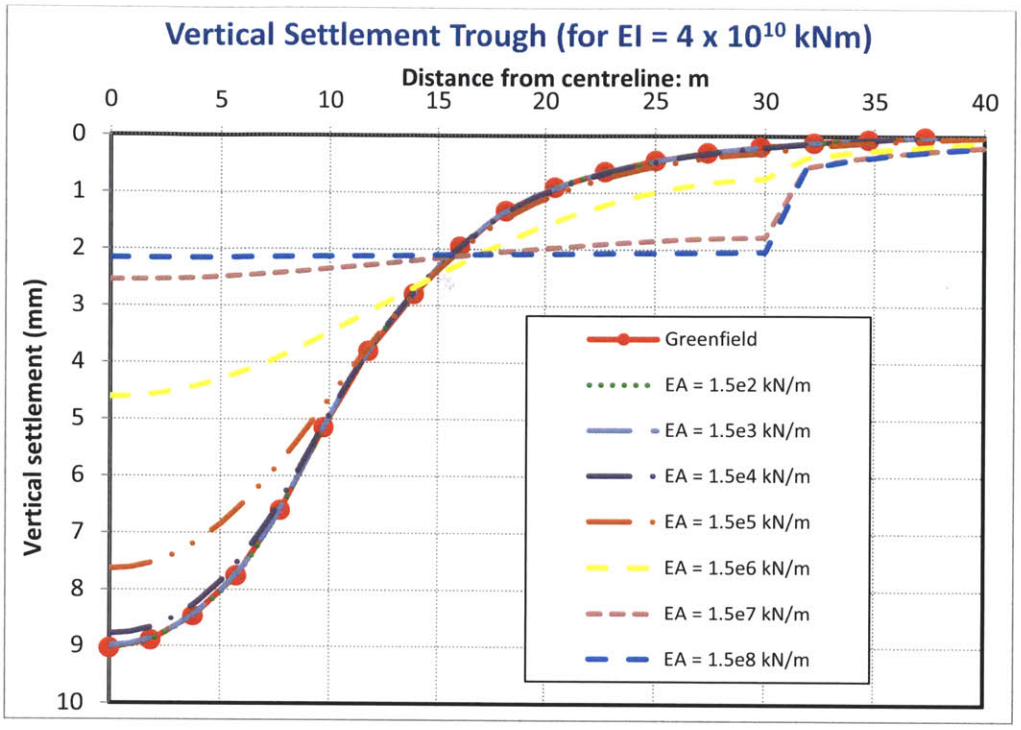

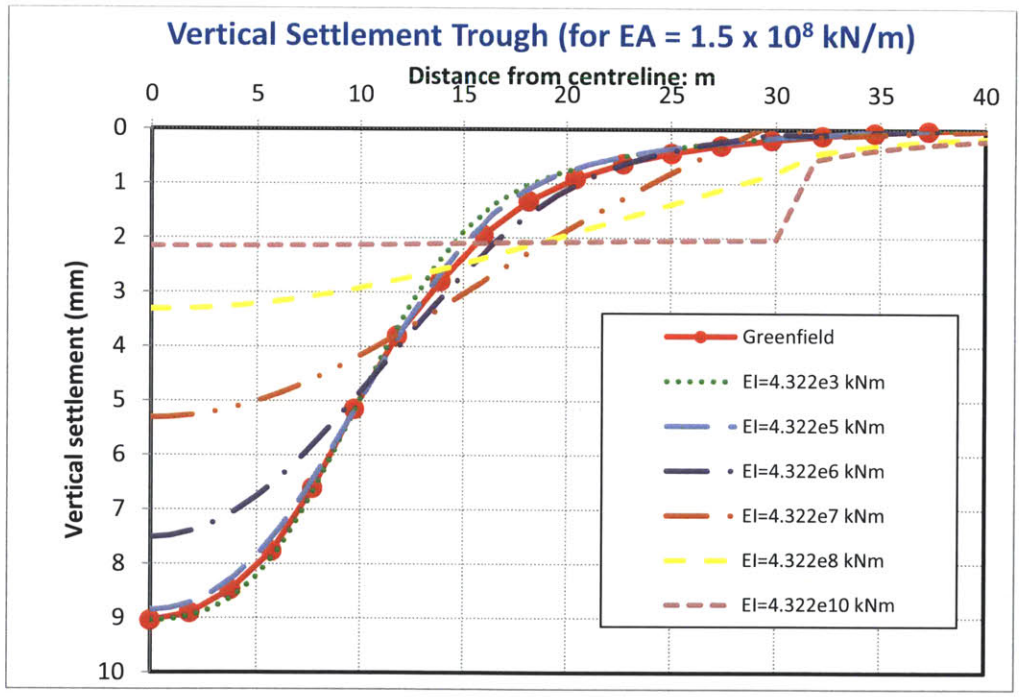

Figure 4.1: Surface settlement troughs for a 20m deep tunnel excavated beneath a 60m wide structure: a) effect of axial stiffness; b) effect of bending stiffness

Figures 4.2(a) and (b) shows the derived deflection ratio modification factors M^{DR} for sagging and hogging as functions of EI and EA respectively. The results reported by Potts and Addenbrooke (1997) are overlaid for comparison. The results show that the HSS model gives lower modification factors M^{DR} for sagging for all combinations of EA and EI analyzed. The largest modification factors for sagging M^{DR} for sagging = 1.01 and 1.26 for the HSS model and the PJ model respectively, which occur at very low bending stiffness (EI = 4 x 10^2 kNm). There is little variation in M^{DR} for sagging for EI $\leq$ 4 x 10^6 kNm. Deflection ratios reduce significantly at higher bending stiffness (EI > 4 x 10^5 kNm). The drop is most drastic for high axial stiffness (EA = 1.5 x 10^8 kN/m), where M^{DR} for sagging reduces from 0.96 to 0 for over the range, EI = 4 x 10^5 to 4 x 10^{10} kNm. For low axial stiffness (EA < 1.5 x 10^5 kN/m), modification factors remain constant at 0.92 – 0.95 for the entire range of EI being varied. On the other hand, it is interesting to observe that the inverse trend of M^{DR} in the hogging zone as identified in Potts and Addenbrooke (1997) at EI > 5 x 10^7 kNm for EA = 1.5 x 10^6 to 1.5 x 10^7 kN/m is not observed in this study. Comparing the modification factors M^{DR} for hogging with Potts and Addenbrooke (1997), for high axial stiffness (EA > 1.5 x 10^5 kN/m), the modification factors M^{DR} for hogging are generally higher, except at EI = 4 x 10^8 kNm where Potts and Addenbrooke (1997) reach its peak M^{DR} for hogging before reversal in trend. Conversely, for low axial stiffness (EA > 1.5 x 10^5 kN/m), the modification factors M^{DR} for hogging are lower than Potts and Addenbrooke (1997). It is interesting to observe that M^{DR} for both sagging and hogging are found to be greater than unity at low bending and axial stiffness, which implies that the presence of the structure at this range of stiffness leads to greater hogging and/or sagging than the greenfield curve.

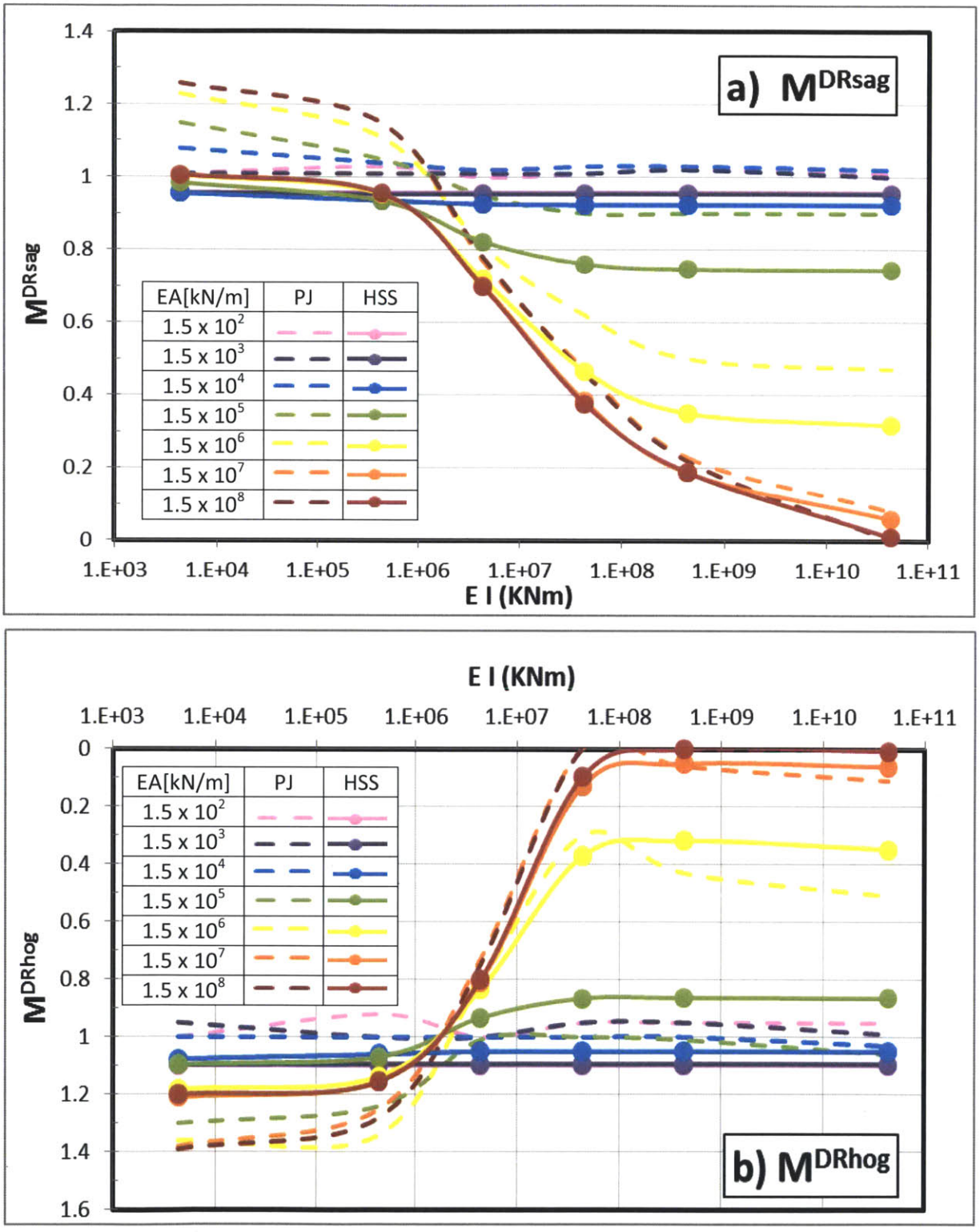

Figure 4.2: Variation of modification factors for deflection ratio with beam flexural stiffness: (a) M^{DRsag}; (b) M^{DRhog}

M^{DR} data in Figure 4.2 are re-plotted in Figure 4.3 as functions of the axial stiffness. The results obtained in Potts and Addenbrooke (1997) are also overlaid on the figure for comparison. It is evident that the HSS model is giving lower modification factors M^{DR} for sagging for all combinations of EA and EI analyzed. The highest modification factors M^{DR} for sagging are 1.01 and 1.26 for HSS model and Potts and Addenbrooke (1997) respectively, both occurring at high axial stiffness (EA = 1.5 x 10^8 kN/m). There is little variation in M^{DR} for low axial stiffness (EA < 1.5 x 10^4 kN/m). Modification factors vary significantly for high bending stiffness (EI = 4 x 10^{10} kNm), from 0.92 to 0.01 for axial stiffness in the range EA = 1.5 x 10^4 to 1.5 x 10^8 kN/m. For low bending stiffness (EI < 4 x 10^5 kNm), modification factors remain constant at 0.96 – 1.01 for the entire range of axial stiffness. However, it is interesting to note that the reversal in trend of modification factor M^{DR} for hogging as identified in Potts and Addenbrooke (1997) for beams with axial stiffness EA > 1.5 x 10^7 kN/m and low bending stiffness (EI = 4 x 10^5 and 4 x 10^6 kNm) is not observed in this study. When comparing the modification factors M^{DR} for hogging obtained from this study with Potts and Addenbrooke (1997), no obvious trend is observed.

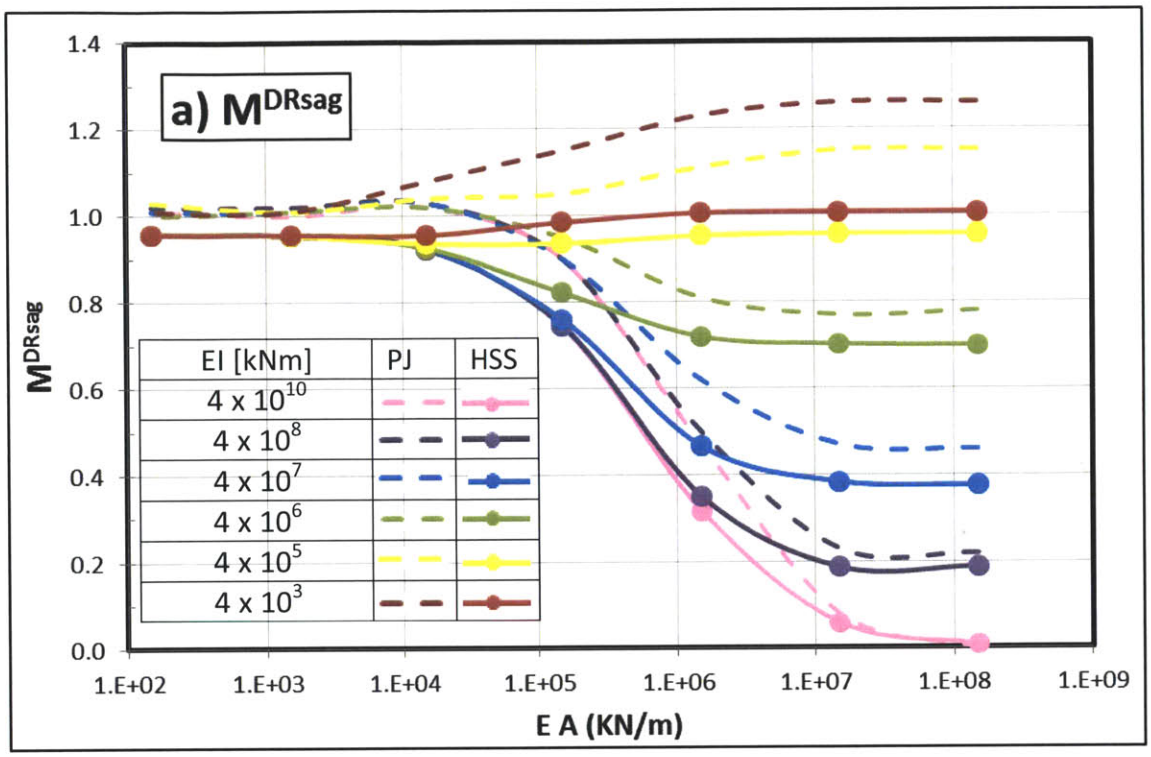

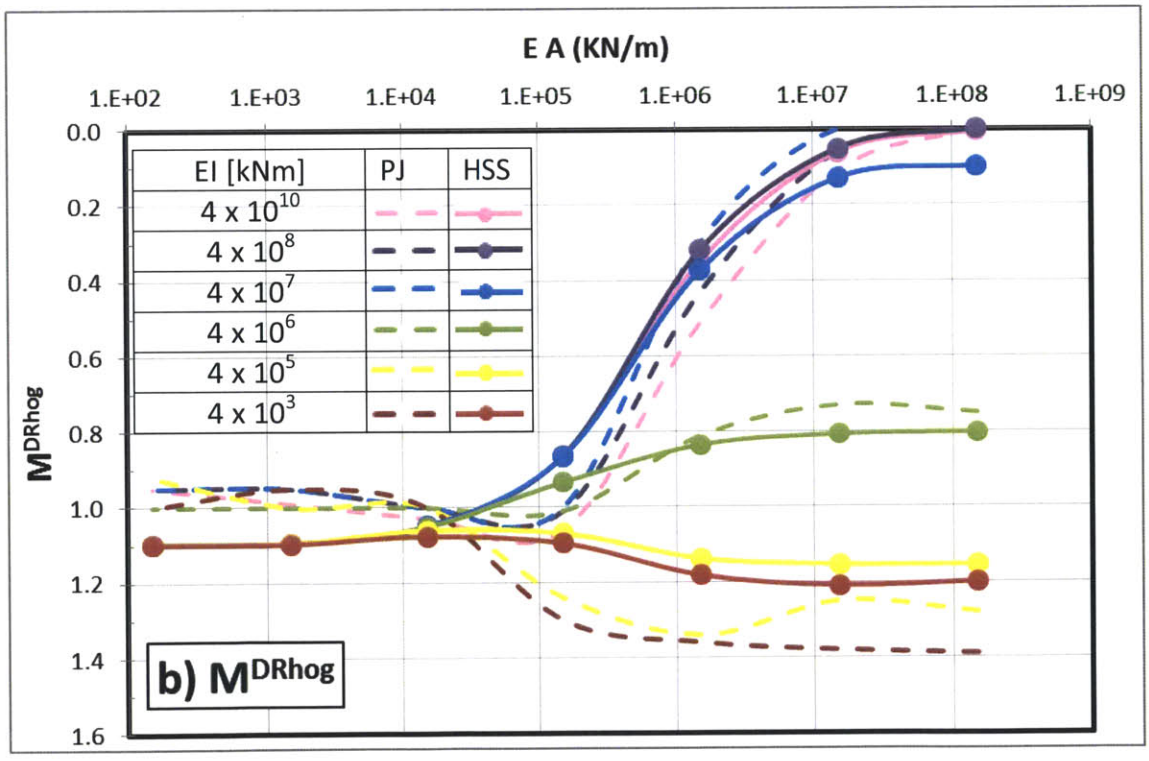

Figure 4.3: Variation of modification factors for deflection ratio with beam axial stiffness: (a) M^{DRsag}; (b) M^{DRhog}

Figures 4.4(a) and (b) show the variation of modification factors for horizontal strains M^{ε} for the selected combinations of EA and EI listed in Table 4.1 for compressive and tensile strain regions respectively. Again, the corresponding results of Potts and Addenbrooke (1997) are overlaid for comparison. For both compressive and tensile horizontal strains, the results from the analyses with different bending stiffness generally overlap with each other, which proves that only the axial stiffness affects horizontal compressive and tensile strains (i.e., these parameters are independent of EI). In Figure 4.4(a), it is evident that $M^{\varepsilon_{hc}}$ is the largest (0.69) at low axial stiffness (EA = 1.5 x 10^2 kN/m) and gradually drops to around zero ($M^{\varepsilon_{hc}}$ = 0.0002 to 0.0014) at high axial stiffness (EA =1.5 x 10^7 kN/m). The current modification factors are smaller than those reported in Potts and Addenbrooke (1997) for all combinations of EA and EI. The largest differences occur at low axial stiffness (EA = 1.5 x 10^2 kN/m). Modification factors in the tensile region $M^{\varepsilon_{ht}}$ (Figure 4.4(b)) are the largest at low axial stiffness (EA = 1.5 x 10^2 kN/m) at 1.05, and gradually drop to around zero ($M^{\varepsilon_{ht}}$ = 0.002) at high axial stiffness (EA =1.5 x 10^7 kN/m). It is interesting to observe that $M^{\varepsilon_{ht}}$ values obtained from this study generally coincide with those of Potts and Addenbrooke (1997). However, it is also worth noting that for high axial stiffness (EA =1.5 x 10^6 to 1.5 x 10^6 kN/m), the value of M^{ε} for compression and tension are both very small, and hence any small change in the magnitude can significantly affect the comparative values from the two soil models.

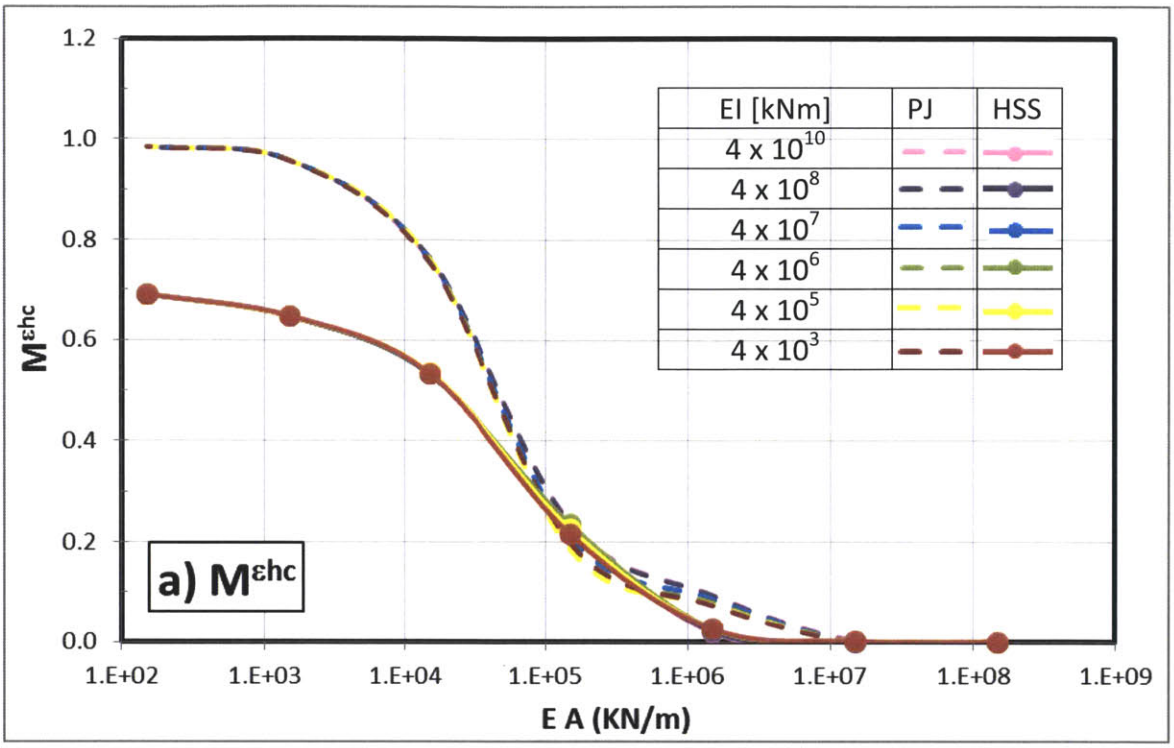

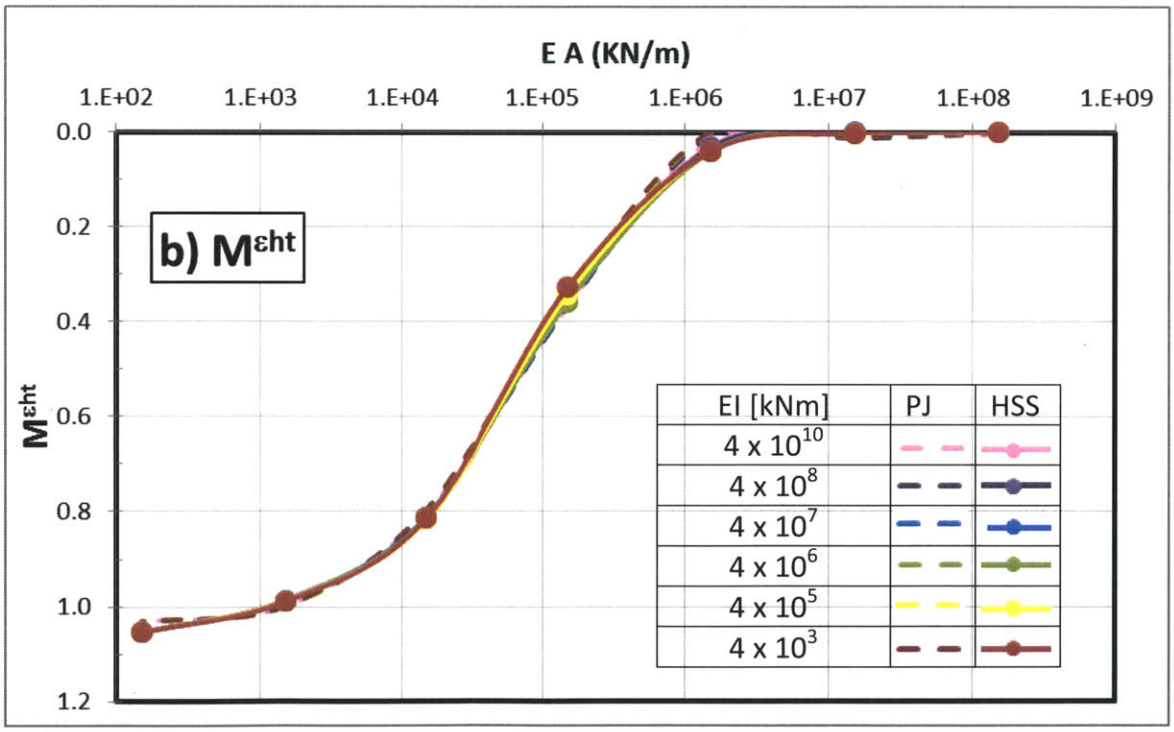

Figure 4.4:Variation of modification factors for horizontal strain with beam stiffness: (a) $M^{\varepsilon hc}$; (b) $M^{\varepsilon ht}$

The results of M^{DR} for sagging and hogging concerning beams with likely values of axial and bending stiffness (i.e., EI = 2 x 10^7 to 4.4 x 10^9 kNm; EA = 6.9 x 10^6 to 3.8 x 10^7 kN/m for 1- to 10-storey building as detailed in Chapter 2) are selected from Table 4.1 and plotted on Figure 4.5 with the design curve (for zero eccentricity) given in Potts and Addenbrooke (1997). It is noted that the design curve is reproduced as M^{DR} vs EI (where EI = $\rho^*(E_s(B/2)^4)$ as given in Potts and Addenbrooke (1997)). It is evident that the results obtained from the HSS model in this study for beams with likely values of axial and bending stiffness fall below the design curves for both sagging and hogging, which represent the upper limit of the analyses carried out in Potts and Addenbrooke (1997). Based on the range of building stiffness analyzed in this study, it is therefore considered that the design curves (for zero eccentricity) for M^{DR} for both sagging and hogging in Potts and Addenbrooke (1997) provide a reasonable first estimate of the effects of soil-structure interaction

Similarly, the results of M^{ε} for compression and tension concerning beams with likely values of axial and bending stiffness are selected and plotted in Figure 4.6 with the design curve (for zero eccentricity) given in Potts and Addenbrooke (1997). It is also evident that the results obtained from the HSS model in this study for beams with likely values of axial and bending stiffness fall below the design curves for both compression and tension regions, which represent the upper limit of the analyses carried out in Potts and Addenbrooke (1997). Based on the range of building stiffness analyzed in this study, it is therefore considered that the design curves (for zero eccentricity) for M^{ε} for both compression and tension in Potts and Addenbrooke (1997) provide a reasonable first estimate of the effects of soil-structure interaction.

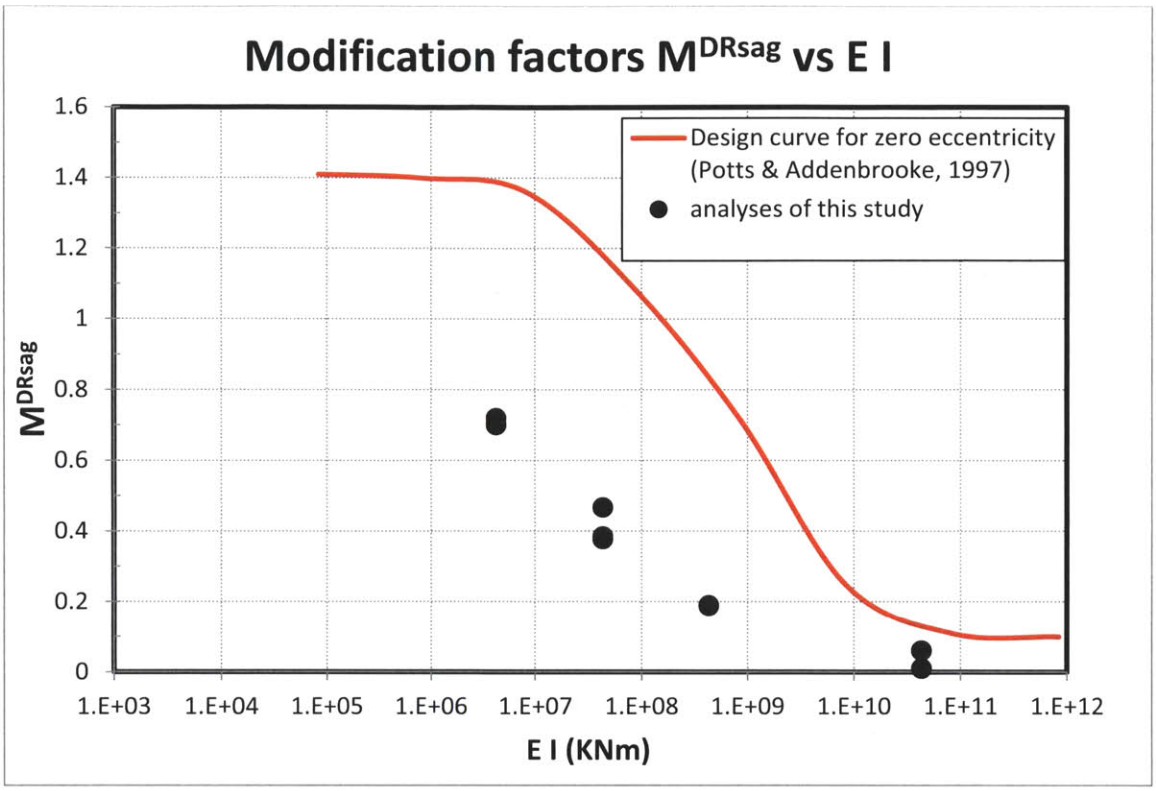

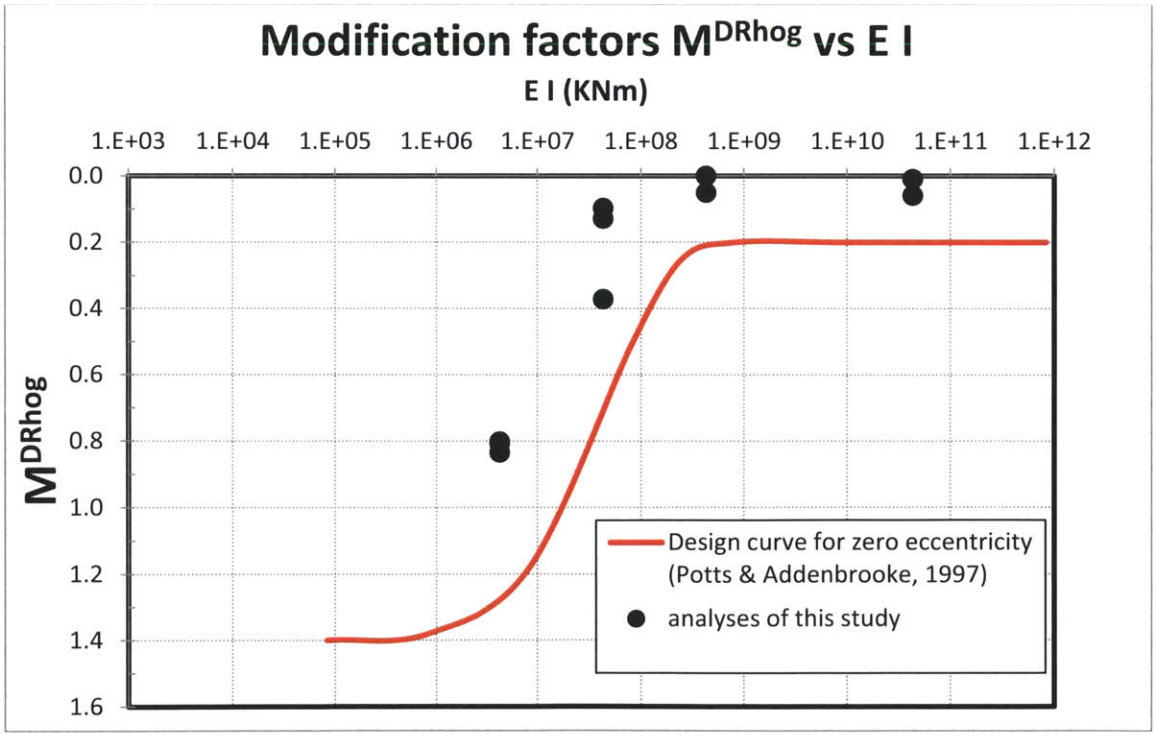

Figure 4.5: Comparison with design curve for zero eccentricity for modification factors M^{DR}: a) sagging; b) hogging

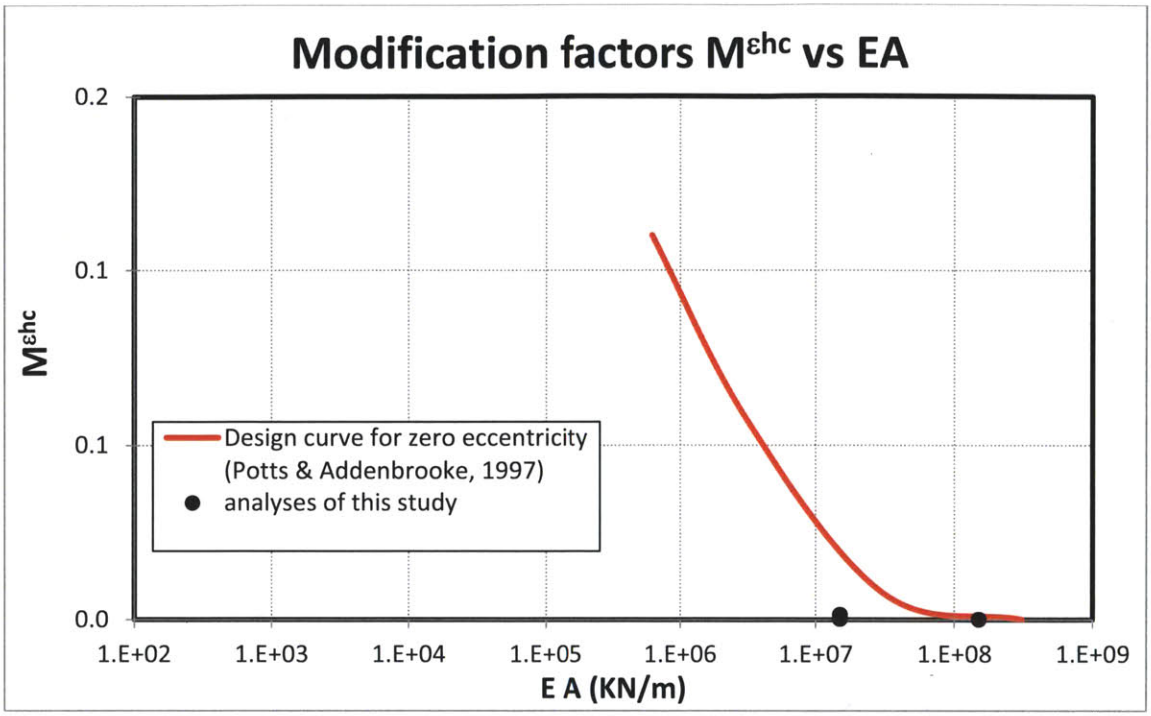

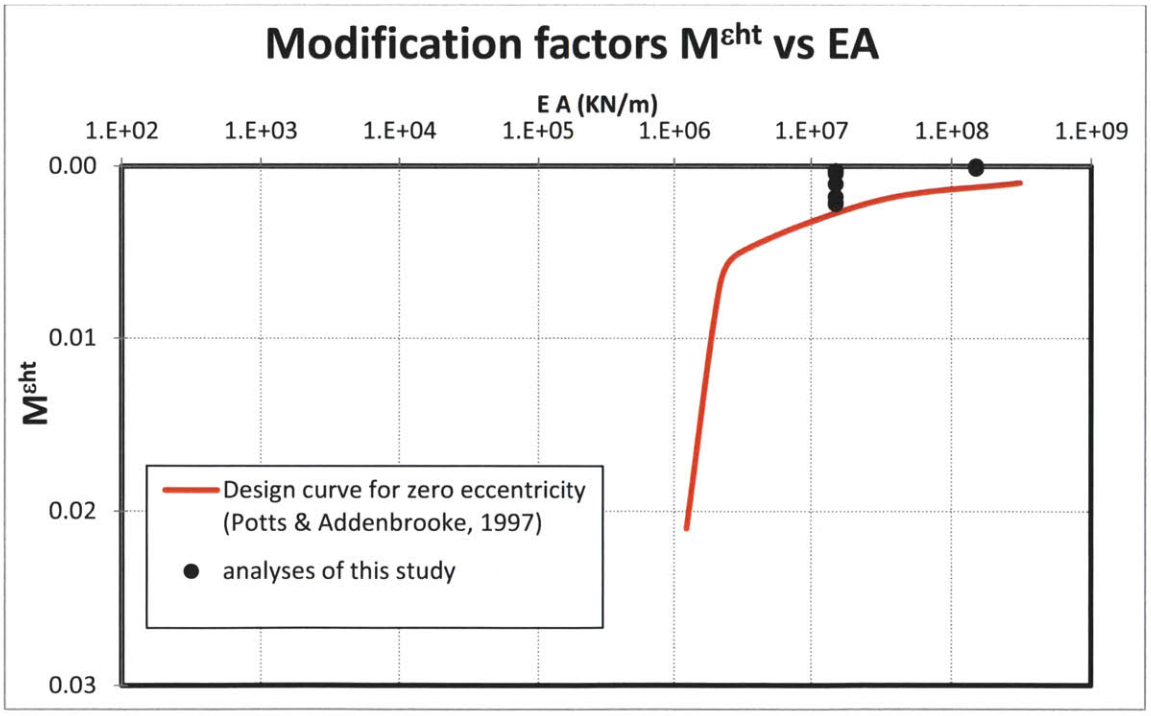

Figure 4.6: Comparison with design curve for zero eccentricity for modification factors horizontal strain: a) compression $M^{\varepsilon hc}$; b) tension $M^{\varepsilon ht}$

4.3 Conclusions

A total of 48 finite element analyses were performed to study the influence of existing buildings on ground movement resulting from a 20m deep tunnel excavated underneath a surface beam of 60m wide with no eccentricity. Bending and axial stiffness (EI and EA) of buildings are varied in these analyses. The results give a very clear message that both the axial and flexural stiffness affect the settlement trough within the range of EA and EI being considered. On the other hand, the results also show that only the axial stiffness affects the horizontal compressive and tensile strains.

Although a different soil model (i.e., HSS model) is used in this study, the variations of modification factors to EI and EA are qualitatively similar to those obtained in Potts and Addenbrooke (1997). The quantitative comparison of the modification factors obtained is summarized below:

(1) HSS model gives lower modification factors M^{DR} for sagging.

(2) For modification factors M^{DR} for hogging, HSS generally gives higher M^{DR} for high axial stiffness and lower M^{DR} for lower axial stiffness.

(3) Modification factors for horizontal strain in compression $M^{\varepsilon_{hc}}$ obtained from HSS model are generally smaller.

(4) Modification factors for horizontal strain in tension $M^{\varepsilon_{ht}}$ obtained from HSS model generally coincide with those of Potts and Addenbrooke (1997). However, as the values of $M^{\varepsilon t}$ and $M^{\varepsilon t}$ are generally very small at high axial stiffness, any small change in the magnitude can significantly affect the ratio of M^{ε} obtained from the two soil models in the high range of axial stiffness.

The results concerning beams with likely values of axial and bending stiffness (for 1- to 10-storey buildings) are selected and plotted on the design curve (for zero eccentricity) for modification factors M^{DR} for sagging and hogging and M^{ε} for compression and tension as given in Potts and Addenbrooke (1997). It is evident that the results obtained from the HSS model in this study for beams with likely values of axial and bending stiffness are falling below the concerning design curves for zero eccentricity, which proves that the design curves for M^{DR} for sagging and hogging and M^{ε} for compression and tension for zero eccentricity given in Potts and Addenbrooke (1997) are still adequate.

It is however noted that the 48 finite element analyses were all performed for a constant tunnel depth (20m to tunnel springline) and the width and eccentricity of the surface beam are unchanged (60m wide beams and zero eccentricity), only with the axial and bending stiffness varied. More analyses by the HSS model, covering different building widths and tunnel depths as well as buildings located at an eccentricity to the tunnel centerline, are required to verify the adequacy of the design curves in Potts and Addenbrooke (1997).

5 Effects of Building Weight

5.1 Introduction

In the previous chapter the building was modeled as a weightless elastic beam. This chapter considers the influence of building weight on tunnelling-induced ground movement.

5.2 Method of analysis

Same as the previous chapter, the analyses focus on a single geometry comprising a circular tunnel of diameter, d = 4.146m located at a depth, H = 20m. The overlying structure is represented by an equivalent elastic beam of width B = 60m located at the ground surface. The centroid of the equivalent beam is centred above the centerline of the tunnel (i.e., with no eccentricity). The soil model and the modeling of soil-structure interaction and tunnel excavation are the same as the previous chapter. All of the analyses use a fixed value of stress release ratio, 1 - β = 97% that produces a greenfield surface volume loss of ΔV_s = 1.5% using the HSS soil model.

Building weight is simulated by an additional calculation step in which the self-weight of the building is represented by a surface surcharge of 50kPa, in drained equilibrium with stresses in the ground prior to tunnel construction. This assumption corresponds to the case where the low permeability clay underneath the building is fully consolidated under

the weight of the building (i.e., the building was constructed long before the tunnel). The surcharge pressure increases the stress and hence, the soil stiffness locally within the foundation soil mass. Displacements are artificially re-zeroed prior to tunnel construction such that all soil strains are defined relative to the drained equilibrium condition associated with the building.

Practical values of bending and axial stiffness, EI and EA, for 1- to 10-storey buildings are provided in Table 3.1 in Chapter 3. The practical range EI = 2.00×10^7 to 4.39×10^9 kNm and EA = 6.90×10^6 to 3.80×10^7 kN/m. In chapter 4, a wider variation of stiffness values EI and EA was adopted (Table 4.1 in Chapter 4 refers) including impractical values of EI and EA in order to study the variation of tunneling-induced ground movements for a wider range of structure stiffness. This chapter will focus on the practical range of bending and axial stiffness for 1- to 10-storey buildings and study the influence of building weight on tunneling-induced ground movements within this range of practical stiffness at a higher resolution. 112 cases of practical building stiffness to be analyzed are plotted on Figure 5.1. The values of EA and EI for 1- to 10-storey buildings are also shown as a line on the figure.

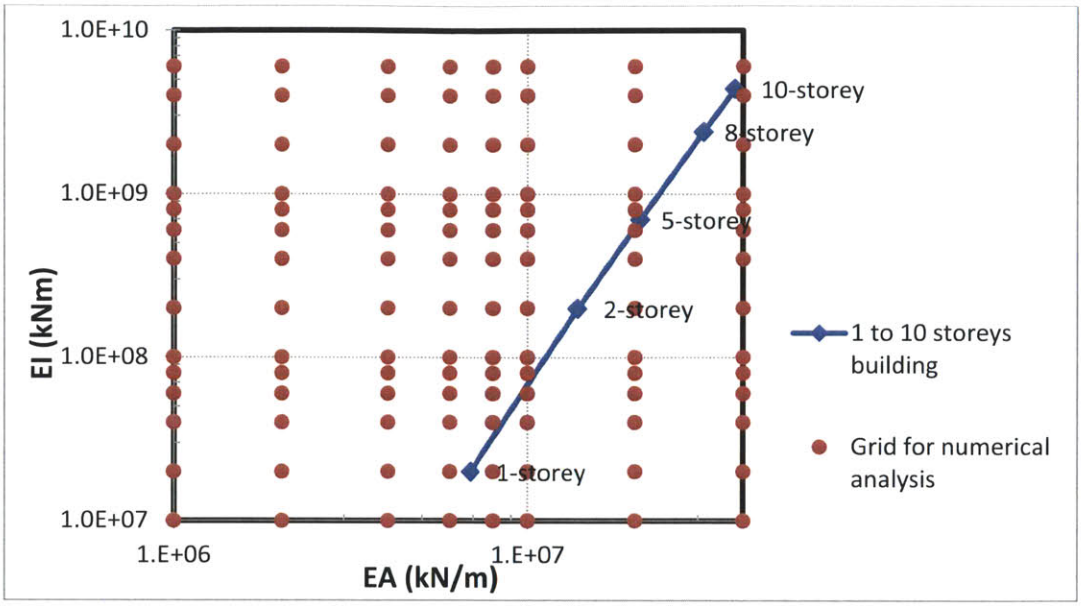

Figure 5.1: Practical range of building bending and axial stiffness (EA and EI)

5.3 Stress state

The existence of structures changes the stress conditions in the underlying soil. On the one hand, building stiffness changes the boundary condition at the ground surface; on the other hand, the building load affects the soil behavior down the level where a tunnel will be constructed (Franzius, 2004). Two finite element analyses were carried out for a 5-storey building with self-weight 50kPa to illustrate the influence of buildings on the stress state of soil prior to tunnel excavation. Figure 5.1 illustrates the effect of building load on mean effective stress p' on centerline of building prior to tunnel construction. The increase in effective stress is most marked at the ground surface, noting that the groundwater table is located at a depth of 2m. The deeper the soil, the smaller the difference in effective stress because overburden dominates the stress field instead of

building load at greater depth. On the other hand, the effect of building load on soil stiffness of a soil element at 10m below centerline of building prior to tunnel construction is plotted on Figure 5.2, which shows that soil stiffness under the 50 kPa building load is higher due to the increased stress level.

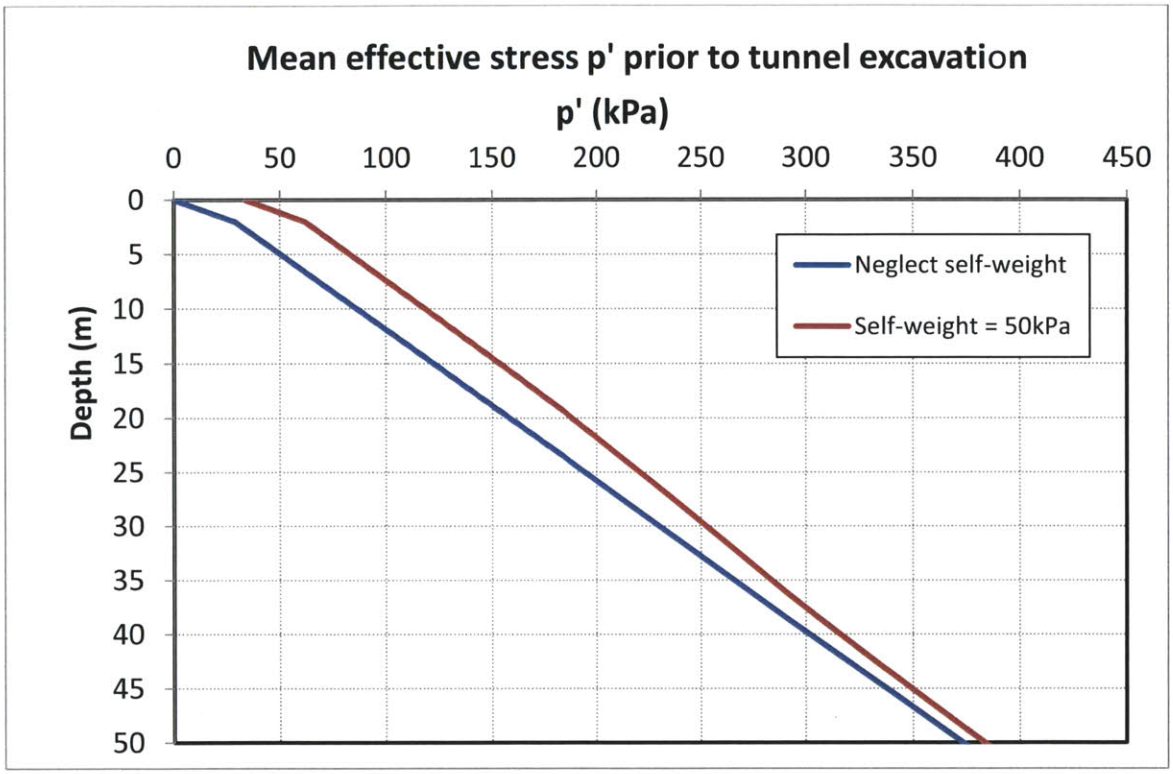

Figure 5.2: Mean effective stress p' profile on centerline of building prior to tunnel construction

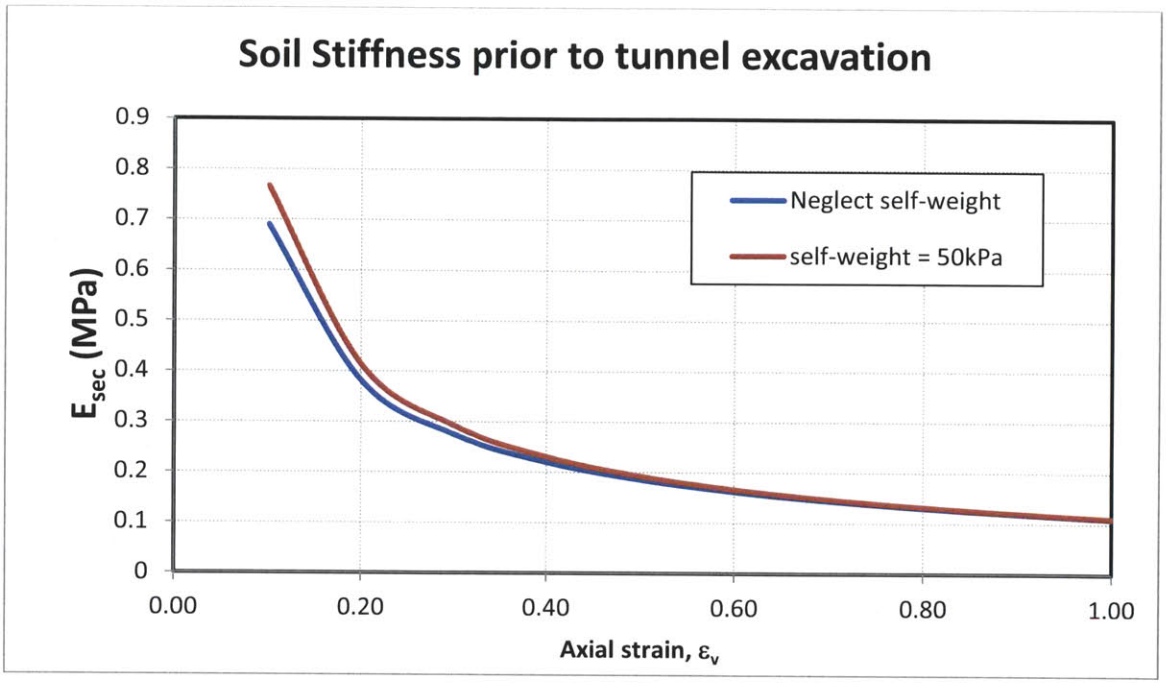

Figure 5.3: Soil stiffness profile at 10m below centerline of building prior to tunnel construction

5.4 Results and Interpretation

A total of 112 finite element analyses were carried out with and without building surcharge respectively to evaluate the influence of building weight on ground movements. These analyses are summarized in Table 5.1 and Table 5.2 below for cases without building load and with building load respectively:

Case No.	B (m)	e (m)	Z (m)	EI kNm	EA kN/m	M^{DRsag}	M^{DRhog}	$M^{\varepsilon ht}$	$M^{\varepsilon hc}$
1	60	0	20	1.00E+07	1.00E+06	0.6293	0.6705	0.0684	0.1382
2	60	0	20	2.00E+07	1.00E+06	0.5614	0.5439	0.0681	0.1419
3	60	0	20	4.00E+07	1.00E+06	0.5083	0.4660	0.0673	0.1448
4	60	0	20	6.00E+07	1.00E+06	0.4850	0.4415	0.0665	0.1463
5	60	0	20	8.00E+07	1.00E+06	0.4701	0.4306	0.0658	0.1471
6	60	0	20	1.00E+08	1.00E+06	0.4596	0.4253	0.0652	0.1476
7	60	0	20	2.00E+08	1.00E+06	0.4327	0.4215	0.0630	0.1492
8	60	0	20	4.00E+08	1.00E+06	0.4143	0.4272	0.0605	0.1508
9	60	0	20	6.00E+08	1.00E+06	0.4069	0.4314	0.0593	0.1516
10	60	0	20	8.00E+08	1.00E+06	0.4029	0.4341	0.0587	0.1520
11	60	0	20	1.00E+09	1.00E+06	0.4004	0.4360	0.0582	0.1523
12	60	0	20	2.00E+09	1.00E+06	0.3949	0.4400	0.0573	0.1530
13	60	0	20	4.00E+09	1.00E+06	0.3921	0.4425	0.0567	0.1533
14	60	0	20	6.00E+09	1.00E+06	0.3911	0.4433	0.0566	0.1534
15	60	0	20	1.00E+07	2.00E+06	0.5984	0.6082	0.0285	0.0817
16	60	0	20	2.00E+07	2.00E+06	0.5156	0.4428	0.0277	0.0846
17	60	0	20	4.00E+07	2.00E+06	0.4515	0.3246	0.0268	0.0870
18	60	0	20	6.00E+07	2.00E+06	0.4207	0.2822	0.0261	0.0880
19	60	0	20	8.00E+07	2.00E+06	0.4019	0.2628	0.0256	0.0889
20	60	0	20	1.00E+08	2.00E+06	0.3880	0.2525	0.0252	0.0895
21	60	0	20	2.00E+08	2.00E+06	0.3479	0.2432	0.0235	0.0910
22	60	0	20	4.00E+08	2.00E+06	0.3183	0.2530	0.0212	0.0933
23	60	0	20	6.00E+08	2.00E+06	0.3048	0.2614	0.0201	0.0948
24	60	0	20	8.00E+08	2.00E+06	0.2971	0.2669	0.0192	0.0955
25	60	0	20	1.00E+09	2.00E+06	0.2914	0.2702	0.0186	0.0957
26	60	0	20	2.00E+09	2.00E+06	0.2813	0.2802	0.0172	0.0970
27	60	0	20	4.00E+09	2.00E+06	0.2754	0.2858	0.0165	0.0976
28	60	0	20	6.00E+09	2.00E+06	0.2734	0.2878	0.0163	0.0978
29	60	0	20	1.00E+07	4.00E+06	0.5822	0.5753	0.0107	0.0461
30	60	0	20	2.00E+07	4.00E+06	0.4883	0.3714	0.0100	0.0483
31	60	0	20	4.00E+07	4.00E+06	0.4180	0.2228	0.0093	0.0498
32	60	0	20	6.00E+07	4.00E+06	0.3848	0.1741	0.0091	0.0508
33	60	0	20	8.00E+07	4.00E+06	0.3633	0.1511	0.0088	0.0514
34	60	0	20	1.00E+08	4.00E+06	0.3470	0.1386	0.0084	0.0518
35	60	0	20	2.00E+08	4.00E+06	0.2993	0.1223	0.0066	0.0533
36	60	0	20	4.00E+08	4.00E+06	0.2560	0.1282	0.0035	0.0548
37	60	0	20	6.00E+08	4.00E+06	0.2341	0.1376	0.0016	0.0560
38	60	0	20	8.00E+08	4.00E+06	0.2209	0.1449	0.0006	0.0567
39	60	0	20	1.00E+09	4.00E+06	0.2122	0.1503	0.0000	0.0572
40	60	0	20	2.00E+09	4.00E+06	0.1929	0.1638	0.0000	0.0582
41	60	0	20	4.00E+09	4.00E+06	0.1825	0.1718	0.0000	0.0587
42	60	0	20	6.00E+09	4.00E+06	0.1790	0.1747	0.0000	0.0589

Case No.	B (m)	e (m)	Z (m)	EI kNm	EA kN/m	M^{DRsag}	M^{DRhog}	$M^{\varepsilon ht}$	$M^{\varepsilon hc}$
43	60	0	20	1.00E+07	6.00E+06	0.5741	0.5604	0.0059	0.0325
44	60	0	20	2.00E+07	6.00E+06	0.4798	0.3463	0.0054	0.0341
45	60	0	20	4.00E+07	6.00E+06	0.4065	0.1882	0.0049	0.0352
46	60	0	20	6.00E+07	6.00E+06	0.3725	0.1338	0.0045	0.0359
47	60	0	20	8.00E+07	6.00E+06	0.3503	0.1080	0.0041	0.0364
48	60	0	20	1.00E+08	6.00E+06	0.3337	0.0939	0.0037	0.0367
49	60	0	20	2.00E+08	6.00E+06	0.2822	0.0764	0.0020	0.0379
50	60	0	20	4.00E+08	6.00E+06	0.2325	0.0818	0.0000	0.0392
51	60	0	20	6.00E+08	6.00E+06	0.2051	0.0908	0.0000	0.0401
52	60	0	20	8.00E+08	6.00E+06	0.1890	0.0980	0.0000	0.0408
53	60	0	20	1.00E+09	6.00E+06	0.1778	0.1029	0.0000	0.0411
54	60	0	20	2.00E+09	6.00E+06	0.1534	0.1151	0.0000	0.0418
55	60	0	20	4.00E+09	6.00E+06	0.1399	0.1232	0.0000	0.0421
56	60	0	20	6.00E+09	6.00E+06	0.1353	0.1264	0.0000	0.0422
57	60	0	20	1.00E+07	8.00E+06	0.5740	0.5571	0.0038	0.0249
58	60	0	20	2.00E+07	8.00E+06	0.4746	0.3303	0.0034	0.0263
59	60	0	20	4.00E+07	8.00E+06	0.4005	0.1687	0.0029	0.0272
60	60	0	20	6.00E+07	8.00E+06	0.3666	0.1123	0.0025	0.0277
61	60	0	20	8.00E+07	8.00E+06	0.3446	0.0854	0.0022	0.0281
62	60	0	20	1.00E+08	8.00E+06	0.3277	0.0704	0.0018	0.0284
63	60	0	20	2.00E+08	8.00E+06	0.2743	0.0542	0.0008	0.0295
64	60	0	20	4.00E+08	8.00E+06	0.2204	0.0576	0.0000	0.0307
65	60	0	20	6.00E+08	8.00E+06	0.1901	0.0661	0.0000	0.0314
66	60	0	20	8.00E+08	8.00E+06	0.1713	0.0726	0.0000	0.0318
67	60	0	20	1.00E+09	8.00E+06	0.1587	0.0775	0.0000	0.0321
68	60	0	20	2.00E+09	8.00E+06	0.1307	0.0891	0.0000	0.0324
69	60	0	20	4.00E+09	8.00E+06	0.1155	0.0960	0.0000	0.0325
70	60	0	20	6.00E+09	8.00E+06	0.1102	0.0989	0.0000	0.0325
71	60	0	20	1.00E+07	1.00E+07	0.5713	0.5522	0.0027	0.0205
72	60	0	20	2.00E+07	1.00E+07	0.4717	0.3211	0.0023	0.0215
73	60	0	20	4.00E+07	1.00E+07	0.3971	0.1570	0.0019	0.0222
74	60	0	20	6.00E+07	1.00E+07	0.3631	0.0990	0.0016	0.0227
75	60	0	20	8.00E+07	1.00E+07	0.3410	0.0714	0.0014	0.0229
76	60	0	20	1.00E+08	1.00E+07	0.3246	0.0580	0.0013	0.0232
77	60	0	20	2.00E+08	1.00E+07	0.2702	0.0406	0.0007	0.0240
78	60	0	20	4.00E+08	1.00E+07	0.2131	0.0426	0.0000	0.0252
79	60	0	20	6.00E+08	1.00E+07	0.1805	0.0502	0.0000	0.0257
80	60	0	20	8.00E+08	1.00E+07	0.1601	0.0566	0.0000	0.0259
81	60	0	20	1.00E+09	1.00E+07	0.1465	0.0612	0.0000	0.0261
82	60	0	20	2.00E+09	1.00E+07	0.1160	0.0723	0.0000	0.0264
83	60	0	20	4.00E+09	1.00E+07	0.0995	0.0788	0.0000	0.0265
84	60	0	20	6.00E+09	1.00E+07	0.0939	0.0811	0.0000	0.0265

Case No.	B (m)	e (m)	Z (m)	EI kNm	EA kN/m	M^{DRsag}	M^{DRhog}	$M^{\varepsilon ht}$	$M^{\varepsilon hc}$
85	60	0	20	1.00E+07	2.00E+07	0.5666	0.5412	0.0009	0.0107
86	60	0	20	2.00E+07	2.00E+07	0.4664	0.3026	0.0007	0.0111
87	60	0	20	4.00E+07	2.00E+07	0.3898	0.1325	0.0007	0.0116
88	60	0	20	6.00E+07	2.00E+07	0.3566	0.0724	0.0007	0.0118
89	60	0	20	8.00E+07	2.00E+07	0.3354	0.0463	0.0007	0.0120
90	60	0	20	1.00E+08	2.00E+07	0.3191	0.0333	0.0007	0.0121
91	60	0	20	2.00E+08	2.00E+07	0.2644	0.0157	0.0004	0.0127
92	60	0	20	4.00E+08	2.00E+07	0.1998	0.0167	0.0000	0.0133
93	60	0	20	6.00E+08	2.00E+07	0.1612	0.0213	0.0000	0.0135
94	60	0	20	8.00E+08	2.00E+07	0.1369	0.0247	0.0000	0.0135
95	60	0	20	1.00E+09	2.00E+07	0.1208	0.0272	0.0000	0.0136
96	60	0	20	2.00E+09	2.00E+07	0.0844	0.0349	0.0000	0.0136
97	60	0	20	4.00E+09	2.00E+07	0.0645	0.0404	0.0000	0.0137
98	60	0	20	6.00E+09	2.00E+07	0.0577	0.0424	0.0000	0.0137
99	60	0	20	1.00E+07	4.00E+07	0.5657	0.5379	0.0003	0.0055
100	60	0	20	2.00E+07	4.00E+07	0.4612	0.2929	0.0004	0.0058
101	60	0	20	4.00E+07	4.00E+07	0.3857	0.1210	0.0004	0.0060
102	60	0	20	6.00E+07	4.00E+07	0.3537	0.0594	0.0004	0.0061
103	60	0	20	8.00E+07	4.00E+07	0.3328	0.0345	0.0004	0.0062
104	60	0	20	1.00E+08	4.00E+07	0.3176	0.0214	0.0003	0.0062
105	60	0	20	2.00E+08	4.00E+07	0.2647	0.0058	0.0002	0.0065
106	60	0	20	4.00E+08	4.00E+07	0.1963	0.0056	0.0000	0.0068
107	60	0	20	6.00E+08	4.00E+07	0.1532	0.0075	0.0000	0.0069
108	60	0	20	8.00E+08	4.00E+07	0.1265	0.0094	0.0000	0.0069
109	60	0	20	1.00E+09	4.00E+07	0.1085	0.0111	0.0000	0.0069
110	60	0	20	2.00E+09	4.00E+07	0.0680	0.0154	0.0000	0.0069
111	60	0	20	4.00E+09	4.00E+07	0.0457	0.0189	0.0000	0.0069
112	60	0	20	6.00E+09	4.00E+07	0.0380	0.0207	0.0000	0.0069

Table 5.1: Analyses with 60m beam with zero eccentricity with practical range of building stiffness (without building load)

Case No.	B (m)	e (m)	Z (m)	EI kN/m	EA kN/m	M DR sag	M DR hog	$M^{\varepsilon ht}$	$M^{\varepsilon hc}$
1	60	0	20	1.00E+07	1.00E+06	1.0191	0.9341	0.0947	0.3423
2	60	0	20	2.00E+07	1.00E+06	0.9232	0.7183	0.0972	0.3399
3	60	0	20	4.00E+07	1.00E+06	0.8412	0.5993	0.0922	0.3376
4	60	0	20	6.00E+07	1.00E+06	0.7982	0.5669	0.0850	0.3382
5	60	0	20	8.00E+07	1.00E+06	0.7670	0.5589	0.0796	0.3381
6	60	0	20	1.00E+08	1.00E+06	0.7463	0.5558	0.0741	0.3380
7	60	0	20	2.00E+08	1.00E+06	0.6836	0.5832	0.0619	0.3419
8	60	0	20	4.00E+08	1.00E+06	0.6424	0.6150	0.0525	0.3442
9	60	0	20	6.00E+08	1.00E+06	0.6240	0.6306	0.0490	0.3444
10	60	0	20	8.00E+08	1.00E+06	0.6137	0.6415	0.0478	0.3454
11	60	0	20	1.00E+09	1.00E+06	0.6070	0.6476	0.0472	0.3458
12	60	0	20	2.00E+09	1.00E+06	0.5948	0.6615	0.0465	0.3464
13	60	0	20	4.00E+09	1.00E+06	0.5869	0.6691	0.0466	0.3462
14	60	0	20	6.00E+09	1.00E+06	0.5843	0.6712	0.0459	0.3462
15	60	0	20	1.00E+07	2.00E+06	1.0079	0.7878	0.0000	0.0812
16	60	0	20	2.00E+07	2.00E+06	0.8875	0.5077	0.0516	0.2027
17	60	0	20	4.00E+07	2.00E+06	0.7937	0.3404	0.0498	0.2024
18	60	0	20	6.00E+07	2.00E+06	0.7374	0.2923	0.0433	0.2039
19	60	0	20	8.00E+07	2.00E+06	0.6967	0.2759	0.0382	0.2056
20	60	0	20	1.00E+08	2.00E+06	0.6652	0.2747	0.0342	0.2068
21	60	0	20	2.00E+08	2.00E+06	0.5662	0.3006	0.0249	0.2128
22	60	0	20	4.00E+08	2.00E+06	0.4843	0.3405	0.0219	0.2166
23	60	0	20	6.00E+08	2.00E+06	0.4504	0.3582	0.0209	0.2171
24	60	0	20	8.00E+08	2.00E+06	0.4303	0.3697	0.0207	0.2171
25	60	0	20	1.00E+09	2.00E+06	0.4205	0.3767	0.0209	0.2176
26	60	0	20	2.00E+09	2.00E+06	0.3960	0.3945	0.0209	0.2177
27	60	0	20	4.00E+09	2.00E+06	0.3843	0.4047	0.0214	0.2180
28	60	0	20	6.00E+09	2.00E+06	0.3798	0.4080	0.0215	0.2182
29	60	0	20	1.00E+07	4.00E+06	0.9958	0.7019	0.0000	0.0468
30	60	0	20	2.00E+07	4.00E+06	0.8795	0.3721	0.0000	0.0455
31	60	0	20	4.00E+07	4.00E+06	0.7800	0.1823	0.0000	0.0433
32	60	0	20	6.00E+07	4.00E+06	0.7132	0.1426	0.0212	0.1140
33	60	0	20	8.00E+07	4.00E+06	0.6678	0.1245	0.0170	0.1156
34	60	0	20	1.00E+08	4.00E+06	0.6284	0.1195	0.0150	0.1171
35	60	0	20	2.00E+08	4.00E+06	0.4928	0.1365	0.0106	0.1219
36	60	0	20	4.00E+08	4.00E+06	0.3718	0.1728	0.0093	0.1238
37	60	0	20	6.00E+08	4.00E+06	0.3243	0.1904	0.0095	0.1238
38	60	0	20	8.00E+08	4.00E+06	0.2998	0.2004	0.0098	0.1240
39	60	0	20	1.00E+09	4.00E+06	0.2840	0.2072	0.0100	0.1241
40	60	0	20	2.00E+09	4.00E+06	0.2522	0.2211	0.0100	0.1241
41	60	0	20	4.00E+09	4.00E+06	0.2352	0.2303	0.0104	0.1241
42	60	0	20	6.00E+09	4.00E+06	0.2290	0.2340	0.0104	0.1241

Case No.	B (m)	e (m)	Z (m)	EI kN/m	EA kN/m	M DR sag	M DR hog	$M^{\varepsilon_{ht}}$	$M^{\varepsilon_{hc}}$
43	60	0	20	1.00E+07	6.00E+06	0.9975	0.6720	0.0000	0.0328
44	60	0	20	2.00E+07	6.00E+06	0.8747	0.3282	0.0000	0.0318
45	60	0	20	4.00E+07	6.00E+06	0.7751	0.1379	0.0000	0.0303
46	60	0	20	6.00E+07	6.00E+06	0.7117	0.0923	0.0136	0.0795
47	60	0	20	8.00E+07	6.00E+06	0.6646	0.0727	0.0110	0.0806
48	60	0	20	1.00E+08	6.00E+06	0.6238	0.0657	0.0110	0.0806
49	60	0	20	2.00E+08	6.00E+06	0.4677	0.0789	0.0064	0.0858
50	60	0	20	4.00E+08	6.00E+06	0.3292	0.1093	0.0058	0.0867
51	60	0	20	6.00E+08	6.00E+06	0.2756	0.1250	0.0064	0.0869
52	60	0	20	8.00E+08	6.00E+06	0.2474	0.1336	0.0065	0.0867
53	60	0	20	1.00E+09	6.00E+06	0.2293	0.1398	0.0066	0.0866
54	60	0	20	2.00E+09	6.00E+06	0.1923	0.1531	0.0066	0.0867
55	60	0	20	4.00E+09	6.00E+06	0.1735	0.1605	0.0070	0.0865
56	60	0	20	6.00E+09	6.00E+06	0.1670	0.1642	0.0070	0.0867
57	60	0	20	1.00E+07	8.00E+06	0.9957	0.6585	0.0000	0.0252
58	60	0	20	2.00E+07	8.00E+06	0.8714	0.3014	0.0000	0.0245
59	60	0	20	4.00E+07	8.00E+06	0.7752	0.1118	0.0000	0.0233
60	60	0	20	6.00E+07	8.00E+06	0.7168	0.0640	0.0000	0.0224
61	60	0	20	8.00E+07	8.00E+06	0.6666	0.0496	0.0077	0.0620
62	60	0	20	1.00E+08	8.00E+06	0.6244	0.0449	0.0066	0.0630
63	60	0	20	2.00E+08	8.00E+06	0.4571	0.0545	0.0047	0.0659
64	60	0	20	4.00E+08	8.00E+06	0.3086	0.0760	0.0045	0.0668
65	60	0	20	6.00E+08	8.00E+06	0.2499	0.0899	0.0047	0.0667
66	60	0	20	8.00E+08	8.00E+06	0.2195	0.0982	0.0047	0.0667
67	60	0	20	1.00E+09	8.00E+06	0.2003	0.1034	0.0048	0.0667
68	60	0	20	2.00E+09	8.00E+06	0.1608	0.1163	0.0000	0.0182
69	60	0	20	4.00E+09	8.00E+06	0.1400	0.1230	0.0000	0.0181
70	60	0	20	6.00E+09	8.00E+06	0.1334	0.1257	0.0000	0.0180
71	60	0	20	1.00E+07	1.00E+07	0.9950	0.6497	0.0000	0.0205
72	60	0	20	2.00E+07	1.00E+07	0.8704	0.2850	0.0000	0.0199
73	60	0	20	4.00E+07	1.00E+07	0.7746	0.0984	0.0000	0.0190
74	60	0	20	6.00E+07	1.00E+07	0.7185	0.0497	0.0000	0.0182
75	60	0	20	8.00E+07	1.00E+07	0.6679	0.0375	0.0060	0.0504
76	60	0	20	1.00E+08	1.00E+07	0.6251	0.0325	0.0051	0.0511
77	60	0	20	2.00E+08	1.00E+07	0.4519	0.0395	0.0036	0.0536
78	60	0	20	4.00E+08	1.00E+07	0.2959	0.0573	0.0036	0.0542
79	60	0	20	6.00E+08	1.00E+07	0.2349	0.0682	0.0037	0.0542
80	60	0	20	8.00E+08	1.00E+07	0.2023	0.0758	0.0037	0.0542
81	60	0	20	1.00E+09	1.00E+07	0.1820	0.0808	0.0038	0.0542
82	60	0	20	2.00E+09	1.00E+07	0.1408	0.0928	0.0000	0.0147
83	60	0	20	4.00E+09	1.00E+07	0.1191	0.0993	0.0000	0.0146
84	60	0	20	6.00E+09	1.00E+07	0.1118	0.1015	0.0000	0.0146

Case No.	B (m)	e (m)	Z (m)	EI kN/m	EA kN/m	M DR sag	M DR hog	$M^{\varepsilon_{ht}}$	$M^{\varepsilon_{hc}}$
85	60	0	20	1.00E+07	2.00E+07	0.9939	0.6211	0.0000	0.0105
86	60	0	20	2.00E+07	2.00E+07	0.8692	0.2588	0.0000	0.0103
87	60	0	20	4.00E+07	2.00E+07	0.7718	0.0731	0.0000	0.0098
88	60	0	20	6.00E+07	2.00E+07	0.7190	0.0289	0.0000	0.0094
89	60	0	20	8.00E+07	2.00E+07	0.6663	0.0143	0.0000	0.0091
90	60	0	20	1.00E+08	2.00E+07	0.6289	0.0102	0.0000	0.0089
91	60	0	20	2.00E+08	2.00E+07	0.4475	0.0129	0.0018	0.0277
92	60	0	20	4.00E+08	2.00E+07	0.2686	0.0223	0.0017	0.0279
93	60	0	20	6.00E+08	2.00E+07	0.2053	0.0285	0.0018	0.0279
94	60	0	20	8.00E+08	2.00E+07	0.1686	0.0321	0.0000	0.0077
95	60	0	20	1.00E+09	2.00E+07	0.1456	0.0346	0.0000	0.0077
96	60	0	20	2.00E+09	2.00E+07	0.0986	0.0435	0.0000	0.0075
97	60	0	20	4.00E+09	2.00E+07	0.0748	0.0489	0.0000	0.0075
98	60	0	20	6.00E+09	2.00E+07	0.0668	0.0509	0.0000	0.0074
99	60	0	20	1.00E+07	4.00E+07	0.9934	0.6157	0.0000	0.0054
100	60	0	20	2.00E+07	4.00E+07	0.8604	0.2450	0.0000	0.0052
101	60	0	20	4.00E+07	4.00E+07	0.7730	0.0596	0.0000	0.0050
102	60	0	20	6.00E+07	4.00E+07	0.7167	0.0200	0.0000	0.0048
103	60	0	20	8.00E+07	4.00E+07	0.6777	0.0064	0.0000	0.0046
104	60	0	20	1.00E+08	4.00E+07	0.6372	0.0036	0.0000	0.0045
105	60	0	20	2.00E+08	4.00E+07	0.4497	0.0043	0.0009	0.0141
106	60	0	20	4.00E+08	4.00E+07	0.2677	0.0078	0.0008	0.0142
107	60	0	20	6.00E+08	4.00E+07	0.1934	0.0095	0.0000	0.0039
108	60	0	20	8.00E+08	4.00E+07	0.1538	0.0123	0.0000	0.0039
109	60	0	20	1.00E+09	4.00E+07	0.1288	0.0140	0.0000	0.0039
110	60	0	20	2.00E+09	4.00E+07	0.0776	0.0183	0.0000	0.0038
111	60	0	20	4.00E+09	4.00E+07	0.0516	0.0225	0.0000	0.0038
112	60	0	20	6.00E+09	4.00E+07	0.0430	0.0242	0.0000	0.0037

Table 5.2: Analyses with 60m beam with zero eccentricity with practical range of building stiffness (with building load)

Figure 5.4 shows the variation of modification factors for deflection ratios (M^{DRsag} and M^{DRhog}, for sagging and hogging zones, respectively) and horizontal strain ($M^{\varepsilon_{hc}}$ and $M^{\varepsilon_{ht}}$, for compression and tension zones, respectively) as functions of the bending and axial stiffness of the structure. From Figure 5.4(a) and (b), it is evident that the bending

stiffness is the dominant parameter affecting the modification factors for deflection ratios in both sagging and hogging zones. The values of M^{DR} for sagging and hogging range from 0.5 to 0.05 and from 0.35 to below 0.05 respectively for 1- to 10-storey buildings. Figure 5.4 (c) and Figure 5.4(d) show that the modification factors for horizontal tensile and compressive strains within the range of practical bending and axial stiffness are only affected by axial stiffness. The values of M^{ε} for tension are very small (below 0.01) and those for compression range from 0.03 to below 0.01 for 1- to 10-storey building.

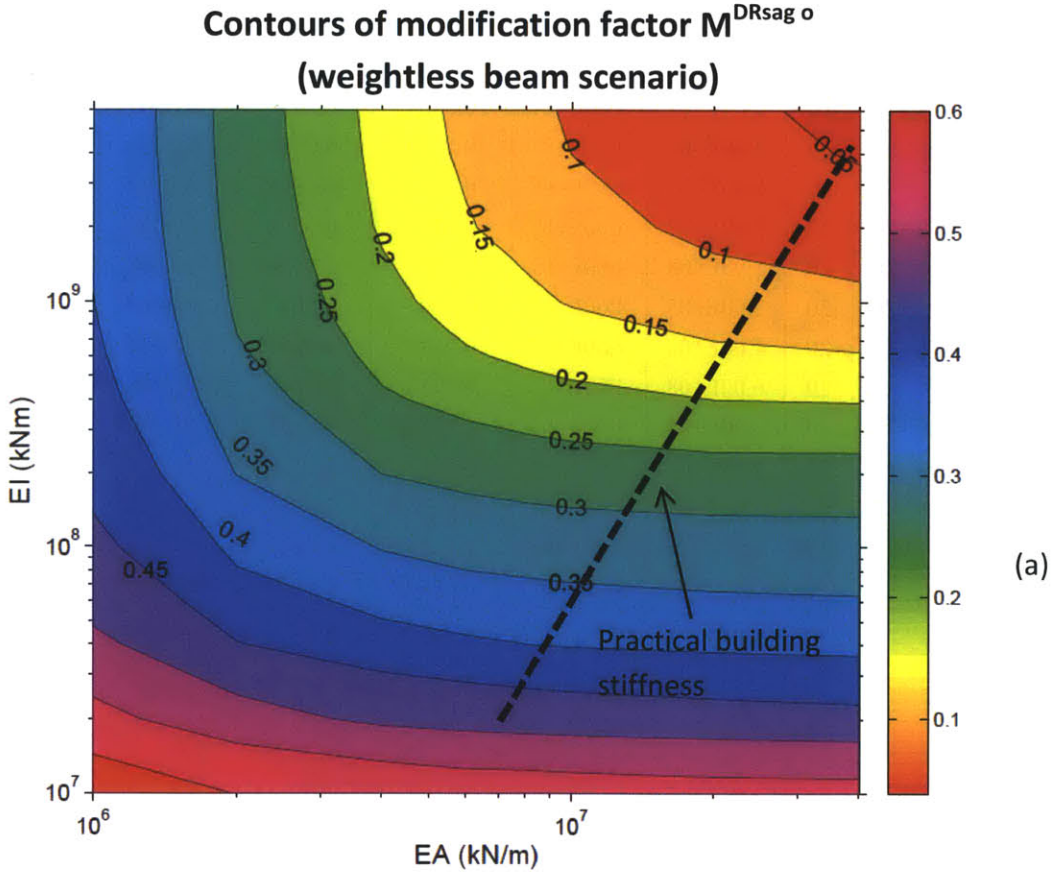

(a)

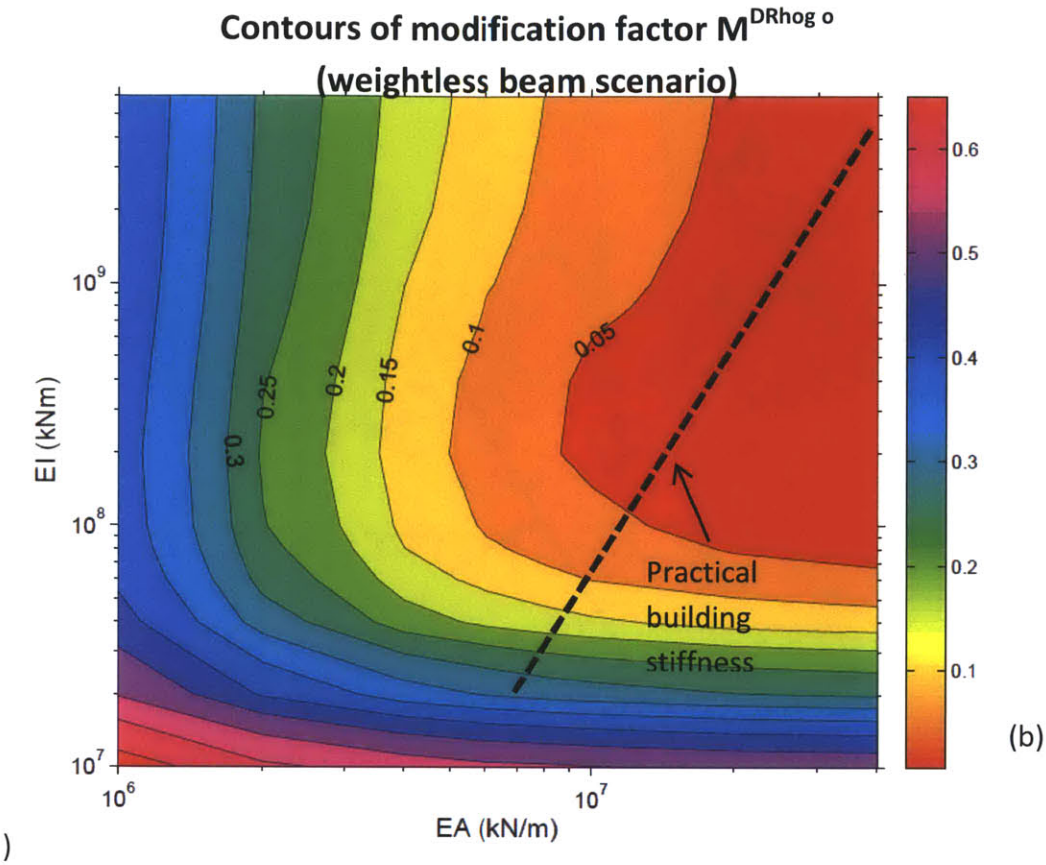
Contours of modification factor M^DRhog o
(weightless beam scenario)
EI (kNm)
EA (kN/m)
0.3
0.25
0.2
0.15
0.1
0.05
Practical
building
stiffness
0.6
0.5
0.4
0.3
0.2
0.1

(b)

)

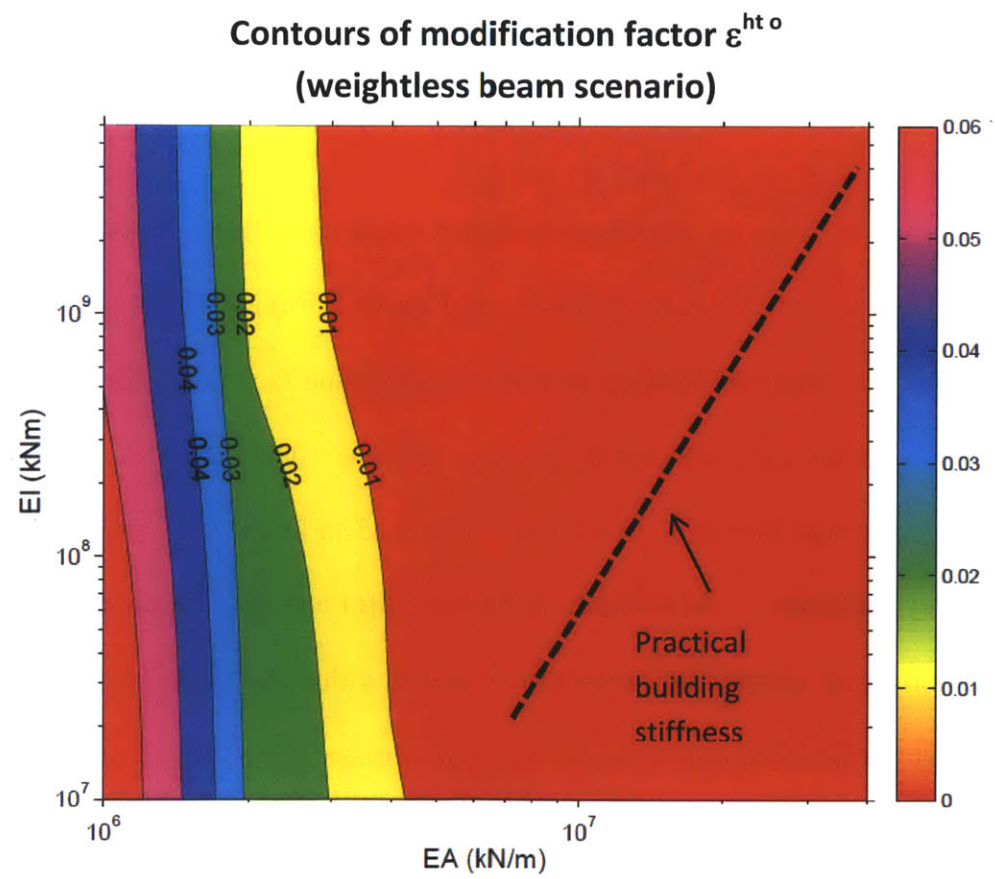
Contours of modification factor ε^ht o
(weightless beam scenario)
EI (kNm)
EA (kN/m)
0.04
0.03
0.02
0.01
Practical
building
stiffness
0.06
0.05
0.04
0.03
0.02
0.01
0

(c)

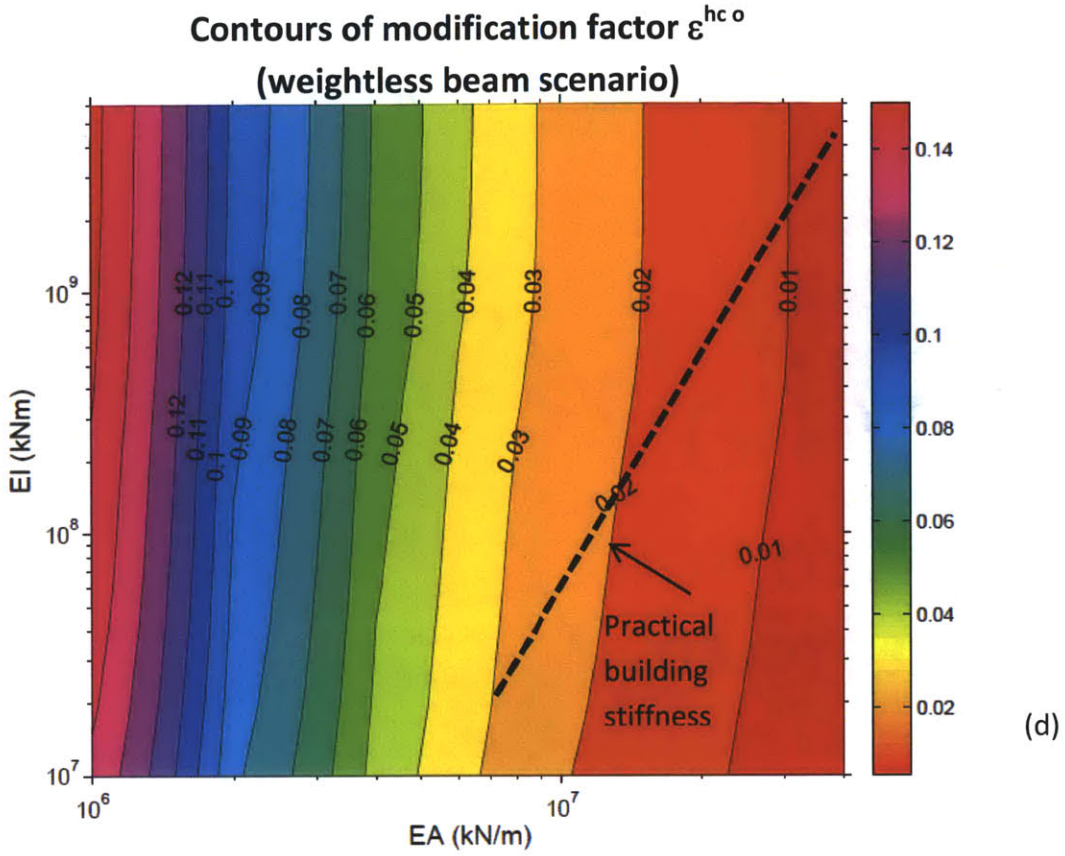

Figure 5.4: Contour plot for modification factors for zero-load cases: (a) $M^{DRsag\ o}$; (b) $M^{DRhog\ o}$; (c) $M^{\varepsilon ht\ o}$; (d) $M^{\varepsilon hc\ o}$

Figure 5.5 shows the variation of modification factors when the self-weight (surcharge effect) of the building is included in the analyses. In Figures 5.5(a) and (b), it is evident that within the practical range of building stiffness, modification factors M^{ε} for sagging and hogging are generally only affected by bending stiffness. The values of M^{DR} for sagging and hogging range from 0.87 to 0.06 and from 0.35 to below 0.05 respectively for 1- to 10-storey buildings. In contrast, in Figure 5.5(c) and (d), the modification factors M^{ε} for horizontal tensile and compressive strains within the range of practical bending and axial stiffness are only affected by axial stiffness. The values of $M\varepsilon$ for tension are very small (below 0.01) and that for compression range from 0.05 to below 0.02 respectively for 1- to 10-storey building.

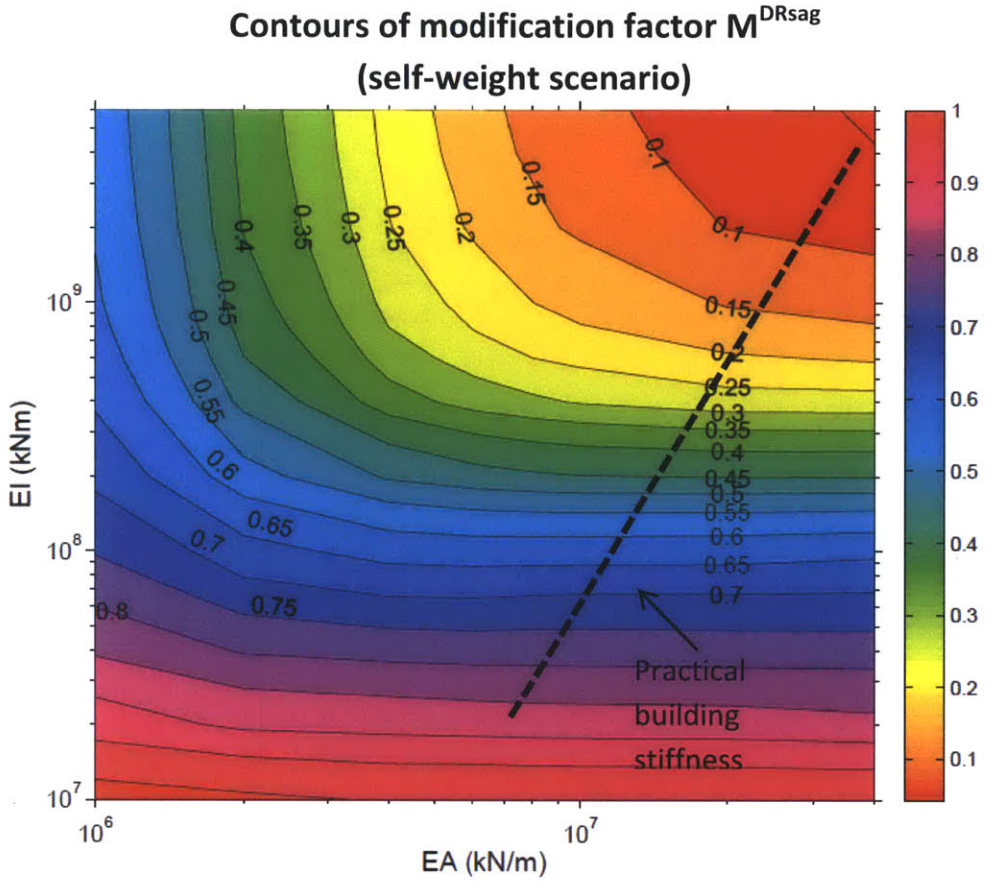
Contours of modification factor M^DRsag
(self-weight scenario)
EI (kNm)
EA (kN/m)
Practical
building
stiffness

(a)

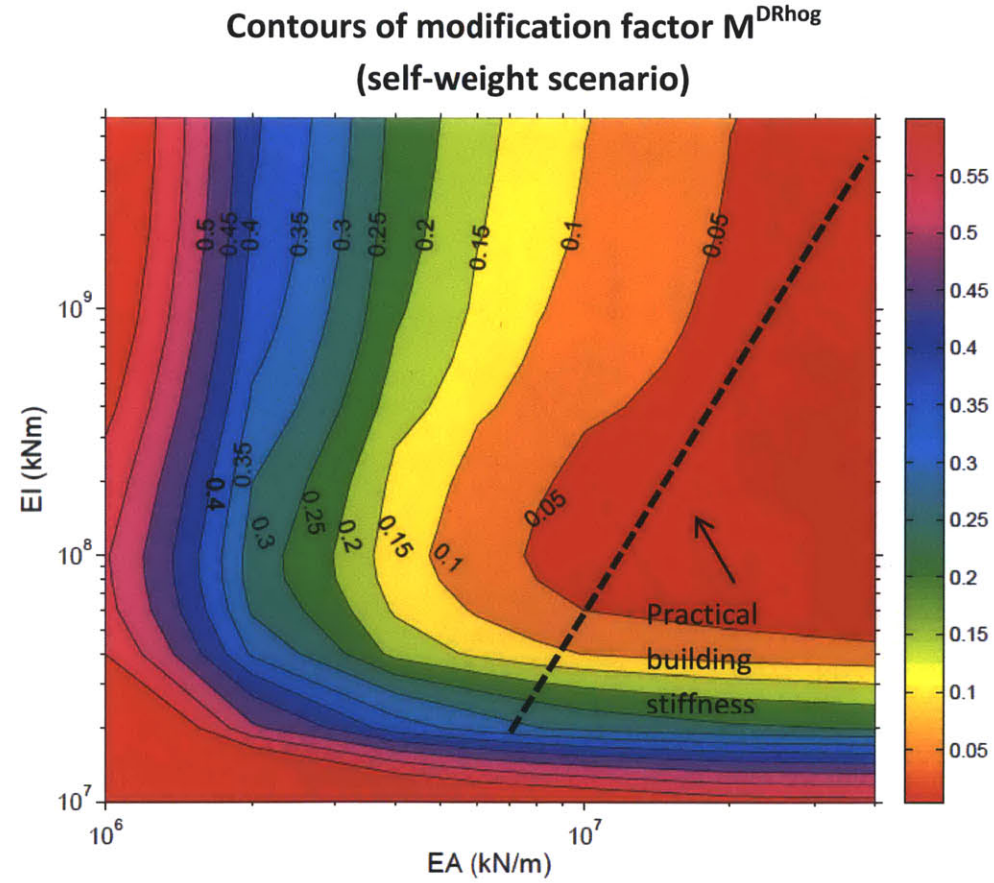
Contours of modification factor M^DRhog
(self-weight scenario)
EI (kNm)
EA (kN/m)
Practical
building
stiffness

(b)

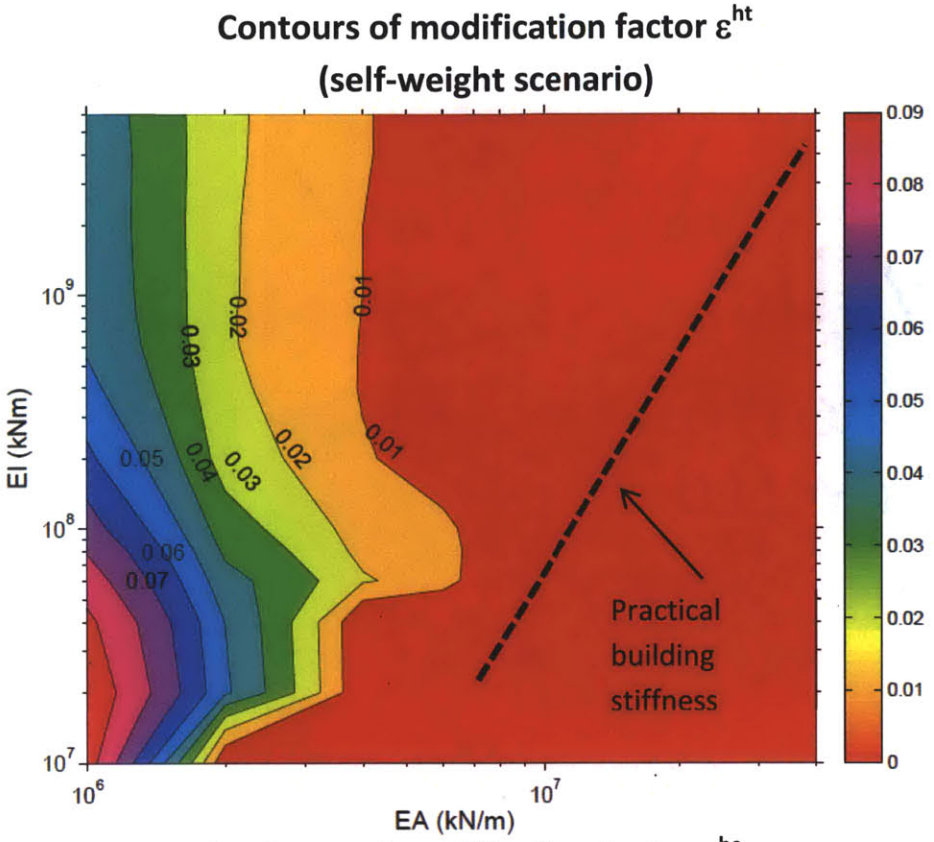

(c)

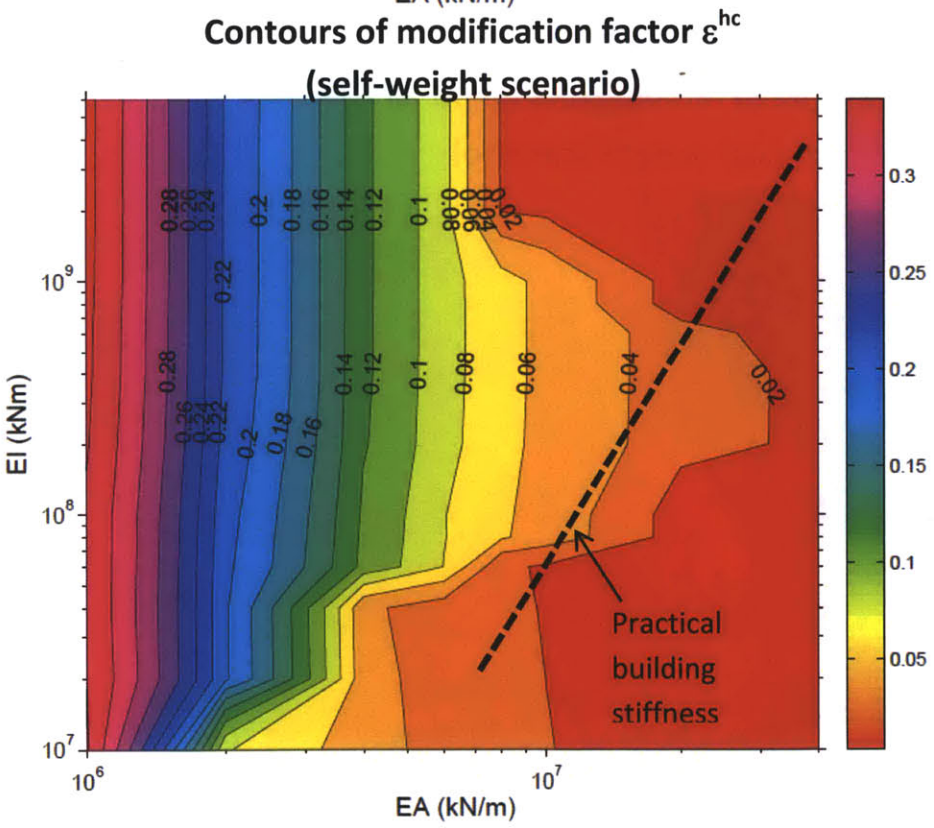

(d)

Figure 5.5 : Contour plot for modification factors for 50 kPa cases: (a) M^{DRsag}; (b) M^{DRhog}; (c) $M^{\varepsilon ht}$; (d) $M^{\varepsilon hc}$

Figure 5.6 summarizes the influence of the surcharge by plotting the ratios of the four modification factors with and without building surcharge. In Figure 5.6(a), it is evident that the modification factor M^{DRsag} for the 50kPa scenario is larger than that for the zero-load scenario (in the ratio of 1.2 to 1.95) within the range of practical building stiffness. In Figure 5.6(b), it is observed that for low building stiffness (1 to 2-storey), the modification factor M^{DRhog} for the 50kPa scenario is less than the zero-load scenario, while for high building stiffness (above 2-storey), the modification factor M^{DRhog} for the 50kPa scenario is larger than that for the zero-load scenario (in the ratio of 1 to around 1.3). It can therefore be concluded that deriving modification factors M^{DRsag} without considering building load is non-conservative for all practical building stiffness. Estimation of the modification factor M^{DRhog} without considering building load is generally non-conservative except for very low building stiffness (2-storey or below). In Figure 5.6(c), it is shown that the ratio of modification factors for horizontal strain in tension $M^{\varepsilon t}$ for the 50kPa scenario to the zero-load scenario is highest for 2-storey buildings (in the ratio of around 5). However, the ratio is less than unity for all other practical stiffness (1-, 5-, 8- and 10-storey). In Figure 5.6(d), it is shown that the ratio of modification factors for horizontal strain in compression $M^{\varepsilon c}$ is larger than unity for 1- to 5-storey buildings and that for 5- to 10-storey buildings is smaller than unity. It can therefore be concluded that deriving modification factors for horizontal strain for tension and compression $M^{\varepsilon t}$ and $M^{\varepsilon c}$ without considering building load is generally non-conservative for building stiffness between 1- to 5-storey..

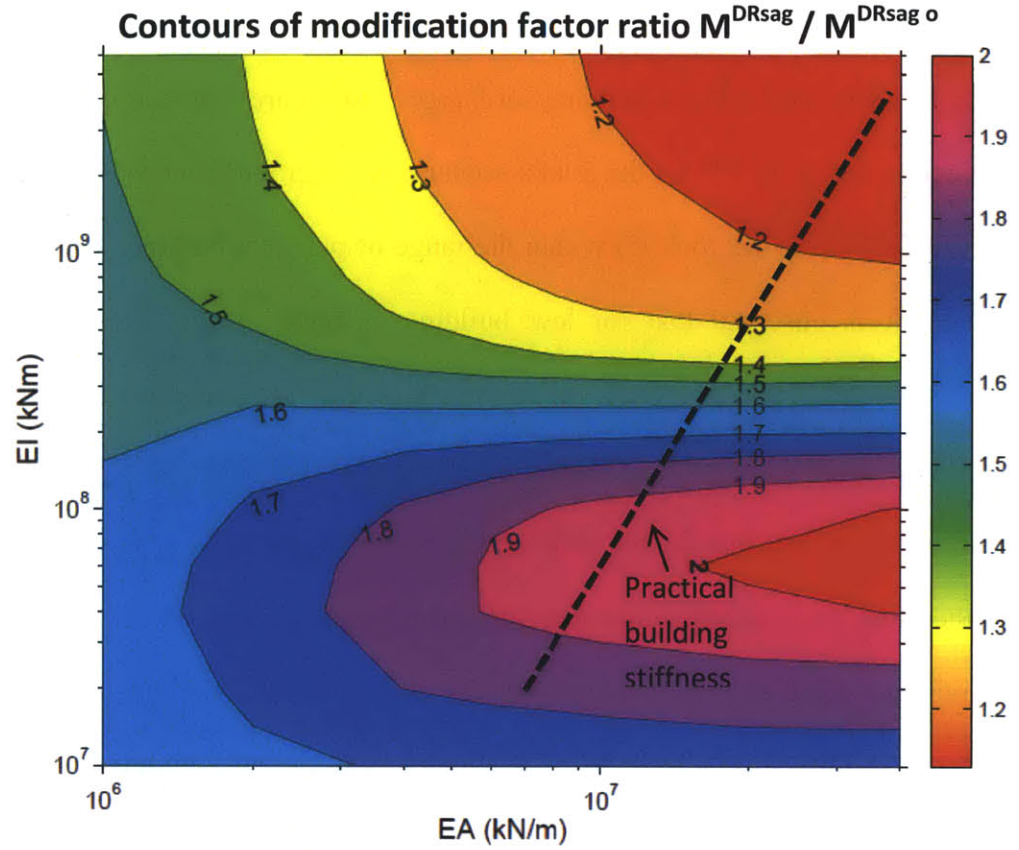
Contours of modification factor ratio M^{DRsag} / $M^{DRsag\ o}$
EI (kNm)
EA (kN/m)
Practical building stiffness

(a)

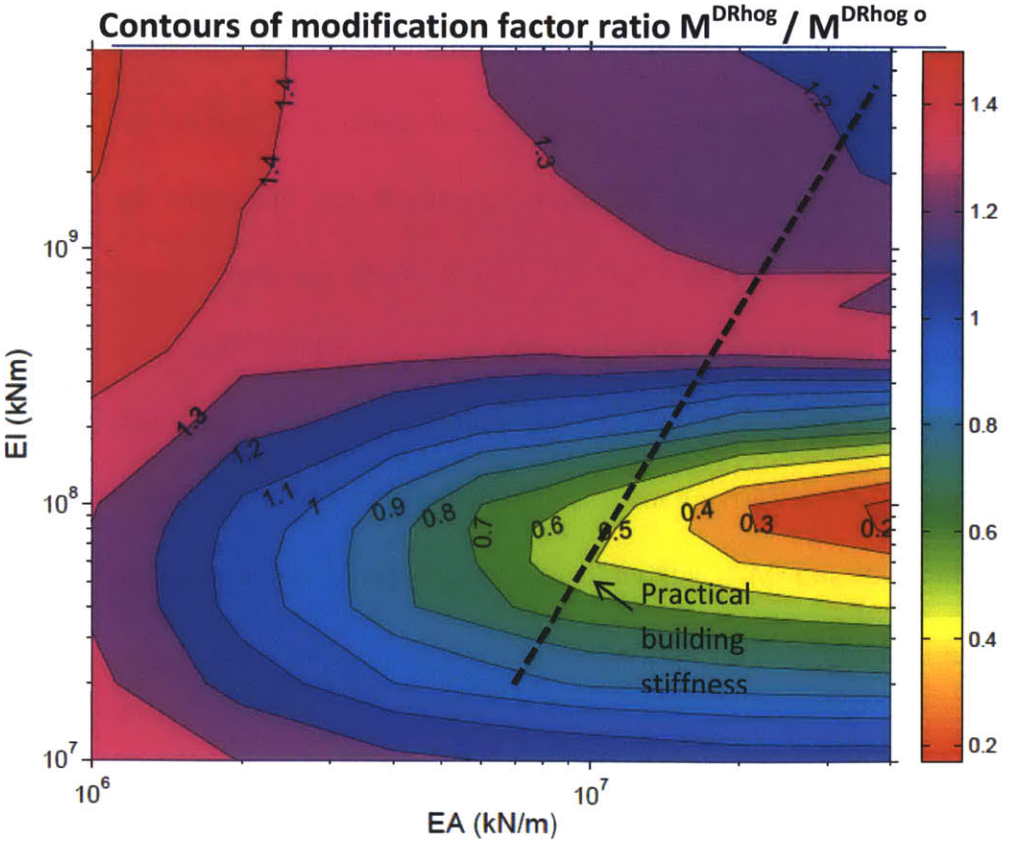
Contours of modification factor ratio M^{DRhog} / $M^{DRhog\ o}$
EI (kNm)
EA (kN/m)
Practical building stiffness

(b)

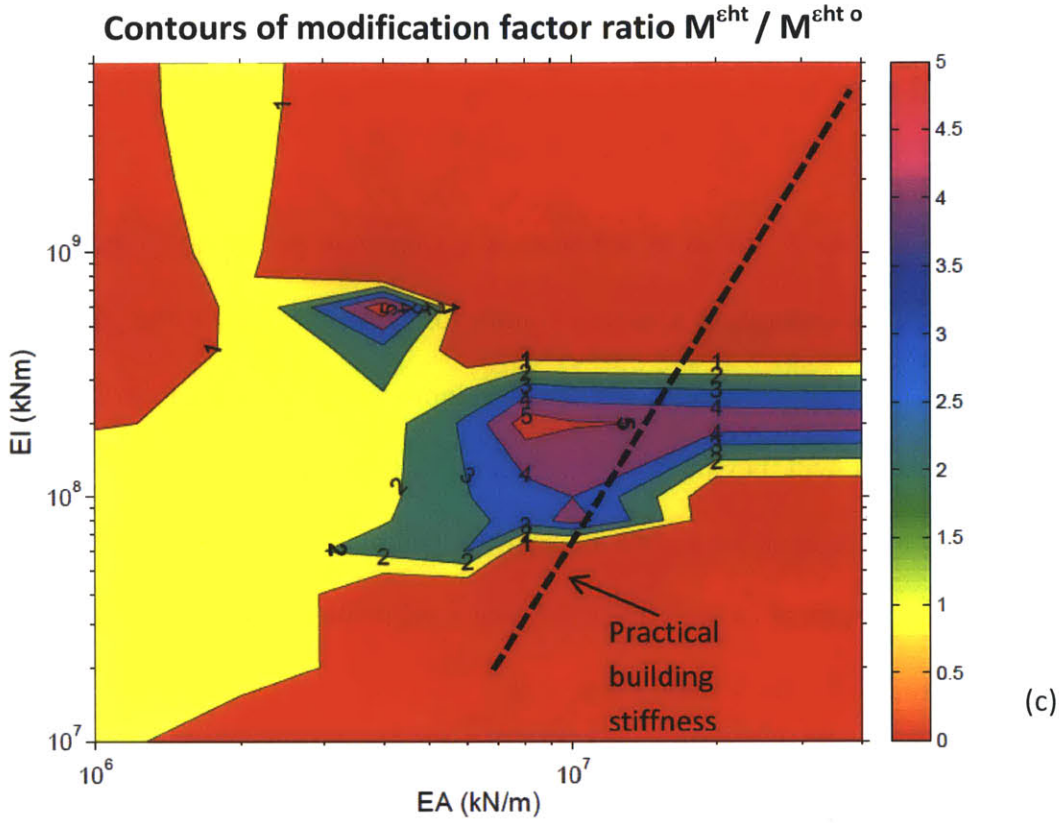

Figure 5.6: Contour plot for ratio of modification factors for 50 kPa to zero load cases: (a) $M^{DRsag} / M^{DRsag\ o}$; (b) $M^{DRhog} / M^{DRhog\ o}$; (c) $M^{\varepsilon ht} / M^{\varepsilon ht\ o}$; (d) $M^{\varepsilon hc} / M^{\varepsilon hc\ o}$

5.5 Volume Loss

As all analyses in this study are set to terminate at a consistent percentage reduction of the initial stress that corresponds to a surface volume loss, $\Delta V_s = 1.5\%$ (for the greenfield case) to represent the field conditions, the actual volume losses obtained from analyses with building surcharge will inevitably cause different surface volume losses. Therefore, the actual volume loss is recorded for all the analyses and plotted against the calculating maximum surface settlement as well as calculating modification factors obtained from this study in Figure 5.7, Figure 5.8 and Figure 5.9:

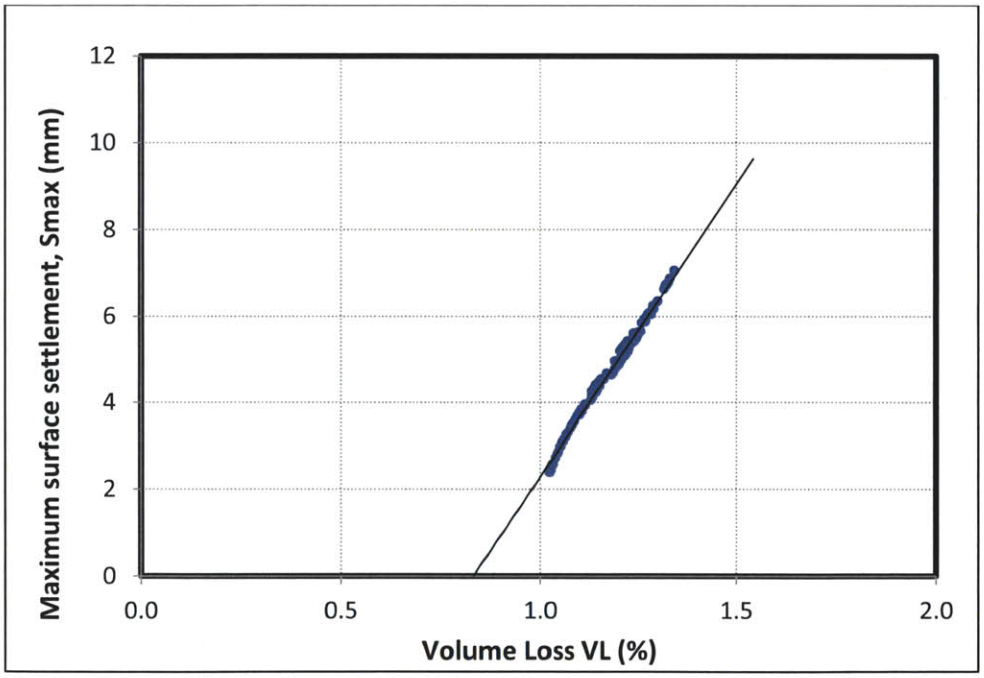

Figure 5.7: Variation of maximum surface settlement and volume loss

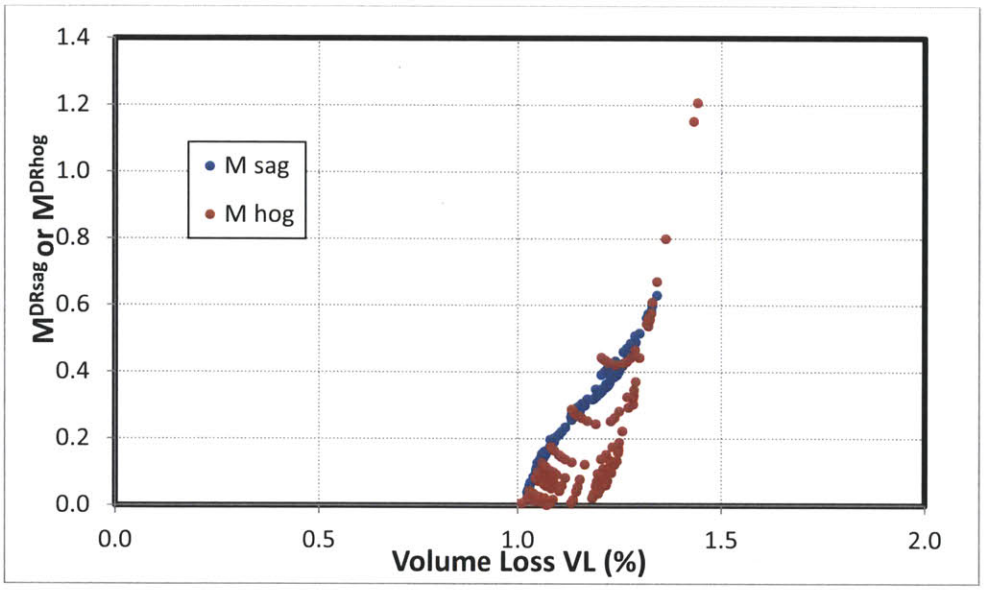

Figure 5.8: Variation of volume loss with modification factors for deflection ratio

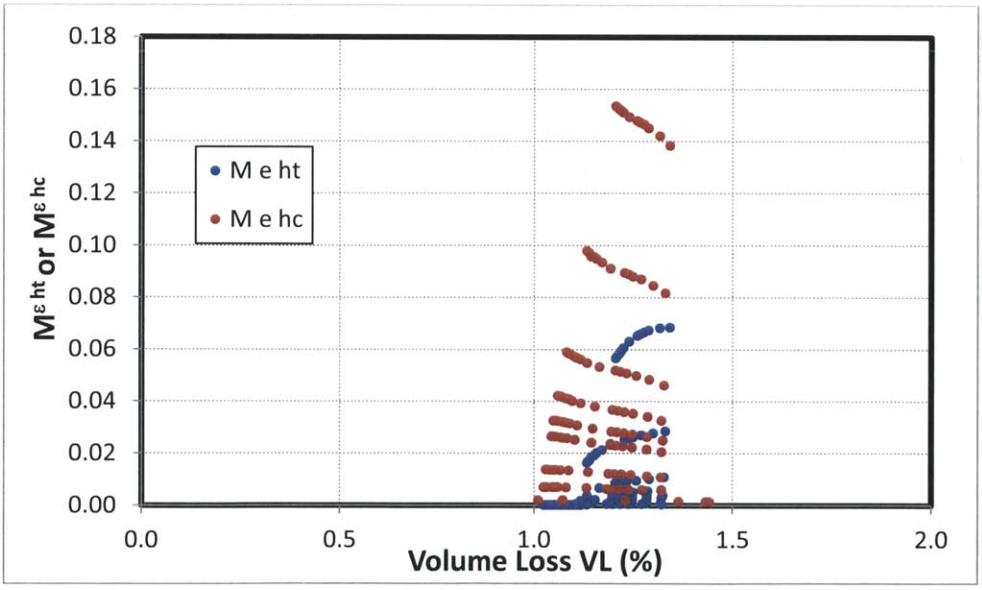

Figure 5.9: Variation of volume loss with modification factors for horizontal strain

Although Figure 5.7 agrees with the results of Potts and Addenbrooke (1997) in that the magnitude of maximum settlement is proportional to volume loss, Figure 5.8 and Figure 5.9 clearly show that the modification factors (for both deflection ratio and horizontal strain) obtained from numerical analyses in this study are not linearly correlated to the volume loss. Therefore, these authors' use of linear extrapolation (based on maximum settlement) is not justified for computing the modification factors. The current analyses made no correction to the results obtained from the numerical analysis so that the results will represent a consistent percentage reduction of the initial stress (fixed β value).

5.6 Conclusions

A total of 112 finite element analyses were carried out for zero-load and 50kPa bulding load respectively to evaluate the influence of building weight on ground movements. Based on the results of these analyses, it is concluded that calculating modification factors without considering building loads is non-conservative for:

(1) For M^{DRsag} – non-conservative for all practical building stiffness

(2) For M^{DRhog} – non-conservative for building higher than 2-storey

(3) For $M^{\varepsilon t}$ – non-conservative for building of 1- to 5- storey

(4) For $M^{\varepsilon c}$ – non-conservative for building of 1- to 5- storey

It is found that neglecting building load can result in non-conservative estimate of modification factors for deflection ratio and horizontal strain for a significant range of practical building stiffness. It is therefore considered that the effect of building weight

cannot be neglected when the boundary effect of building stiffness on the ground is used as a tool to reduce the estimated values of greenfield settlement trough or deflection ratio and horizontal strain of existing buildings in a building damage assessment.

6 Summary and Conclusions

6.1 Summary

The goal of the current study is to assess the influence of an existing structure on tunneling-induced ground movements. This is accomplished through 2D numerical simulations that are compared with similar prior studies reported by Potts and Addenbrooke (1997). The current study uses the Plaxis finite element code together with the hardening soil (HS and HSS) family of constitutive models in order to represent the undrained shear behavior of clay.

Two scenarios of building load conditions: (1) weightless beam (building); (2) assuming uniform surcharge of 50 kPa above the beam (representing building self-weight), are considered. The first scenario is discussed in Chapter 4. 48 finite element analyses were carried out for a wide range of building axial and bending stiffness EA and EI, and the focus was to compare the modification factors for deflection and horizontal strain obtained using Hardening Soil Small (HSS) model with the results of Potts and Addenbrooke (1997) who used a non-linear elastic model (PJ model by Jardine et al., 1986). The second scenario was discussed in Chapter 5. 112 finite element analyses were carried for a grid of EA and EI covering the practical values of stiffness for 1- to 10-storey buildings for both the weightless and the self-weight loading conditions, and the focus was to assess whether assuming weightless structure in calculating modification factors is a conservative approach to assess tunneling-induced ground movements and building damage. Before these finite element analyses were carried out, in Chapter 3,

the input parameters of the hardening soil family of constitution models were calibrated for the case of London clay and compared with results of Potts and Addenbrooke (1997), in order to identify a hardening soil family of constitutive model that matches the stiffness behavior simulated in Potts and Addenbrooke (1997) to enable a direct comparison. The fitted hardening soil family of constitution model was used to estimate the greenfield settlement trough resulting from a tunnel excavation, which was compared with the empirical settlement trough.

6.2 Conclusions

As the calculating modification factors in this study are obtained by dividing the calculating deflection ratio and horizontal strain by its greenfield value, it is crucial that the soil model used in assessing the modification factors for deflection ratio and horizontal strain is capable of estimating an accurate greenfield settlement trough. Based on the results of the numerical analyses conducted in this study, the greenfield settlement trough obtained by the best-fitted HSS model is found to be narrower and fits the empirical trough better than the prior study, and this forms an important bearing for using HSS model to conduct the numerical analyses in the current study. The results also indicated that the choice of soil model has an important influence on the prediction of greenfield ground settlement.

Based on the 48 finite element analyses conducted for the weightless building scenario, the modification factors deviated from the results in Potts and Addenbrooke (1997) in

different extent. However, it was found that modification factors for practical values of bending and axial stiffness obtained in this study still fall within the design curves promulgated in Potts and Addenbrooke (1997). It is therefore concluded that the design curves (for zero eccentricity) of modification factors for deflection ratios (in both the sagging and hogging modes) and horizontal strains (in both tension and compression) in Potts and Addenbrooke (1997) provide a reasonable first estimate of the effects of soil-structure interaction.

Based on the 112 finite element analyses conducted for both the weightless and the building self-weight scenarios in the range of practical building stiffness (1- to 10-storey), it is found that neglecting building load can result in non-conservative estimate of modification factors for deflection ratios and horizontal strains for a significant range of practical building stiffness. It is therefore considered that the effect of building weight cannot be neglected when the boundary effect of building stiffness on the ground is used as a tool to reduce the estimated values of greenfield settlement trough or deflection ratio and horizontal strain of existing buildings in a building damage assessment.

References

1. Attewell P.B. (1978). "Ground movements caused by tunneling in soil," Proceeding of Conference of Large Movements and Structures," Cardiff, Pentech Press (1978), p. 812-948.

2. Benz T. (2006). Small-strain stiffness of soils and its numerical consequences. Ph.D. Thesis, University Stuttgart.

3. Boscardin M.D. and Cording E.G. (1989). "Building response to excavation-induced settlement," Journal Geo Engrg, ASCE, 115;1;1-21.

4. Burland J.B., Broms B.B. and de Mello, V.F.B. (1977). "Behavior of foundations and structures," – SOR Review, Session 2, Proc. 7th European Conf on SMandFE, Brighton, 1;13-29.

5. Burland J.B. (1995). "Assessment of risk of damage to buildings due to tunneling and excavation," Earthquake Geotechnical Engineering, Ishihara (ed). Balkema, Rotterdam.

6. Burland J.B. and Wroth C.P. (1974). "Settlement of buildings and associated damage," Settlement of structures, BGS conference, Cambridge, 1974, p. 611-651.

7. Cording E. J. and Hansmire W. H. (1975) "Displacements around soft ground tunnels," General Report 5th Pan American Conference on Soil Mechanics and Foundation Engineering Buenos Aires, Session IV, 571-632.

8. Zymnis D.M. (2007). Evaluation of analytical mehods to interpret ground deformations due to soft ground tunneling. MSc Thesis, MIT.

9. Dimmock P.S. and Mair R.J. (2008). "Effect of building stiffness on tunneling-induced ground movement," Tunneling and Underground Space Technology 23 (1008) p.438-450.

10. Franzius J.N. (2003). Behaviour of buildings due to tunnel induced subsidence. PhD Thesis, Imperial College.

11. Franzius J.N., Potts D.M., Addenbrooke T.I., Burland J.B. (2004). "The influence of building weight on tunneling-induced ground and building deformation," Soils and Foundations, Vol 44, No. 1, 25-28, Feb. 2004, Japanese Geotechnical society.

12. Franzius J.N., Potts D.M. and Burland J.B. (2005). "The influence of soil anisotropy and K_0 on ground surface movement resulting from tunnel excavation," Geotechnique 55, No. 3, 189-199.

13. Fraser R.A. and Wardle L.J. (1976). "Numerical analysis of rectangular rafts on layred foundations," Geotechnique, 1976, 26, No.4, 613-630.

14. Jardine R.J., Potts D.N., Fourie A.B. and Burland J.B. "Studies of the influence of non-linear stress-strain characteristics in soil-structure interaction," Geotehnique, 1986, 36, No. 3, 377-396.

15. Kimura T and Mair, RJ (1981). "Centrifugal testing of model tunnels in soft clay," the 10th International Conference on Soil Mechanics and Foundation Engineering, 15-6-1981 to 19-6-1981, Stockholm, Sweden pp. 319-322.

16. Kusakabe O., Fujita K. and Miyazaki Y. (1999). "Ground and structure response to a hand driven decline in London clay," International Symposium on Geotechnical Aspects of Underground Construction in Soft Ground (IS-Tokyo 99), Tokyo, Japan, p.75-80.

17. Leca and New (2007). "Settlements induced by tunneling in Soft Ground," Tunneling and Underground Space Technology 22 (2007) 119-149.

18. Macklin, S.R. (1999). "The prediction of volume loss due to tunnelling in overconsolidated clay based on heading geometry and stability number", Ground Engineering, v 32, n 4, p 30-33, 1999.

19. Mair, R.J. and Taylor, R.N. (1997) "Bored tunnelling in the urban environment," Proc. 14th Intl. Conf. Soil Mechs. and Found. Engrg, Hamburg, (4), 2353-2385.

20. Marto (1958) "Concerning an approimatae equation of subsidence trough and its time factors," International strata control congress, Leipzig, 191-205.

21. National Coal Board (1975). Subsidence Engineers Handbook. National Coal Board Production Dept., U.K.

22. New and O' Reilly (1991). "Tunneling induced ground movement; predicting their magnitude and effects," 4th International Conference on Ground Movements and Structures. University of Wales college Cardiff, Cardiff, Wales.

23. Peck, R. B. (1969) "Deep excavations and tunneling in soft ground," Proc. 7th International Conference Soil Mechanics and Foundation Engineering, Mexico City, State of the Art Volume, 225-290.

24. Pinto, F. and Whittle, A.J. (2011). "Ground movements due to shallow tunnels in soft ground: 1. Analytical solutions," submitted to ASCE Journal of Geotechnical and Geoenvironmental Engineering.

25. Pinto, F., Zymnis, D. and Whittle, A.J. (2011). "Ground movements due to shallow tunnels in soft ground: 2. Analytical interpretation and prediction," submitted to ASCE Journal of Geotechnical and Geoenvironmental Engineering.

26. Polshin, D.E. and Tokar, R.A. (1957). "Maximum allowable non-uniform settlement of structures," Proc 4th Int Conf SMandFE, London, 1;402.

27. Potts D.M. and Bond A.J. (1994). "Calculation of structural forces for propped retaining walls," Proc. 13th Int. Conf. Soil Mech. and Foundation Engng, New Delhi, 1994, 2, 823 – 826.

28. Potts D.M. and Addenbrooke (1997). "A structure's influence on tunneling-induced ground movements," Proc. Instn. Civ. Engrs. Geotech. Engng. 1997, Vol 125, April, PP109-125.

29. Potts D. M. and Zdravkovic L. (2001). Finite element analysis in geotechnical engineering application. Thomas Telford.

30. Sagaseta, C. (1987) "Analysis of undrained soil deformation due to ground loss," Geotechnique, 37(3), 301-320.

31. Sagaseta, C. and Gonzalez, C. (2001) "Prediccion teorica de subsidencias," Chapter 6.2 Aspectors Geotecnicos de la Ampliacion del Metro de Madrid.

32. Schanz T., Vermeer P.A. and Bonnier P.G. (1999). "The hardening soil model: Formulation and verification," In R B J Brinkgreve, Beyond 2000 in Computational Geotechnics, Balkema, Rotterdam, p. 289-291.

33. Schmidt, B. (1969). Settlements and ground movements associated with tunneling in soils. PhD Thesis, University of Illinois, Urbana.

34. Timoshenko S. (1957). Strength of materials – Part I, D van Nostrand Co, Inc. London.

35. Verruijt, A. and Booker, J.R. (1996) "Surface settlements due to deformation of a tunnel in an elastic half plane," Geotechnique, 46(4), 753-756.

36. Whittle, A.J. and Sagaseta, C. (2001). "Analyzing the effects of gaining and losing ground," ASCE Journal of Geotechnical and Geoenvironmental Engineering, 255-290, (doi 10.1061/40659(2003)9).